ISBN 978-82-326-2168-2 (printed version)
ISBN 978-82-326-2169-9 (electronic version)
ISSN 1503-8181

Doctoral theses at NTNU, 2017:48

Anne Mai Ersdal

Model predictive load-frequency control

NTNU
Norwegian University of
Science and Technology
Faculty of Information Technology,
Mathematics and Electrical Engineering
Department of Engineering Cybernetics

NTNU
Norwegian University of
Science and Technology

Doctoral theses at NTNU, 2017:48

NTNU

NTNU
Norwegian University of
Science and Technology

Anne Mai Ersdal

Model predictive load-frequency control

Thesis for the degree of Philosophiae Doctor

Trondheim, February 2017

Norwegian University of Science and Technology
Faculty of Information Technology,
Mathematics and Electrical Engineering
Department of Engineering Cybernetics

NTNU
Norwegian University of
Science and Technology

NTNU
Norwegian University of Science and Technology

Thesis for the degree of Philosophiae Doctor

Faculty of Information Technology, Mathematics and Electrical Engineering Department of Engineering Cybernetics

© Anne Mai Ersdal

ISBN 978-82-326-2168-2 (printed version)
ISBN 978-82-326-2169-9 (electronic version)
ISSN 1503-8181
ITK-report: 2017-6-W

Doctoral theses at NTNU, 2017:48

Printed by Skipnes Kommunikasjon as

Summary

The decrease in frequency quality seen in the Nordic power system over the past two decades is a clear token of the major changes that power systems all around the world are facing. These changes are to a large extent connected to the green shift in energy production, which results in less controllable power production. Additionally, there are bottlenecks in the Nordic transmission grid, which at times exclude some of the resources from participating in frequency control, and the power trading between the Nordic and the Continental European system is increasing, which means that the Nordic system is being subjected to higher and more unpredictable consumption.

One important mean for improving the frequency quality is to improve the load frequency control (LFC), which is the continuous operation of keeping produced and consumed power equal all times. With the Nordic power system in mind, an important task will be to implement a fully operable automatic generator control (AGC), which automatically controls the power-production set point of each generator. AGC was first implemented in the Nordic system in 2013, and due to unexpectedly high expenses, it is still not fully up and running. This thesis aims at investigating model predictive control (MPC) as a control design method for AGC, with application to the Nordic power system. It is believed that the natural handling of multiple inputs and system constraints, as well as the optimizing nature of MPC makes it a promising candidate for AGC.

The main contribution of this thesis is an MPC-based solution to the LFC/AGC problem, where state feedback is achieved through a state estimator and a simplified system model is used both in the MPC predictions and the state estimator. System constraints include production limits and limits on generation rate of change, as well as constraints on tie-line power transfer capacity. In order to include constraints on the individual generating units, and not only on the aggregated generating units of the simplified model, the participation factors of each generator are included as optimization variables. Simulations on a proxy model show that the MPC-based solution outperforms a traditional PI-based solution. In order to make the controller more robust against fluctuations in produced wind power, a multi-stage nonlinear MPC (MNMPC) is also presented. Based on estimates of the worst-case deviation in produced wind-power, the MNMPC makes sure there is enough available transfer capacity on tie lines to make use of all resources in case of large deviations in wind-power production. The approach of stochastic NMPC (SNMPC) is also tested as an alternative to the MNMPC. The SNMPC has the theoretical advantage of stochastic guarantees for constraint fulfillment in the presence of disturbances (deviations in

produced wind power), while the MNMPC shows better tractability and is less likely to encounter feasibility issues.

Using the power transfer in high voltage direct current (HVDC) lines as controllable inputs to the system is also investigated as a method for improving angle stability, which is a different part of power system stability. The method of backstepping was applied in this part of the thesis, which is a control-design method that is not based on online optimization, contrary to the MPC. The work shows that HVDC-lines can contribute in stabilizing the overall stability of a power system.

Preface

This thesis is submitted in partial fulfillment of the requirements for the degree of Philosophiae Doctor (PhD) at the Norwegian University of Science and Technology (NTNU). The research has been conducted at the Department of Engineering Cybernetics (ITK) from August 2011 to October 2016. Funding for the research has been provided by the Research Council of Norway Project 207690 Optimal Power Network Design and Operation, for which I am very grateful.

First of all, I would like to show my gratitude to my supervisor Professor Lars Imsland for all his encouragement, guidance and valuable inputs throughout this period. I am very grateful for his support, and would like to thank him for always taking the time to answer all my questions and offering his advise. It has been very inspiring to have a supervisor who is so committed, and takes a genuine interest in my work. I would also like to thank my co-supervisor Professor Kjetil Uhlen for all his guidance, comments and suggestions. His eminent knowledge and experience within power systems has been a very important contribution to this thesis, and I have learned a great deal from cooperating with him.

During the spring of 2013 I had the privilege of visiting Professor Nina F. Thornhill at Imperial College London. This was a very inspiring time, and I would like to thank both Professor Thornill and Dr. Davide Fabozzi for close collaboration and very valuable inputs to my work. In many ways it defined the path I took in my research, and this thesis would not have been the same without it.

I would also like to thank the members of my thesis committee, Professor Bikash Pal, Associate Professor Sébastien Gros, and Professor Marta Molinas, for the efforts and time you have spent on reviewing this thesis.

During my time at the department, I have enjoyed close friendship and good colleagueship with Anders Willersrud, Tor Aksel Heirung, Joakim Haugen, Brage Rugstad Knudsen, Bjarne Grimstad, Parsa Rahmanpour, Hodjat Rahmati, Eleni Kelasidi, Mansoureh Jesmani, and several others. I have had a great time, sharing discussions, laughs and fellowship. I was also fortunate to make many new friends during my time in London, and would like to take the opportunity to express my gratitude to Inês M Cecílio, Sara Budinis, Adele Slotsvik, Pedro Rivotti, Yuanyuan Ma, Dionysios Xenos, Denis Schulze, and Alexandra Krieger for the warm and welcoming atmosphere.

I would also like to thank my parents and my sister. Firts of all for being survivors, and secondly for their unconditional support and encouragement, especially after Edith's arrival. Finishing this thesis would not have been easy without you, and without all your help with babysitting and daily dinner invitations. A special

thank you to my father for introducing me to Engineering Cybernetics, and for always helping me with my math homework. I am also deeply grateful to Ørjan for always being there to support, encourage and comfort me, and for always being so helpful and understanding. And last, but not least, I want to thank Edith; for sleepless nights, new priorities, and for being an endless source of love and motivation.

Anne Mai Ersdal
Tromsø, February 2017

Contents

Abbreviations

AC	Alternating current
ACE	Area control error
AGC	Automatic generator control
AVR	Automatic voltage regulator
CMPC	Centralized model predictive control
CPM	Control performance measure
DAE	Differential algebraic equation
DC	Direct current
DMPC	Distributed model predictive control
EKF	Extended Kalman filter
FACTS	Flexible alternating current transmission system
FCR	Frequency containment reserves
FRR	Frequency restoration reserves
HVDC	High voltage direct current
IP	Interior point
KF	Kalman filter
LFC	Load frequency control
LP	Linear programming
MNMPC	Multi-stage nonlinear model predcitive control
MPC	Model predictive control
NERC	North American electric reliability corporation
NLP	Nonlinear programming
NMPC	Nonlinear model predictive control
NNMPC	Nominal nonlinear model predictive control
OCP	Optimal control problem
PI	Proportional integral
PID	Proportional integral derivative
PM	Prediction model
PMU	Phasor measurement unit
PRM	Plant replacement model
PSS	Power system stabilizer
RMPC	Robust model predictive control
RNMPC	Robustified nonlinear model predictive control
RR	Replacement reserves
SMPC	Stochastic model predictive control
SNMPC	Stochastic nonlinear model predictive control

SQP	Sequential quadratic programming
TSO	Transmission system operator
QP	Quadratic programming

Chapter 1

Introduction

This chapter presents some background information on power systems in general, and the Nordic power system in particular. Power systems all around the world are currently facing large changes, much because of the green shift seen in power production, and the challenges related to this will be discussed. This aim of this thesis is to investigate model predictive control (MPC) as a mean to solve some of these challenges, and the basics of MPC and nonlinear MPC (NMPC) will therefore be presented as well.

1.1 Introduction to Power Systems

Modern power systems are large, complex, dynamical systems whose main task is to provide electric energy to the end user, i.e. the industry, households, agriculture and so on. The structure of these power systems can be divided into four main parts: Generation, transmission, distribution and demand, see Figure 1.1.

Since the 1990s the energy markets have been liberalized. In a typical liberalized model, there are several private companies who generate power using their own individual power stations, and who compete against each other in selling it. The transmission of the power is usually operated by one transmission system operator (TSO), which has monopoly and is independent of the generation companies. The distribution of power to the end users is also handled by several private companies, which own and manage the distribution network in their area. Finally there are the companies who are responsible for retail, by buying power from the generation companies and selling it to the end users.

Generation

The main sources of electrical energy to the power system is the kinetic energy of water and the thermal energy derived from fossil fuels and nuclear fission (Kundur, 1994). The task of the prime movers (often turbines) is to convert this kinetic energy into mechanical energy, which in turn is converted into electrical energy by the synchronous generators. A synchronous generator is a generator where, at steady state, the frequency of the delivered output current is synchronized with the rotation of the generator rotor. When many such generators work together in a network, they will all synchronize with the same network frequency at steady state.

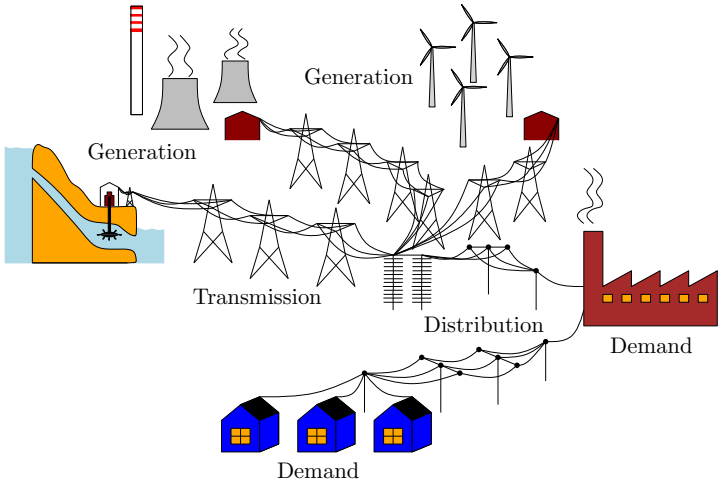

Figure 1.1: Overview of power system structure.

Transmission

Traditionally, the large power plants have been placed near the primary source of energy and the produced electricity is transmitted over long distances to the end users. To minimize the energy loss, which is proportional to the current squared, the transmission lines operate at very high voltages. The transmission network usually has a mesh structure, which allows for flexibility and redundancy in transporting power from source to end users. The transmission network is what connects all the generating units and loads together, so that an action of any individual component influence all the other components of the system (Machowski et al., 2008).

Distribution

The distribution network brings the energy to the consumers, operating at lower voltages than the transmission network. Traditionally, there has not been any generating units connected to the distribution network, but this is changing, as smaller, renewable-energy based power plants enter the market.

Demand

The power demand from the end users is ever-changing and can, individually, change quite rapidly and in an unpredictable manner. However, when adding all this individual power demands into one total power demand, the changes are less fluctuating and more predictable. The variations in total power demand depends on the season, weather conditions, time of day and so on.

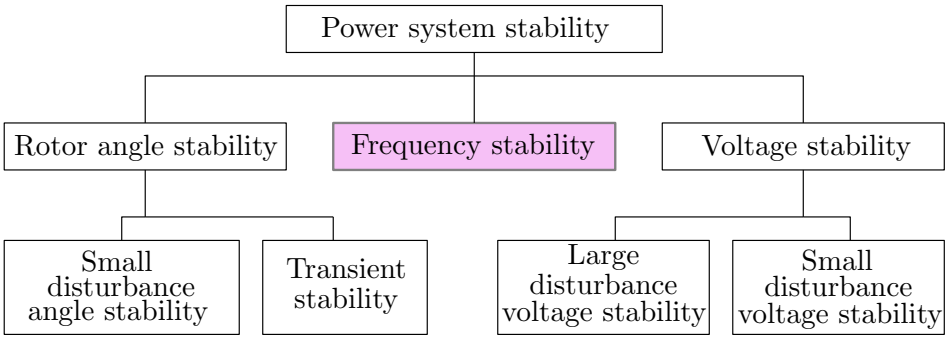

Figure 1.2: Classification of power system stability (Machowski et al., 2008).

1.1.1 Power System Stability

In Kundur et al. (2004), the definition of power system stability is given as:

> The ability of an electric power system, for a given initial operating condition, to regain a state of operating equilibrium after being subjected to a physical disturbance, with most system variables bounded so that practically the entire system remains intact.

When discussing power system stability, it is normal to divide the concept into three parts: rotor angle stability, frequency stability and voltage stability, see Figure 1.2.

The rotor angle stability is the system's ability to maintain synchronization of the generators after a severe (transient angle stability) or smaller (small disturbance angle stability) momentary disturbance. These faults are often caused by short circuits in the transmission network, and are often cleared without having to interfere with the amount of mechanical power provided by the prime movers. The rotor angle stability is fairly well preserved using power system stabilizers (PSS), thyristor exciters, fast fault clearing and so on (Bevrani et al., 2011).

Voltage stability is the system's ability to maintain the voltages of the system at acceptable levels after being subjected to a disturbance. The voltage stability is strongly coupled with the reactive power balance in the power system, and it is stabilized by the automatic voltage regulator (AVR) which controls the internal voltage of the generators.

Contrary to rotor angle stability, the frequency stability of a system is related to long-term imbalance between generation and consumption of active power. This active power imbalance will initially be covered by the kinetic energy of the rotating masses in the system (turbines, generators, motors), causing the frequency to change in a similar manner to the level in a water tank: as the water level rises/falls when there is a surplus/shortage of supplied water, so does the frequency of a power system when there is a surplus/shortage of produced power. However, this is no permanent solution, and such a power imbalance requires actions to be made so

that the mechanical input from the prime movers match the network loads, which in turn will restore the frequency back to the wanted level. This is what is referred to as load frequency control (LFC), which is the main topic of this thesis. Since this thesis focuses on frequency stability and not voltage stability, the term power will in the following refer to active power.

1.1.2 Power markets

The balancing of power supply and demand are in most systems managed by power markets. In these markets, production and consumption are balanced for each hour of the upcoming twenty-four hours, and they take into account known variations in power production as well as daily/weekly/annually deterministic load variation patterns. However, there are still several factors that are uncertain, mainly connected to temperatures, wind and unforeseen system errors (Statnett, 2012). Because of this, there are also intra-day markets where power is traded up to one hour before the operating hour. Even though these intra-day markets contribute to correct possible deviations from the original market balance, there will always be unforeseen system faults and changes in generation or load also within the operating hour. The imbalance caused by these unforeseen factors is continuously covered by the LFC, which is operated and maintained by the TSO.

1.1.3 Load Frequency Control

The main task of LFC is to maintain frequency stability, which means keeping the system frequency at a desired level when changes in consumption or generation appear. This is done by continuously adapting the power production against the consumption during the operating hour. Since storing of large amounts of power in general is inefficient (Machowski et al., 2008), the power must be produced as it is consumed. In addition to this main control task, another incentive is to keep the costs associated with LFC at a minimum. LFC of interconnected power systems is often implemented as a three-level hierarchical control structure. These three levels, in increasing hierarchical order, are often referred to as primary, secondary and tertiary control[1] (Machowski et al., 2008). Secondary control is often referred to as automatic generator control (AGC), and this term will be applied in the following. Figure 1.3 shows the nature of how primary control, AGC and tertiary control cooperate to compensate for a power imbalance. It also shows the timescales of when they are required to activate in the Nordic power system.

Primary control

Primary controllers, often referred to as governors, are local, continuous, automatic controllers situated at the generating units. They are proportional controllers which

[1] Also known as frequency containment reserve (FCR), frequency restoration reserve (FRR) and replacement reserve (RR) (ENTSO-E, 2012).

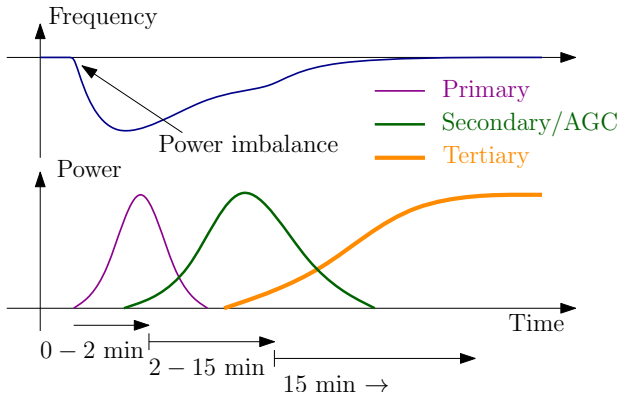

Figure 1.3: Activation of primary, secondary/AGC and tertiary control after power imbalance.

alter the mechanical input power from the turbine based on the deviation in angular speed from a given nominal speed, and they are required to act instantaneously. For stable operations the governor much ensure that an increase in shaft speed will reduce the turbine mechanical output and vice versa. In steady state, the following relationship is desirable

$$\frac{\Delta c}{\Delta \omega_m} = -\frac{1}{\rho} \tag{1.1}$$

where Δc is the change in valve positioning, $\Delta \omega_m$ the deviation in generator angular speed from the nominal angular speed, and ρ a positive constant called the speed-droop coefficient. The effective gain of the governing system is $K = 1/\rho$. It is the droop which decides how much the output power should adjust (trough the input c) when the shaft speed changes. Or put in another way, it decides how much the speed should change when there is a demand for higher or lower power delivery from the turbine. Preferably, the change in speed should be small, which is achieved with a small droop. However, depending on the type of turbine, there are limitations on the droop connected to how rapid changes in c they can handle. If generators connected to the same system all have $\rho > 0$, there will always be a unique load-sharing frequency.

AGC

When the system is subjected to a long-term power imbalance, the primary controllers alone will not be able to restore the frequency to its initial state. The primary control will stabilize the frequency with an offset, unless replaced by the AGC. This is done by altering the set point to the governor and thus changing the power output at $\Delta \omega_m = 0$. The AGC is slower than primary control, and it is centralized, often automated, and dispatch the control signal in a discrete manner. In most systems today, AGC is implemented as proportional integral (PI)-based controllers (Bevrani, 2014) which produce one input per area. This is then dis-

tributed to the generating units of each area using participation factors, α, which define the contribution of the individual generating units to the total generation (Machowski et al., 2008).

When there are multiple areas connected by tie lines with given power-flow set points, the AGC also tries to restore the power flow on the tie lines to these set points. The control input is then a combination of the frequency offset and the tie-line offset called the area control error (ACE). Because the Nordic power system is operated as a unity with common markets, there is no need to minimize tie-line offsets, as long as the power flow is kept within the tie-line boundaries. Hence, such tie-line set points will not be included in this work.

Tertiary control

Tertiary control is additional to, and slower than, AGC and primary control. It is mainly executed manually by the TSO, and its purpose is to ensure (Machowski et al., 2008)

- Adequate AGC spinning reserves[2].
- Optimal dispatch of units participating in AGC.
- Restoration of bandwidth of AGC.

Tertiary control is executed either via changing the AGC set point or by connecting or disconnecting generating units that participate in tertiary control.

1.1.4 The Nordic power system and challenges within LFC

In Europe there are two isolated systems (Cyprus and Iceland) and five synchronous areas: the Continental European, the Baltic (which is synchronized with Russia), the Nordic, the British, and the Irish synchronous area (ENTSO-E, 2015), see Figure 1.4. In a synchronous area, the power systems of each country are connected to each other using alternating current (AC) lines, and all the generators are synchronous; sharing a common system frequency. This has the effect that every component of a synchronous area will be affected by faults or disturbances appearing anywhere in that area. The individual synchronous areas are again connected to each other using direct current (DC) interconnection which does not spread the effect of faults etc.

This thesis focuses on the Nordic power system, which consists of Norway, Sweden, Finland, and the eastern part of Denmark, that is the island of Zealand. In the Nordic system, there has been a negative trend with regards to frequency quality and LFC over the past two decades. The aim is to keep the frequency between 49.9 and 50.1 Hz, however, as seen in Figure 1.5, which displays the minutes spent

[2]Spinning reserves is the difference between the sum of the power ratings of all operating units and their actual load, i.e. "available" power of on-line generating units.

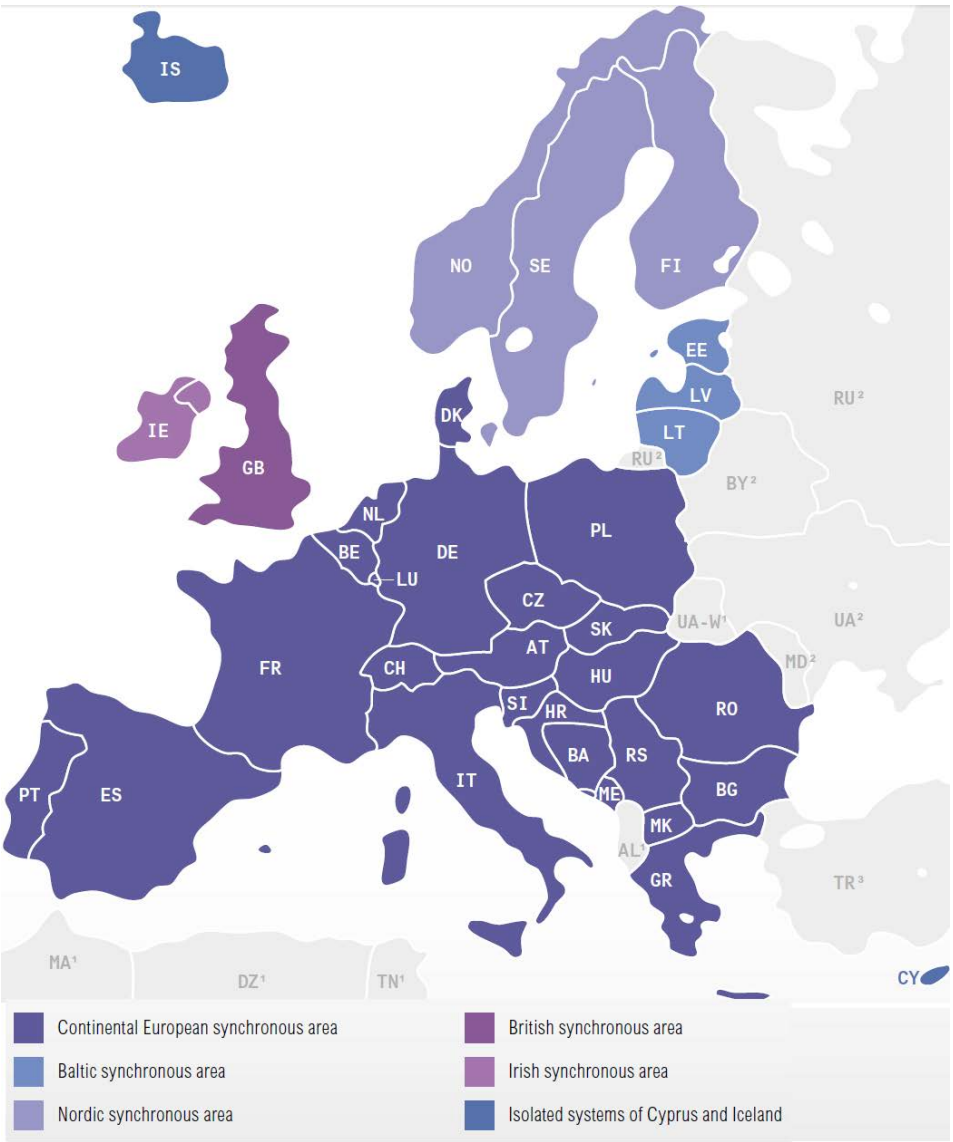

Figure 1.4: Synchronous and isolated areas in Europe (ENTSO-E, 2015).

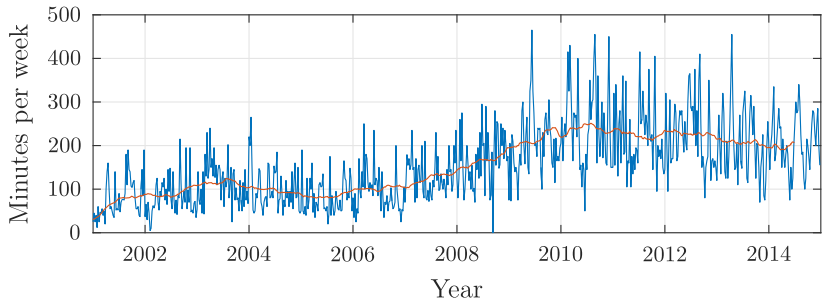

Figure 1.5: Minutes per week spent outside $49.9 - 50.1$ Hz in the Nordic system (Statnett, 2015).

outside this band per week, this has shown to be increasingly difficult. There are many factors that contribute to this development, and some of the main challenges will be further elaborated in the following. They all share the feature that they are connected to the great changes seen in power systems all around the world.

Traditionally, power systems has been supplied by large power stations consisting of mainly hydro-, nuclear-, coal-, or gas turbines. Except for nuclear energy, these are all sources of energy which results in flexible power production: As long as there is water in the reservoirs, coal to burn, etc., you can produce as much power as you want, only limited by the dimensions of the turbine. This power was then consumed by traditional consumers, such as households and industry, and there were not much trading of power between different synchronous areas, such as between the Nordic system and the Continental European system. This situation has changed a lot over the past two decades, much because of the climate changes. It is believed that the dominant cause of the climate changes is the CO_2 emission from human activities, which is largely dominated by combustion of fossil fuels in power stations around the world. This has led to a growth of new renewable energy, such as wind, solar, wave, etc., and the European Union has stated that by 2020, 20% of the energy consumption in Europe should come from renewable energy. Figure 1.6 shows the development of generating capacity in the Nordic power system over the past 15 years, divided into hydro, thermal (nuclear and fossil), and renewable energy sources excluding hydro (RES-H). It shows that during the past 15 years, the percentage of RES-H has increased, and the environmental aim is for it to increase even further. This poses great challenges with regards to LFC, since RES-H is mainly uncontrollable power production, which means that the TSO cannot simply ask e.g. a large wind farm to produce more power. It all depends on the amount of wind at the time. With less controllable power available in the system, the task of continuously balancing production against consumption becomes more difficult, and this is one of the main reasons for the decrease in frequency quality (Statnett, 2015).

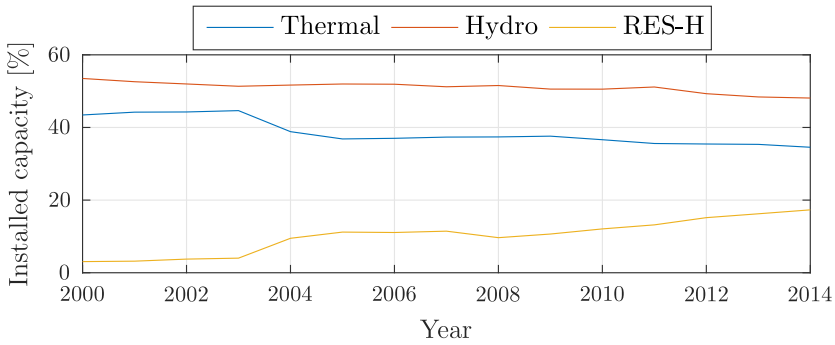

Figure 1.6: Installed generation capacity in the Nordic power system (Nordel, 2008; ENTSO-E, 2014).

This increase in uncontrollable power production is present all across Europe, and one way of making all the synchronous areas of Europe less affected is by increasing the DC-connections between them, allowing them to cooperate in the task of fading out non-renewable energy. One idea is to use the hydro-dominant Nordic system as a battery for the increasingly wind- and sun influenced Continental European system. This means more power transfer in and out of the Nordic system, resulting in higher and more unpredictable consumption, which also contributes to the decrease in frequency quality (Statnett, 2015).

In addition to the challenges related to the green shift in energy production, the Nordic system has not been expanded concurrent with the increasing energy need and the tighter connection to Continental Europe, leaving it under-dimensioned and operating close to its maximum transfer capacity (Statnett, 2015). This has led to an increasing amount of of bottlenecks, which at times excludes some of the resources from participating in LFC, and according to Statnett (2015) there is a tendency to a strong correlation between frequency incidents (i.e. minutes spent outside $49.9 - 50.1$ Hz) per week and the number and duration of bottleneck congestions that week.

The last challenge mentioned here is the challenge of the hourly production set-point shifts. The change in power-production set points happens on the hour in the Nordic system, while the change in consumption naturally happens during the hour. This leads to a large deviation between production and consumption at every hour shift, resulting in large frequency deviations. In addition, the change in power flow on the connecting DC lines also happens on the hour, which amplifies the problem as the connection and trading with Continental Europe increase.

Figure 1.5 also shows that the number of frequency incidents has stabilized and decreased some since 2011. This is mainly because of actions taken by the Nordic TSOs since 2008, some of which temporary, resulting in better market solutions, more flexible power exchange with Continental Europe, and also an improved LFC.

In fact, the Nordic system did not practice AGC until 2013, and it is still not fully up and running, much because of unexpectedly high expenses due to incomplete AGC market solutions (Statnett, 2015). This is however an ongoing project, and the frequency quality is still far from the wanted levels. It is expected that the temporary solutions will be replaced by among others a fully operable AGC in the years to come, which is considered to be an important part of improving the frequency quality. It is therefore of interest to find methods of conducting AGC which aid the power system in resolving some of the issues related to bottlenecks and the increasing amount of uncontrollable power production, and it is believed that MPC could be an efficient solution.

1.2 Introduction to model predictive control

Model predictive control (MPC) is an advanced control method which has its roots in optimal control, and it is one of the few advanced control methods that has made a significant impact on industrial control engineering (Maciejowski, 2002). MPC comes in many shapes and sizes, however, they all share the same basic concept: a model of the system to be controlled is used to predict and optimize the future system behavior. This is done by solving an optimal control problem (OCP), which forms the heart of an MPC. A general discrete-time OCP is as follows

$$\min_{x_k, u_k \forall k=1,\ldots,M} \; J\left(x_k, u_k\right) \tag{1.2a}$$

subjected to

$$x_0 - x_{init} = 0 \tag{1.2b}$$
$$x_{k+1} - f\left(x_k, u_k, w_k\right) = 0 \;\forall\; k = 1, \ldots, M \tag{1.2c}$$
$$g\left(x_k, u_k\right) \leq 0 \;\forall\; k = 1, \ldots, M \tag{1.2d}$$
$$r\left(x_M\right) \leq 0 \tag{1.2e}$$

where x_k are the dynamic system states, u_k the controllable system inputs, and w_k the system disturbance. Equation (1.2b) is the fixed initial state, (1.2c) the system model, (1.2d) the path constraints, and (1.2e) the terminal constraints. The objective function

$$J\left(x_k, u_k\right) = \sum_{k=0}^{M-1} L\left(x_k, u_k\right) + E\left(x_M\right) \tag{1.3}$$

is a central part of the OCP, and it consists of a stage cost $L\left(x_k, u_k\right)$ and a terminal cost $E\left(x_M\right)$ (often referred to as the Lagrange term and the Mayer term, respectively). When solving the OCP, one finds the inputs u_k which minimize the objective function $J(\cdot)$ over the control horizon M, while fulfilling all system constraints (1.2b)-(1.2e). The objective function $J(\cdot)$ and the control horizon M are

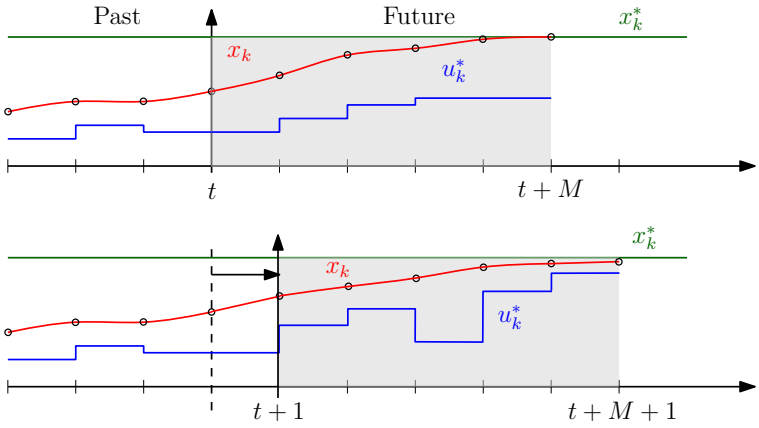

Figure 1.7: The receeding-horizon principle, $k = 1, \ldots, M$.

the main tuning variables of the OCP. The objective function states what is actually regarded as optimal and what should be prioritized, while the control horizon dictates how much of the future system behavior that should be included. In the objective function it is common to punish deviations from a wanted steady state or state trajectory x_k^*, so that the optimal input u_k^* steers the state to this value.

The solution to the OCP are optimal inputs M timesteps into the future, and if the system model was perfect, and no unknown disturbances acted on the system, these inputs would steer the system towards x_k^* as predicted. However, no system model is perfect, and even if it was, the OCP only provides optimal input M timesteps into the future. What should the input be when M timesteps have passed? This is solved by what is known as the receding-horizon principle, see Figure 1.7: At each time step, the first optimal input from the OCP, u_0^*, is applied to the system, and at the next timestep measurements from the system are used to update the system model, and a new OCP is solved, giving an updated optimal input. Again, only the first of these inputs is applied to the system. This is repeated at every timestep, which introduces feedback to the controller, and the result is the MPC. Figure 1.8 depicts the general composition of an MPC, with the system model, measurements y_k, and the OCP. The figure also includes the Kalman filter, which produces the state and disturbance estimates $\{\hat{x}_k, \hat{w}_k\}$. The Kalman filter is discussed in the next section.

The path constraints (1.2d) can include constraints on both states and inputs, and this intuitive inclusion of constraints is one of the benefits of an MPC. In addition to this, it naturally handles multivariable control[3], and feedforward from known or measurable disturbances are easily included through w_k in (1.2c). An MPC will also often make it possible to operate closer to the constraints, which leads to more profitable operation in many cases.

[3]Control systems with multiple inputs and/or multiple outputs.

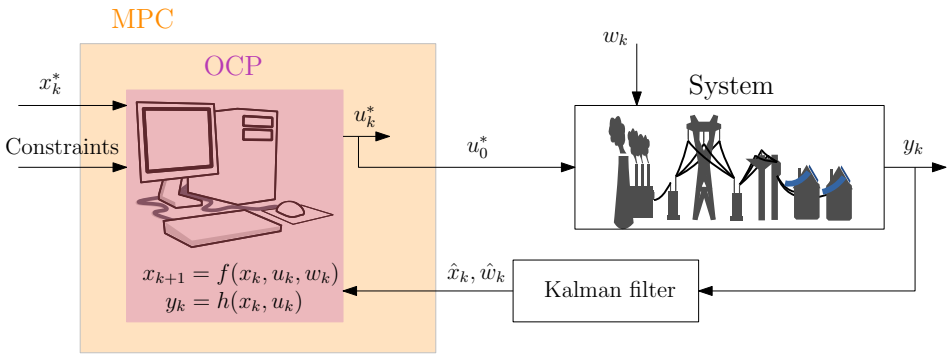

Figure 1.8: General composition of an MPC.

1.2.1 Feedback and updating the system model

The MPC predicts and optimizes the behavior of the system model, not the actual system itself. And in order for the MPC to function properly it is important that the model accurately (enough) reflects the most interesting properties of the actual system. However, it is also important that the model is not too detailed and complicated, as the OCP must be solved in time for the next timestep. One must therefore expect model errors and unknown/unmodelled disturbances in an MPC, and updating the system model in order to maintain good quality predictions is always necessary. One way of achieving this is through Kalman filtering.

The original Kalman filter (KF) was published by Rudolf E. Kalman in 1960, and it is a method for estimating the states of a linear system. A KF is a recursive algorithm which exploits knowledge of both the system as well as the disturbances it is subjected to, in order to estimate the state vector so that the mean squared estimated error is minimized. The KF is run at each time step, and it involves four main steps: the incrementation of time, the integration, the computation of the Kalman gain, and the measurement update. After the time is incremented, the estimate is integrated forward in time using a system model. This estimate is then refined during the measurement update, using the current measurement and the Kalman gain. The Kalman gain is the solution to the Riccati equation (Simon, 2006), and it will in general decide how much to trust the model and how much to trust the measurements (through provided information of their respected accuracy). The Kalman filter (KF) has become popular within many areas of application, especially since the extended Kalman filter (EKF) for non-linear systems was introduced in the late 1960s (Simon, 2006). The KF adapts the state estimate to fit the measurements from the true system response, and thereby updating the system model. The KF can also be modified to include estimation of unmeasurable, time varying disturbances, so that they can be included in the feed-forward part of the MPC.

1.2.2 Solving the OCP

Solving an OCP is the same as solving a general optimization problem where (1.2b)-(1.2e) are all seen as equality and inequality constraints. A general optimization problem can be defined as

$$\min_{\upsilon} \quad \Gamma(\upsilon) \tag{1.4a}$$

subject to

$$\Theta(\upsilon) = 0 \tag{1.4b}$$
$$\Sigma(\upsilon) \leq 0 \tag{1.4c}$$

where υ are the optimization variables, $\Gamma(\upsilon)$ the objective function, $\Theta(\upsilon)$ the equality constraints, and $\Sigma(\upsilon)$ the inequality constraints. Comparing to the OCP (1.2), (1.2b) and (1.2c) are equality constraints, while (1.2d) and (1.2e) are inequality constraints.

General optimization problems are solved through numerical optimization using iteration-based algorithms, and there are many different types of optimization problems, which can be solved by many different algorithms. There are however some common classifications, and optimization problems sharing the same classification can in general be solved by the same algorithms. It is common to classify optimization problems using two different axes: convex vs. non-convex and linear vs. non-linear. An optimization problem such as (1.4) is said to be convex if the objective function and the inequality constraint function are convex and the equality constraint function is linear, otherwise it is non-convex (Nocedal and Wright, 2006). A convex optimization problem is in general much easier to solve than a non-convex optimization problem, and all local optima are global optima, hence a global solution is always found (if a solution exists). Non-convex optimization problems can be more challenging, as they tend to have several stationary points and local optima. In a non-convex optimization problem one can find either a local or a global solution, the former can however be a quite challenging task, and many algorithms return a local optima. The axis of linear vs. non-linear is based on whether the system constraints (including the system model of an OCP) and the objective function are linear or nonlinear, which results in the following three classifications

- **Linear programming (LP)**. In an LP formulation, the objective function is linear, and so are all system constraints. Optimization problems of this type are always convex, and they are probably the most widely solved optimization problems, especially within financial and economic applications (Nocedal and Wright, 2006). They are easily solved with well known algorithms, and will always produce a global optimum.

- **Nonlinear programming (NLP)**. In an NLP formulation, either the system constraints or the objective function are nonlinear. These problems tends

to arise naturally in physical systems, however, they are more difficult, and hence more time consuming, to solve. An NLP can be either convex or non-convex, and this is what decides the difficulty of the NLP and which algorithms that can be used to solve it. A convex NLP can often be solved efficiently using the same type of algorithms that are efficient for LP formulations.

- **Quadratic Programming (QP)**. The QP formulation is a special case of NLP, where the system constraints are linear, while the objective function is quadratic. The characteristics of a QP can be exploited to find efficient algorithms, and if a QP is convex it is often similar in difficulty to an LP (Nocedal and Wright, 2006). Convexity of a QP is rather simple to identify, as it is given by positive semi-definiteness of the Hessian H of the objective function $\Gamma(\upsilon) = c^T\upsilon + \upsilon^T H\upsilon$. A QP can always be solved or shown to be infeasible in a finite amount of computations (Nocedal and Wright, 2006).

An OCP with a linear system model is often either an LP or a QP (unless there are other nonlinear constraints), while an OCP with a nonlinear system model as equality constraint always will be a non-convex NLP. The distinction between linear and nonlinear system model is therefore important when it comes to the solvability and efficiency of an OCP, and it is the most important classification for an MPC: linear MPC and nonlinear MPC (NMPC). In this thesis, NMPC is applied, and hence a non-convex NLP is solved at each time step. The two most common classes of algorithms used to solve NLPs are sequential quadratic programming (SQP) methods, and interior-point (IP) methods. See Nocedal and Wright (2006) for more information on numerical optimization.

Continuous-time OCP

It is from now on assumed that the system model of (1.2) is nonlinear, and hence that the discrete-time OCP is an NLP. As seen from (1.2a), the OCP has $2M$ optimization variables consisting of both the states x_k and the inputs u_k, $k = 1, \ldots, M$, and the NLP solver actually solves both the simulation problem and the optimization problem at the same time. When dealing with system models and objective functions that are continuous, forming a continuous-time OCP, there will be infinitely many optimization variables: $x(t)$, $u(t)$, $\forall t \in [0, T]$, where T is the continuous-time control horizon. There are in general two approaches for solving continuous-time OCPs: indirect or direct approaches (Biegler, 2010). The indirect approach is often described as "first optimize, then discretize". This leads to a boundary value problem, which is often quite difficult to solve. The direct approach can be described as "first discretize, then optimize". Here, the control trajectory is parameterized in finite dimension, leaving a discrete-time OCP, which can be solved as an NLP. The most common methods for parameterization is single shooting, multiple shooting, and collocation (Biegler, 2010).

Collocation has been the method of choice in this thesis, and the details for the collocation setup is therefore presented here. Given a general continuous-time OCP

$$\min_{x(t),u(t)\forall t=0,\ldots,T} J\left(x(t),u(t)\right) \tag{1.5a}$$

subjected to

$$x(0) - x_{init} = 0 \tag{1.5b}$$
$$\dot{x}(t) - f\left(x(t),u(t),w(t)\right) = 0 \ \forall \ t = 0,\ldots,T \tag{1.5c}$$
$$g\left(x(t),u(t)\right) \leq 0 \ \forall \ t = 0,\ldots,T \tag{1.5d}$$
$$r\left(x(T)\right) \leq 0 \tag{1.5e}$$

With collocation this OCP is discretized in both control and states on a fixed grid. The optimization horizon T is first divided into N elements of length h, and within each element the state profile is approximated using polynomial representation of order $K+1$. A common choice of polynomial representation is the Lagrange interpolation polynomial, and with $K+1$ interpolations points in element i, the state in element i is approximated as (Biegler, 2010)

$$t = t_i + h_i\tau \tag{1.6}$$
$$x^K(t) = \sum_{j=0}^{K} l_j(\tau)x_{ij} \tag{1.7}$$

where

$$l_j(\tau) = \prod_{k=0,\neq j}^{K} \frac{\tau - \tau_k}{\tau_j - \tau_k} \tag{1.8}$$

and $t \in [t_i, t_{i+1}]$, $\tau \in [0,1]$, $\tau_0 = 0$, $\tau_j < \tau_{j+1}$ and $j = 0,\ldots,K-1$. This approximation has the property that the approximated states x^K and the actual states x are equal at each interpolation point τ_j, see Figure 1.9.

The same can be done for the state time derivative, and by using these approximations one can get equations which ensures that the equation for the time derivative is fulfilled at the collocation points. These are called the colloctaion equations, and for the Lagrange polynomial they are as follows

$$\sum_{j=0}^{K} x_{ij}\frac{dl_j(\tau_k)}{d\tau} = h_i f(x_{ik},u_{ik}) \tag{1.9}$$

for $k = 1,\ldots,K$ and $i = 0,\ldots,N-1$.

In order to ensure continuity of the state profile in the element junctions, continuity equations are needed. For Lagrange interpolation profiles they are as follows

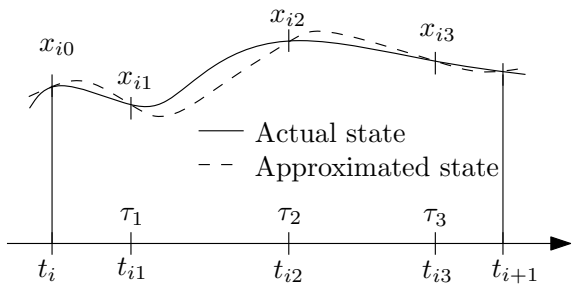

Figure 1.9: Polynomial approximation of state profile for one finite element (Biegler, 2010).

$$x_{i+1,0} = \sum_{j=0}^{K} l_j(1) x_{ij} \tag{1.10a}$$

$$x_{0,0} = x_0 \tag{1.10b}$$

for $i = 0, \ldots, N-1$.

Combining all of these equation results in the following NLP

$$\min_{x_{ik}, u_i \forall i=0,\ldots,N-1, k=0,\ldots,K} J\left(x_{ik}, u_i\right) \tag{1.11a}$$

subjected to

$$x_{00} - x_0 = 0 \tag{1.11b}$$

$$\sum_{j=0}^{K} \dot{l}_j(\tau_k) x_{ij} - h_i f\left(x_{ik}, u_i, w_{ik}\right) = 0 \ \forall \ i = 0, \ldots, N-1, k = 0, \ldots, K \tag{1.11c}$$

$$x_{i+1,0} - \sum_{j=0}^{K} l_j(1) x_{ij} = 0 \ \forall \ i = 0, \ldots, N-1 \tag{1.11d}$$

$$g\left(x_{ik}, u_{ik}\right) \leq 0 \ \forall \ i = 0, \ldots, N-1, j = 0, \ldots, K \tag{1.11e}$$

$$r(x_{N0}) \leq 0 \tag{1.11f}$$

Note that the input u_i is constant over each element i. The continuous-time OCP (1.5) is thus transformed into a discrete-time OCP (and in the case of a nonlinear system model, an NLP). It is mentioned that (1.11) contains implicit system equations, while the general discrete-time OCP formulation (1.2) has explicit system equations. This will not, however, affect the algorithms solving the OCP. Throughout this thesis, the number of elements N is chosen so that their length h is consistent with the control signal dispatching, and within each of these elements, the state profile is approximated using a Lagrange polynomial of order 3.

Feasibility

An important concept for all constrained optimization problems is that of the feasible region. The feasible region for the optimization problem (1.4) are those values of v where the constraints (1.4b) and (1.4c) are fulfilled. If this region is non-empty, the optimization problem is feasible, and if there exists no values of v where all constraints are fulfilled, the optimization problem is infeasible, i.e. it cannot be solved. Translated to OCP and MPC: If no system input can be found that fulfills all input constraints, and at the same time results in a system trajectory which fulfills all state constraints, the OCP is infeasible. This is a severe situation, as no updated optimal input can be produced, and it is important to have a strategy for dealing with infeasibility. One possible solution is to reuse the input calculated at the previous timestep. Either by keeping the input unchanged, or by using the control signal u_1^* from the previous timestep. This provides no guarantees for neither feasibility nor optimality, but it will work just fine in many situations.

Another possibility is to add slack variables to the soft constraints. Soft constraints are often state constraints connected to control quality, i.e. violating them will not cause any immediate danger. On the contrary, there are hard constraints, which are often related to input constraints that cannot be physically violated. One example being a valve, which cannot open more than 100%. The slack variables ϵ, which must be positive, are added to the soft constraints, and they are also added to the optimization variables

$$g_s\left(x_k, u_k\right) \leq \epsilon_k \tag{1.12a}$$

$$\epsilon_k \geq 0 \tag{1.12b}$$

where $k = 1, \ldots, M$. In order not to use the slack variables unless absolutely necessary, use of ϵ is penalized in the objective function

$$J\left(x_k, u_k, \epsilon_k\right) = \sum_{k=0}^{M-1} L\left(x_k, u_k\right) + E\left(x_M\right) + \gamma \epsilon_k \tag{1.13}$$

where γ is a constant of appropriate dimension. In this way, the soft constraints $g_s\left(x_k, u_k\right)$ are allowed to exceed zero in severe situations. In (1.13), ϵ is linearly included in the objective function, resulting in what is known as an exact penalty, which means that as long as γ is large enough, the constraint will not be violated unless there is no feasible solution to the original problem (Maciejowski, 2002).

Other possible solutions for dealing with infeasiblity is to actively manage the horizon or the constraints definition at each timestep, and through this avoid infeasiblity.

1.2.3 Nominal stability of nonlinear MPC

It is common to consider nominal stability of an NMPC, which is stability of the NMPC with no model uncertainty or unmeasurable disturbance. If one could have

an infinite optimization horizon in the NMPC, one could prove nominal asymptotic stability using Lyapunov theory (Grüne and Pannek, 2011). But solving an infinite horizon optimization problem is difficult in general, and the closed-loop NMPC with finite horizon (as described in Section 1.2) is not necessarily stable. First of all, it does not make sense to look at the stability of the solution to the OCP, as this is not what is actually implemented. What is actually implemented is only the first of the optimized inputs, before a new OCP is solved. In addition it only considers the system behavior M timesteps into the future, and does not care what happens after that. Because of this, methods for ensuring nominal asymptotic stability of an NMPC with finite optimization horizon has developed.

One way is to add stabilizing constraints to the NMPC. Either as equilibrium terminal constraints, demanding that the final state of the optimization horizon is equal to the systems steady state $x_M = x^*$, or as regional terminal constraints and terminal cost (Grüne and Pannek, 2011). In the latter, the terminal cost (Mayer term) $E(x_M)$ which is added to the objective function, is defined so that there exists a controller $u_k = \kappa\left(x_k\right) \forall k \geq M$ such that: (a) $E(x_M)$ works as a Lyapunov function for the closed loop system on a region $\mathbb{X}_0$ around x^*, (b) ensures that $\mathbb{X}_0$ is a forward invariant set for the closed loop system. In order to guarantee that the controller $u_k = \kappa\left(x_k\right)$ is feasible for all $k \geq M$, one must add a regional terminal constraint, ensuring that the predicted state at timestep M is inside $\mathbb{X}_0$. This is also known as recursive feasibility; ensuring that a feasible solution exists at the next timestep. Recursive feasibility is an important part of nominal stability analysis, as no stability can be proven without feasibility guarantees. With recursive feasibility it is guaranteed that as long as the OCP is feasible at the first timestep, it will also be feasible for all future timesteps. By applying either of these methods, asymptotic stability can be proven using Lyapunov theory (Grüne and Pannek, 2011).

The methods described above are often good for theoretical purposes, but there are some practical issues related to implementing them, and they are seldom applied in industry. For terminal equilibrium constraints the system needs to be controllable to x^* in finite time, and for regional constraint set and terminal cost a Mayer term which can be used to prove stability might be difficult to find. Unison for both the methods is that the optimization horizon often becomes relatively large.

Grüne and Pannek (2011) provides another method to prove asymptotic stability through the choice of objective function J and optimization horizon T. By designing the Lagrange term of the objective function so that it fulfills certain bounds, a lower bound for the optimization horizon which guarantees stability can be found. Finding both these lower bounds as well as the Lagrange term which fulfills them, can be a difficult task. The method can however be used to design a good objective function, even though it may not necessarily prove stability (Grüne and Pannek, 2011).

1.2.4 Robust MPC

The previous section treated the question of stability when no model uncertainty or unmeasurable disturbances are present. A system model is an approximation of a real life system, and it is often desirable that the model is rather simple and low dimensional. This is often achieved by designing the model to reflect certain important system properties, rather than modeling every detail of the system. This approach results in a model-plant mismatch that naturally introduces uncertainty. In addition, there are also other external disturbances which influence the real system, and in order to perform a meaningful control analysis and design, these uncertainties need to be described by an uncertainty model (Levine, 2010). Such uncertainty models often define an admissible set of plant models $\mathcal{F}$, and an admissible set of uncertain external input signals $\mathcal{W}$, which allows for system analysis such as: Is closed-loop stability guaranteed for every system model in $\mathcal{F}$? Will all system constraints be fulfilled for every external disturbance in $\mathcal{W}$? It is also common to divide between stochastic and deterministic disturbance models, where the elements of $\mathcal{F}$ and $\mathcal{W}$ are assigned different probabilities with a stochastic model, and seen as equally likely to occur in a deterministic model (Levine, 2010).

Within MPC, the issue of uncertainty is often addressed through robust MPC (RMPC), which considers uncertainties that are deterministic and lie in a bounded set (Mesbah, 2016; Bemporad and Morari, 1999). The work on RMPC has been dominated by min-max OCP formulations:

$$\min_{x_k^{w,f}, u_k \forall k=1,\dots,M} \left[\max_{w\in\mathcal{W}, f\in\mathcal{F}} J\left(x_k^{w,f}, u_k\right) \right] \tag{1.14a}$$

$$x_0^{w,f} - x_{init} = 0 \ \forall \ w \in \mathcal{W}, f \in \mathcal{F} \tag{1.14b}$$

$$x_{k+1}^{w,f} - f(x_k^{w,f}, u_k, w_k) = 0 \ \forall \ k = 1, \dots, M, w \in \mathcal{W}, f \in \mathcal{F} \tag{1.14c}$$

$$g(x_k^{w,f}, u_k) \leq 0 \ \forall \ k = 1, \dots, M, w \in \mathcal{W}, f \in \mathcal{F} \tag{1.14d}$$

$$r(x_M^{w,f}) \leq 0 \ \forall \ w \in \mathcal{W}, f \in \mathcal{F} \tag{1.14e}$$

In these OCP formulations, the optimization seeks to find minimizing inputs for the disturbances in $\mathcal{F}$ and $\mathcal{W}$ that maximize the objective function, while fulfilling system constraints for all possible disturbances, see for example Rawlings and Mayne (2009); Mayne et al. (2000); Löfberg (2003). Under certain assumptions and modifications, open loop min-max MPC (one common input sequence for all possible uncertainties) can be proven to be robust asymptotically stable (Mayne et al., 2000). This approach does however often results in large and complex optimization problems, often leading to conservative results or infeasible optimization problems (Scokaert and Mayne, 1998). To improve feasibility and ease computational load, various approaches has been proposed, e.g. using closed-loop (or feedback) min-max where the concept of feedback is implemented in the control horizon (Mayne, 2001), or tube-based MPC which is based on the precomputation of invariant sets (Langson et al., 2004). However, as problem dimensions grow,

closed-loop min-max and tube-based MPC still gives prohibitive complexity and conservative results. Another approach which shows better tractability results, is multi-stage MPC, which includes feedback, and where the disturbance is represented by a scenario tree where the scenarios are combinations of the extreme values of the disturbance (Lucia et al., 2013).

An alternative approach considers the uncertainty to be of probabilistic nature, i.e. it is stochastic and possibly unbounded. For many systems the stochastic system uncertainties can be adequately characterized, and it is natural to explicitly account for the probabilistic occurrence of uncertainties (Mesbah, 2016). This approach is commonly known as stochastic MPC (SMPC), and the stochastic description of the uncertainties are used to define chance constrains (Li et al., 2002; Primbs and Sung, 2009):

$$\min_{x_k, u_k \forall k=1,\ldots,M} E\left[J\left(x_k, u_k\right)\right] \tag{1.15a}$$

$$\mathcal{P}\left[x_0 - x_{init} = 0\right] \geq 1 - \sigma \tag{1.15b}$$

$$\mathcal{P}\left[x_{k+1} - f(x_k, u_k, w_k) = 0\right] \geq 1 - \sigma \ \forall \ k = 1, \ldots, M \tag{1.15c}$$

$$\mathcal{P}\left[g(x_k, u_k) \leq 0\right] \geq 1 - \sigma \ \forall \ k = 1, \ldots, M \tag{1.15d}$$

$$\mathcal{P}\left[r(x_M) \leq 0\right] \geq 1 - \sigma \tag{1.15e}$$

where $w \in \mathcal{W}$ and $f \in \mathcal{F}$ are assigned probability distributions, and $\mathcal{P}[\cdot]$ denotes the dependencies on the stochastic variables w and f. These chance constraints enable systematic use of the stochastic description of uncertainties to define stochastic levels of acceptable closed-loop constraint violation through σ (Mesbah, 2016), i.e. a small constraint violation probability is allowed. Chance-constrained optimization problems are hard to solve in general, and establishing theoretical properties such as recursive feasibility and stability, poses a major challenge (Mesbah, 2016). To obtain tractable solutions, sample-based approximations such as the scenario approach (Campi et al., 2009) has been presented as an alternative. In the scenario approach only a finite number of uncertainty realizations are considered, and the chance-constrained optimization problem is approximated by replacing the chance constraint with hard constraints associated with the extracted disturbance realizations only.

1.3 Software

All models and controllers in this thesis are implemented in Python using Casadi. Casadi is a framework for solving dynamic OCPs, and it has been developed with focus on allowing users to implement their method of choice with any complexity, rather than being a black-box OCP-solver (Andersson, 2013). The name Casadi originates from its form as a minimalistic computer algebra system (Cas) with a general implementation of automatic differentiation (ad). It is interfaced to various NLP solvers, and in using these solvers from Casadi there is no need to implement

functions for the derivatives, as they are automatically generated and interfaced by Casadi using automatic differentiation (Andersson, 2013).

1.4 Research objective

The main contribution of this thesis is the development of MPC-based control strategies to improve the frequency control of power systems, with the Nordic power system as a case study. As discussed in Section 1.1.4, the Nordic system is facing challenges related to an increasing amount of energy from intermittent energy resources, a heavier loaded network with many bottlenecks, and an increase in power trade with Continental Europe. These are all factors which has contributed to a decrease in frequency quality over the past two decades, and the aim of this thesis is to examine how use of MPC for AGC can help solve some of these challenges and improve frequency quality.

1.5 Outline and Contributions

This thesis is divided into four main parts. The first two parts consider different ways of improving LFC through the use of NMPC, the third part compares two different approaches for achieving robustness of the NMPC, and the fourth part considers the use of a backstepping controller to control power flow in high voltage direct current (HVDC) lines to improve angle stability. In the three first parts, a simulation model is used as a proxy for the physical system, as the transmission grid is a critical infrastructure which cannot be used as a test-bed. The power system model used as a proxy in this thesis was developed at SINTEF Energy Research (Norheim et al., 2005), and it reflects the real production and most interesting bottlenecks in the Nordic power system. All of the presented NMPCs are based on continuous-time nonlinear system models which are simplifications of the proxy model, and the method of collocation is applied to form an NLP which is solved using the IPOPT algorithm (Wächter and Biegler, 2006). Since the functions for the derivatives are automatically generated by Casadi (using automatic differentiation), the IPOPT is based on the exact Hessian. Each chapter contains a peer-reviewed conference or journal paper, and is therefore self-contained and can be read independently. As such, there will be some repetition in some of the chapters, especially the introduction, the modeling and the basic MPC-introduction in Chapter 2 and 3. As an explanatory comment, it is mentioned that the robustified NMPC (RNMPC) of Chapter 3, and the multi-stage NMPC (MNMPC) of Chapter 4 is the same controller.

- In **Chapter 2** a nominal NMPC, which does not take into account disturbances or uncertainties, is presented. The main contribution of this part is an MPC-based solution to the LFC problem, where state feedback is achieved

through a state estimator, and a simplified power system model is used both in the NMPC predictions and the state estimator. The participation factor of each generating unit is included as optimization variables, and suggestions are made as to how one can ensure tie-line power transfer margins through slack variables. An approach for including pricing information in the objective function is also presented.

This part consists of Ersdal et al. (2016a), which is based on preliminary results in Ersdal et al. (2013) and Ersdal et al. (2014).

- In **Chapter 3** the NMPC from Chapter 2 is made more robust against variations in produced wind power. The main contribution of this part is using knowledge of estimated worst-case variations in wind-power production to ensure available power-transfer capacity between different areas, where the wind-power capacity is concentrated in one area, leaving that area vulnerable to deviations in wind-power production.

  This part consists of Ersdal et al. (2016b), which is based on preliminary results in Ersdal et al. (2014).

- In **Chapter 4** a stochastic NMPC is implemented, which is an alternative approach for achieving robust NMPC. This approach is compared to the multi-stage NMPC of Chapter 3. The main contribution is the comparison of these two scenario-based approached, the discussion of their pros and cons, and how they are connected to solving the issue of robust LFC.

  This part consists of Ersdal and Imsland (2017).

- **Chapter 5** concerns a different subject than the previous chapters. It is possible to directly control the power flow in an HVDC line, and this is exploited to use HVDC lines that connect different power systems as a mean to increase the angle stability of the power systems. The controller is also designed using a different approach than in the previous chapters, namely the method of backstepping. Even though this is a different subject than LFC, angle stability is still an important aspect within power system stability, and it is vital for safe operation of a power system that they both are attended to. It is also worth mentioning that controlling the power flow through HVDC-lines, also can be used within LFC, even though this is not the subject of this chapter.

  This part consists of Ersdal et al. (2012).

- **Chapter 6** concludes the thesis.

1.5.1 Publications

The following list of publications form the basis of this thesis.

- Ersdal, A.M. and Imsland, L. (2017). Scenario-based approaches for handling uncertainty in MPC for power system frequency control. In *IFAC World Congress (submitted)*.
- Ersdal, A.M., Imsland, L., Uhlen, K., Fabozzi, D., and Thornhill, N.F. (2016b). Model predictive load-frequency control taking into account imbalance uncertainty. *Control Engineering Practice*, 53:139-150.
- Ersdal, A.M., Imsland, L., and Uhlen, K. (2016a). Model predictive load-frequency control. *Power Systems, IEEE Transactions on,* 31(1):777-785.
- Ersdal, A.M., Imsland, L., and Uhlen, K. (2012) Coordinated control of multiple HVDC links using backstepping. In *Control Applications (CCA), 2012 IEEE International conferences on*, pages 118-1123.

The following additional papers are not directly included in the thesis, but acts as preliminary and background work.

- Ersdal, A.M., Fabozzi, D., Imsland, L., and Thornhill, N.F. (2014). Model predictive control for power system frequency control taking into account imbalance uncertainty. In *IFAC World Congress*, volume 19, pages 981-986.
- Ersdal, A.M., Cecílio, I.M., Fabozzi, D., Imsland, L., and Thornhill, N.F. (2013). Applying model predictive control to power system frequency control. In *Innovative Smart Grid Technologies Europe (ISGT EUROPE), 2013 4th IEEE/PES*. IEEE.

The following publication was written in the period of the PhD study, but is not included in the thesis.

- Cecílio, I.M., Ersdal, A.M., Fabozzi, D., and Thornhill, N.F. (2013). An open-source educational toolbox for power system frequency control tuning and optimization. In *Innovative Smart Grid Technologies Europe (ISGT EUROPE), 2013 4th IEEE/PES*. IEEE.

Chapter 2

Model predictive load-frequency control

The work in this chapter was published in Ersdal et al. (2016a), which is an extension of the work in Ersdal et al. (2013) and Ersdal et al. (2014).

Summary

A nonlinear model predictive controller (NMPC) for load frequency control (LFC) of an interconnected power system is investigated. The NMPC is based on a simplified system model of the Nordic power system, and it takes into account limitations on tie-line power flow, generation capacity, and generation rate of change. The participation factors for each generator are optimization variables, and suggestions are made as to how one can ensure tie-line power transfer margins through slack-variables, and pricing information through the objective function. The solution of NMPC for LFC is completed by including a Kalman filter for state estimation. The presented NMPC is compared against a conventional LFC/AGC scheme with proportional integral (PI) controllers. Simulations show that the NMPC gives better frequency response while using cheaper resources. This chapter illustrates that NMPC could be a realistic solution to some of the LFC problems power systems are facing today.

2.1 Introduction

During the last two decades, power systems around the world has seen great development and change. First with the liberalizations of the power markets during the 1990's, and in the later years as an increasing amount of renewable energy resources and distributed generation enters the systems. In addition, the energy need around the world is steadily increasing, and all of these factors are causing challenges, especially with regards to load frequency control (LFC).

Traditionally, LFC has had a hierarchical structure with primary, secondary, and tertiary control[1]. The primary and secondary control is automatic, often PI-based, and tuned based on operator practice (Bevrani, 2014), while tertiary control is

[1] Also known as frequency containment reserves (FCR), frequency restoration reserves (FRR) and replacement reserves (RR).

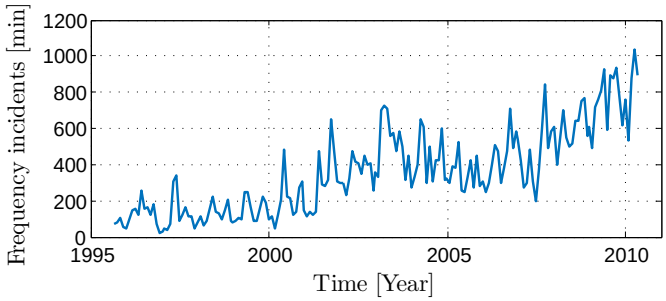

Figure 2.1: Number of frequency incidents, i.e. minutes spent outside 49.9 and 50.1 Hz, in the Nordic system (Whitley and Gjerde, 2011).

manually executed by the transmission system operator (TSO). Secondary control is often referred to as automatic generator control (AGC), and this term will be applied in the following. In the Nordic network, consisting of Norway, Sweden, Finland and the eastern part of Denmark, hydro power is the main provider of primary control, while other generating units such as thermal and nuclear power generators as well as some controllable loads participate in tertiary control (Statnett, 2012). AGC was first implemented in 2012/2013 in the Nordic system and it is still not fully up and running. However, it is likely that hydro power will be the main provider for AGC as well.

In the Nordic system the aim of LFC is set to keep the frequency within 49.9 and 50.1 Hz. However, during the last decades the minutes spent outside this band has been steadily increasing, as seen in Figure 2.1. According to Statnett, the Norwegian TSO, two of the main reasons for this is a heavier loaded network with an increasing amount of bottlenecks, which at times excludes some of the resources from participating in LFC, and also an increasing amount of uncontrollable production, such as intermittent energy resources (Statnett, 2012). The latter is especially important during night and summer, when there is less traditional production which can participate in LFC and balance out any unpredicted power imbalance.

Due to the development seen the last decades, there has been many suggestions to how power systems can be equipped to better cope with these challenges. In Chang-Chien et al. (2011) it is suggested how wind generators can participate in LFC, while others concentrate on effective energy storage (Suvire et al., 2012), or how network loads can be included in LFC (Short et al., 2007). There has also been suggestions to new methods for executing LFC, such as including primary control in local decentralized generators (Marinovici et al., 2013), or improving LFC by applying fuzzy logic (Yousef et al., 2014), sliding mode control (Vrdoljak et al., 2010), internal model control (Saxena and Hote, 2013), and various PID tuning methods (Tan, 2010).

Model predictive control (MPC) is another possibility for LFC which has received attention. In McNamara et al. (2013) MPC is used for controlling power flows in high voltage direct current (HVDC) links to improve LFC, and in Halvgaard et al. (2012) MPC is applied for building climate control to benefit LFC. MPC has also been used for preventing severe line-overloads in power systems. In Otomega et al. (2007); Carneiro and Ferrarini (2010) MPC is proposed as a special protection scheme aimed at preventing thermal overloads on network lines during emergencies. In Otomega et al. (2007) the MPC relies on a direct current (DC) approximation of the actual power flows, whereas Carneiro and Ferrarini (2010) has added a thermodynamical model of the conductors and weather information to determine possible thermal overloads. In Almassalkhi and Hiskens (2015) a hierarchical MPC control scheme is suggested, where the upper-level controller finds the optimal energy schedule and the lower control level serves as a cascade mitigation corrective scheme in case of large disturbances. Also here the MPC relies on a DC approximation of the network power flow.

In this work MPC will be applied for AGC in a larger power system, which is also the topic in Shiroei et al. (2013); Mohamed et al. (2012), but there the MPC is based on a model equal to the one used for simulation. In this work the MPC is based on a simplified equivalent of the full power system, and constraints on the generation capacity and generation rate of change are included, as well as constraints on tie-line power transfer capacities. A solution to how one can guarantee available transfer capacity on the tie-lines is also presented, and a proposal to how economy can be considered in the MPC and AGC decision making is included. Any participation from loads in LFC is omitted in this work, and hydro generators are the sole provider of primary control and AGC.

This chapter is an extension of the work presented in Ersdal et al. (2013, 2014). In Ersdal et al. (2013) a single-area model is considered and there is no model-plant mismatch, and in Ersdal et al. (2014) this is extended to a two-area model with tie-line limitations. In Ersdal et al. (2014) the MPC is also extended to take into account uncertainty in wind power production. This topic is not further addressed here, in part due to considerations related to computational complexity, but such uncertainty-aware intelligence can also, in principle, be included when the hourly set-points to the AGC are calculated (unit commitment), see for example Dvorkin et al. (2015) and the references therein. Such an approach would be compatible with the MPC-based AGC controller presented here. In this work, the implementation of slack variables are relevant in this context, as they enable the MPC to exploit back-off margins to important constraints to handle uncertainties.

The main contribution of this chapter is the presentation of a solution to the LFC problem, where

- The participation factor of each generator is included in the optimization problem.
- State feedback to the MPC is achieved through a state estimator.

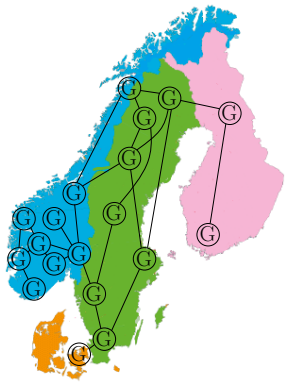

Figure 2.2: An overview of the generators in the SINTEF model (Norheim et al., 2005).

- A simplified power system model is used both in the MPC predictions and state estimation.

The MPC will not function as an emergency protective scheme, but as an everyday LFC controller which corrects production set-points both during normal and more severe operating conditions. In other words, this is a scheme for frequency restoration. The technical solution is analyzed without discussion of the market aspect of it. However, we believe that this could be implemented as an auction-based scheme similar to the present LFC implemented in the Nordic system.

The remainder of the chapter is organized as follows. In Section 2.2 the proxy model used to represent the Nordic power system is presented, followed by a simpler model to be used in the MPC. The details of the controller is given in Section 2.3, before the case study of the Nordic system is presented in Section 2.4 along with some simulation results. Section 2.5 gives a short discussion about the results, before the conclusion in Section 2.6.

2.2 Modelling

The Nordic power system is represented by a proxy model, which is a reduced version of a model developed by SINTEF Energy Research, where the placement of the generators and transmission lines reflects the real production and the most interesting bottlenecks in the Nordic power system (Norheim et al., 2005). The version implemented here consists of 15 hydro generators, 5 non-hydro generators, 21 composite loads, and 36 nodes. The placement of the generators can be seen in Figure 2.2.

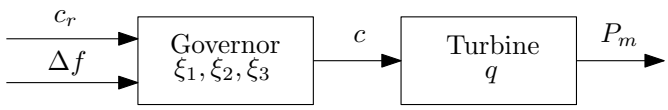

Figure 2.3: Overview of governor and turbine states, inputs and output.

2.2.1 Proxy Model

The proxy model is described by a differential algebraic equation (DAE)

$$\dot{x} = f(x, z, u, w) \tag{2.1a}$$
$$0 = g(x, z, u, w) \tag{2.1b}$$

where x are the dynamic system states, z the algebraic system states, u the controlled inputs to the system, and w the system disturbance.

The Swing Equation

For each generator k, the generator dynamics are given by the swing equation

$$\dot{\delta}^k = \omega_n \Delta\omega^k \tag{2.2a}$$
$$\Delta\dot{\omega}^k = \frac{1}{H^k}\left(P_m^k - P_e^k - D^k\left(\Delta\omega^k - \Delta\omega_s\right)\right) \tag{2.2b}$$

where δ is the rotor angle, $\Delta\omega$ the rotor angular velocity relative a reference frame, $\Delta\omega_s$ the inertial rotor angular velocity relative a reference frame, ω_n the angular velocity of this reference frame, P_m the mechanical power produced by the rotor, $P_e = \mathcal{R}e\left(E_g I_g^\star\right)$ the electrical power acting on the rotor, H the inertia constant and D the damping coefficient. The internal voltage of the generator is $E_g = |E_g|\, e^{j\delta}$, and $I_g^\star$ is the complex conjugate of the current delivered from the generator into the network. In this work, voltage control is assumed to be much faster than the dynamics of interest, and is therefore not considered. Hence the internal generator voltages $|E_g|$ are assumed constant.

The Turbine and Governor Dynamics

Because hydro turbines are the main provider for primary control in the Nordic network, and most likely will be the main provider for AGC as well, only the hydro turbine and governor dynamics are modeled in this work. The remaining generating units will produce a constant amount of power.

A simplified diagram of the hydro turbine and governor dynamics are given in Figure 2.3. They are modeled as the nonlinear model of Machowski et al. (2008), usually denoted HYGOV, and has the states q, ξ_1, ξ_2, and ξ_3. The valve opening is c, and c_r is the valve opening set point provided to the generating unit by the TSO. Given a large power system consisting of m generators, where m_h of these

are hydro turbines, the total system dynamics can be written as (2.1a) with

$$x = \begin{bmatrix} \delta^k & \Delta\omega^k & q^i & \xi_1^i & \xi_2^i & \xi_3^i \end{bmatrix}^T \tag{2.3}$$

$$u = c_r^i \tag{2.4}$$

where $k = 1, \ldots, m$ and $i = 1, \ldots, m_h$. In total $2m + 4m_h$ dynamic states, and m_h controllable inputs.

Network Current Equation

The current flow in the network is found using the internal node representation. Defining all currents as positive into node k, Kirchoff's current law for each node gives

$$I_g^k + I_L^k + \sum_{i=1}^{n} Y_{ki} U_i = 0 \tag{2.5}$$

where I_g^k is the current delivered from generator k, I_L^k the load current from load k, Y_{ki} the systems admittance matrix at position (k, i), U_i the voltage at node i, and n the number of nodes in the network. The current injected from generator k into node k is

$$I_g^k = \frac{E_g^k - U^k}{j{x'_d}^k} \tag{2.6}$$

where ${x'_d}^k$ is the generator transient reactance. The active power load at node k is modeled as a constant current I_l^k and the reactive power load as a constant admittance Y_l^k, such that the total current from load k is

$$I_L^k = -I_l^k - U^k Y_l^k \tag{2.7}$$

This means that the power flow is dependent on the nodal voltage, but not dependent on the system frequency. System loads are in general often both voltage and frequency dependent, however it could be argued that some of the frequency-dependency of the loads are modeled through the damping term of the swing equation (2.2). In addition, the frequency-dependency of the loads in the Nordic power system is relatively low compared to the total power consumption.

Combining (2.5) - (2.7) gives an equation with two unknown: $|U|$ and θ, the magnitude and angle of the nodal voltages, respectively. This makes up the algebraic system equation (2.1b), with a total of $2n$ algebraic states z. The disturbances w acting on the system are the absolute values of the active load currents as well as the produced power from non-hydro generators, resulting in a total of $n + m - m_h$ disturbances.

$$z = \begin{bmatrix} \left|U^k\right| & \theta^k \end{bmatrix}^T \tag{2.8}$$

$$w = \begin{bmatrix} \left|I_l^k\right| & P_m^p \end{bmatrix}^T \tag{2.9}$$

where $k = 1, \ldots, n$ and $p = m_h + 1, \ldots, m$.

2.2.2 Prediction Model

The model presented in the previous section is a large and complex model, and in many cases it can be both sufficient and beneficial to consider a smaller, simplified power system model. One example is the prediction model (PM) used in an MPC. To find this PM, the larger model of the previous section is first divided into N areas connected to each other by tie lines. The states, inputs and disturbances of the PM are defined as $\bar{x}$, $\bar{u}$, and $\bar{w}$. These are all given relative an initial steady state where the power supply and demand in the system are balanced, both with regards to active and reactive power. This initial steady state is also used for linearization points when this is needed.

The dynamics affecting the frequency response of a power system are relatively slow, and neglecting the fast dynamics reduces the complexity of the model (Bevrani, 2014). The nodal voltages and the electromechanical dynamics of the swing equation are considered to be fast dynamics, and can therefore be neglected. The dynamics of area i, including the generators, can in this case be represented by one single differential equation (Bevrani, 2014)

$$\Delta\dot{\bar{f}}^i = \frac{1}{2\bar{H}^i}\left(\Delta\bar{P}_m^i - \Delta\bar{P}_D^i - \Delta\bar{P}_{tie}^i\right) \tag{2.10}$$

where $\Delta\bar{f}$ is the deviation from the nominal frequency f_s, $\Delta\bar{P}_m$ the total change in mechanical power from primary control and AGC combined, $\Delta\bar{P}_D$ the total change in load power, $\Delta\bar{P}_{tie}$ the change in total power flow from the area on all its tie lines, and $\bar{H}$ the inertia of the rotating masses of the area. The change in total tie-line power flow from area i is (Bevrani, 2014)

$$\Delta\dot{\bar{P}}_{tie}^i = 2\pi\left(\Delta\bar{f}^i\sum_{j=1,j\neq i}^{N}\bar{T}_{ij} - \sum_{j=1,j\neq i}^{N}\bar{T}_{ij}\Delta\bar{f}^j\right) \tag{2.11}$$

where $\Delta\bar{f}^{i/j}$ is the local frequency in area i/j, and $\bar{T}_{ij}$ the synchronizing torque coefficient between area i and j. The frequency deviation of the entire system is defined as

$$\Delta\bar{f} = \frac{\sum_{i=0}^{N}\bar{H}^i\Delta\bar{f}^i}{\sum_{i=0}^{N}\bar{H}^i} \tag{2.12}$$

The equations for the hydraulic turbines and governors can be simplified by modeling all the hydraulic power stations of an area as one aggregated hydraulic turbine and governor. The dynamics of the turbine can in turn be represented by a linearized version of the nonlinear model used in the proxy model. This gives the following dynamic equation for the aggregated turbine of area i

$$\Delta\dot{\bar{q}}^i = -\frac{2}{\bar{T}_w^i\bar{c}_{ss}^2/\bar{q}_{ss}}\left(\Delta\bar{q}^i - \frac{\bar{q}_{ss}^{i2}}{\bar{c}_{ss}^{i2}}\Delta\bar{c}^i\right) \tag{2.13a}$$

$$\Delta\bar{P}_m^i = \bar{A}_t^i\bar{h}_{ss}^i\left(3\Delta\bar{q}^i - 2\frac{\bar{q}_{ss}^{i2}}{\bar{c}_{ss}^{i2}}\Delta\bar{c}^i\right) \tag{2.13b}$$

where $\bar{T}_w$ is the water starting time, and $\Delta\bar{c}$ and $\Delta\bar{q}$ the change in valve opening and water flow rate from $\bar{c}_{ss}$ and $\bar{q}_{ss}$, respectively. When modeling the aggregated governor, one of the time constants can be neglected, as it is several times smaller than the others. The resulting governor dynamic equations for area i are

$$\Delta\dot{\bar{\xi}}_2^i = -\frac{1}{\bar{T}_r^i}\Delta\bar{\xi}_2^i + \Delta\bar{c}^i \tag{2.14a}$$

$$\Delta\dot{\bar{\xi}}_3^i = \mathrm{sat}_{\dot{c}}^i\left(\frac{1}{\bar{T}_g^i}\left(\Delta\bar{c}_r^i - \Delta\bar{f}^i + \frac{\bar{r}^i}{\bar{T}_r^i}\Delta\bar{\xi}_2^i - \left(\bar{r}^i + \bar{\rho}^i\right)\Delta\bar{c}^i\right)\right) \tag{2.14b}$$

$$\Delta\bar{c}^i = \mathrm{sat}_c^i\left(\Delta\bar{\xi}_3^i\right) \tag{2.14c}$$

where $\bar{r}$ and $\bar{\rho}$ are the transient and static droop coefficients, $\bar{T}_r$ and $\bar{T}_g$ time constants, and $\mathrm{sat}_{\dot{c}/c}(\cdot)$ saturations.

Depending on the number of areas N, the simplified system is represented by one differential equation

$$\dot{\bar{x}} = \bar{f}\left(\bar{x}, \bar{u}, \bar{w}\right) \tag{2.15}$$

which consists of $5N$ dynamic state variables $\bar{x} = \begin{bmatrix}\bar{x}^1 & \cdots & \bar{x}^N\end{bmatrix}^T$, N controlled inputs $\bar{u} = \begin{bmatrix}\bar{u}^1 & \cdots & \bar{u}^N\end{bmatrix}^T$, and N disturbances $\bar{w} = \begin{bmatrix}\bar{w}^1 & \cdots & \bar{w}^N\end{bmatrix}^T$, where $\bar{x}^i = \begin{bmatrix}\Delta\bar{f}^i & \Delta\bar{q}^i & \Delta\bar{\xi}_2^i & \Delta\bar{\xi}_3^i & \Delta\bar{P}_{tie}^i\end{bmatrix}^T$, $\bar{u}^i = \Delta\bar{c}_r^i$, and $\bar{w}^i = \Delta\bar{P}_D^i$. The bar notation represents the simplified system states, inputs and parameters.

2.3 Controller

2.3.1 Control problem

The main task for the LFC is to maintain frequency stability, which means keeping the system frequency at a desired level when changes in generation or load appear. This is done by adjusting the produced power P_m so that it always matches the system load. Maintaining this frequency stability also includes avoiding bottleneck congestions, and staying within other system bounds.

In addition to this main control task, another incentive is to keep the costs associated with LFC at a minimum. Lowering the use of all resources are important, however, the cost of primary control is often higher than AGC, and lowering the use of primary control by keeping the frequency closer to f_n through use of AGC is desirable. When using AGC, the TSO has to pay more per delivered MWh the more they require the AGC-participating generators to deviate from the initial hourly set point. This means that keeping the input $\bar{u}$ in the prediction model as close to its hourly set-point value $\bar{u}_0$ as possible will minimize the costs of AGC.

2.3.2 MPC

MPC is a framework for advanced control that has seen widespread use, especially within chemical process industries, and it is believed that the optimizing and

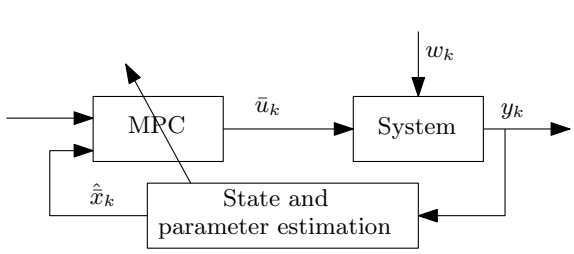

Figure 2.4: Overview of MPC-loop.

constraint-handling nature of MPC makes it suitable also for frequency control. MPC uses a model of the system to predict how it will behave in the future, and then optimizes the controlled input with regards to an objective function measuring predicted performance. Mathematically, it can be formulated as a continuous time optimal control problem on the form (2.16a) subject to (2.16b) - (2.16d) (Biegler, 2010)

$$\min_{\bar{x}(\cdot),\bar{u}(\cdot)} J\left(\bar{x}(t),\bar{u}(t)\right) \tag{2.16a}$$

$$\bar{x}(0) - \bar{x}_0 = 0 \text{ Fixed initial state} \tag{2.16b}$$

$$\dot{\bar{x}}(t) - f\left(\bar{x}(t),\bar{u}(t),\hat{\bar{w}}(t)\right) = 0 \text{ System model} \tag{2.16c}$$

$$g\left(\bar{x}(t),\bar{u}(t)\right) \leq 0 \text{ Constraints} \tag{2.16d}$$

where $\bar{x}(t)$ are the system states, $\bar{u}(t)$ the controlled inputs, $\hat{\bar{w}}(t)$ the predicted disturbances, and $J\left(\bar{x}(t),\bar{u}(t)\right)$ the control objective function.

Figure 2.4 shows the basics of how an MPC works. The idea is to solve an optimization problem at each time step to find the optimal system input $\bar{u}(t)$ over a fixed time horizon with respect to the objective function $J(\cdot)$, and then apply the first element of $\bar{u}(t)$ as input to the system. The loop is closed by the measurements $y(t)$, and a state estimator is also included as the MPC needs knowledge of the entire state vector $\bar{x}(t)$.

2.3.3 MPC Design for AGC

An MPC will be applied for AGC in this work. The MPC will be based on the prediction model (PM) of Section 2.2.2, and it will control the Nordic power system represented by the proxy model, from now on referred to as the plant replacement model (PRM), of Section 2.2.1. This means that there is a natural model-plant mismatch between the PRM and the PM, which always is the case when applying MPC in real world situations. The control of, and contribution from tertiary control is omitted in this work, as it is manually operated. The dynamic equation of the PM (2.15) is implemented as the system model (2.16c), and the constraints (2.16d) includes limitations on generation capacity and generation rate of change. In some

of the examples of Section 2.4 limitations on the tie-line power transfer are also included.

The saturations in (2.14) are nonlinear, implying that we have nonlinear equality constraints (2.16c), and nonlinear MPC (NMPC) must be used. For the same reason, the optimization problem in (2.16) is non-convex. The continuous time optimization problem (2.16) in the NMPC is solved with direct methods, that is, it is discretized and transformed into a nonlinear program (NLP) using collocation. The NLP is then solved using the interior point optimizer IPOPT (Wächter and Biegler, 2006) with exact Hessian, all implemented in Casadi (Andersson, 2013).

The saturations will not only introduce nonlinearity to the PM, they are also non-smooth functions which can cause numerical problems when solving the NLP using IPOPT. The problem is that the second-order derivative of the Lagrange function (known as the Hessian) is not necessarily Lipschitz continuous[2], which can prevent the convergence of IPOPT. This problem can be dealt with by introducing smooth approximations of the saturation functions. Given the saturation of a variable σ, which is limited by the upper and lower limits σ_{max} and σ_{min}:

$$\text{sat}(\sigma) = \min(\sigma_{max}, \max(\sigma_{min}, \sigma)). \tag{2.17}$$

In this thesis, the following approximation of Equation (2.17) is applied to approximate the saturations in (2.14), where $\kappa > 0$ is an approximation factor.

$$\text{sat}(\sigma) \approx \min\left(\sigma_{max}, \hat{\sigma}\right) \approx \frac{1}{2}\left(\sigma_{max} + \hat{\sigma} - \sqrt{\left(\sigma_{min} - \hat{\sigma}\right)^2 + \kappa^2}\right) \tag{2.18a}$$

where

$$\hat{\sigma} = \frac{1}{2}\left(\sigma_{min} + \sigma + \sqrt{\left(\sigma_{min} - \sigma\right)^2 + \kappa^2}\right) \approx \max(\sigma_{min}, \sigma) \tag{2.18b}$$

This leads to a smooth saturation function which will have a second-order derivative that is Lipschitz continuous.

The MPC implemented here is a centralized MPC (CMPC), i.e. it is based on a model of the full system and it controls all the controllable inputs to the system. An alternative approach would be a distributed MPC (DMPC) where separate MPCs, based on single-area models, would be responsible for controlling each area. A natural choice of areas could then be by country or by control area. There are several examples where DMPC has been applied for LFC, such as Venkat et al. (2008); Mohamed et al. (2011), and the main benefits of distributed control are smaller optimization problems for each MPC, hence shorter optimization time, and less demands for communication. This is very beneficial when considering large power systems, such as in continental Europe or North America. The main drawback of DMPC is that it may result in poor systemwide control performance

[2]A function is said to be Lipschitz continuous if it is limited how fast the function can change. See e.g. Khalil (2002) for details.

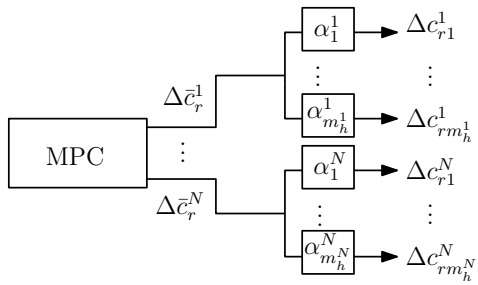

Figure 2.5: Illustration of generator participation factors, where m_h^i is the number of hydro generators in area i.

if the subsystems interact significantly (Venkat et al., 2008), which is the case in most power systems. When considering the Nordic power system it is important to keep in mind that it is quite small compared to the Central European system or the Eastern Interconnection in North America, and it is mainly Norway and Sweden which supply primary control and AGC through hydro power. This means that in this case there is not that much to gain by distributing the control when it comes to optimization time, especially when considering that the CMPC presented here is based on a simplified model with a rather small amount of optimization variables. In addition to this, using a DMPC would complicate the tie-line constraint handling, which is an important feature of the presented controller.

Including Participation Factors in the NMPC

In the PM, there is one input for each area of the system. This leads to N optimal inputs from the NMPC: $\Delta\bar{c}_r^i$, where $i = 1, \ldots, N$. These N inputs will then be distributed to the hydro generators of each area by individual participation factors α_j^i. As described in Figure 2.5

$$c_{rj}^i = c_{r0j}^i + \alpha_j^i \Delta\bar{c}_r^i \tag{2.19}$$

where $j = 1, \ldots, m_h^i$ and m_h^i is the number of hydro generators in area i. Bear in mind that $\sum_{i=0}^{N} m_h^i = m_h$.

However, each of the inputs c_r have individual constraints, and in order to be able to account for each of them in the NMPC, the participation factors α are included as optimization variables in the NMPC. In this way, individual constrains on generation and generation rate of change for each hydro generator can be included in, and accounted for by the NMPC. It also allows for greater flexibility and better use of the NMPC's strengths on coordination of multiple inputs. This is however at the expense of a larger optimization problem. With this modification, the PM now has $5N$ dynamic states, m_h optimization variables (controllable inputs), and N disturbances.

Including Economics in the NMPC

One of the obvious opportunities of an NMPC is to include the pricing of AGC in the objective function. Economic MPC refers to an MPC where the objective function is an economic profit function, often linearly dependent on state and input (Rawlings and Amrit, 2009), as opposed to the more widespread quadratic objective function:

$$J\left(\bar{x},\bar{u}\right)=\int_{t=0}^{T}\bar{x}^{T}Q\bar{x}+\bar{u}^{T}R\bar{u}\ dt \tag{2.20}$$

Some previous work has focused on the use of economic MPC for LFC, such as Hovgaard et al. (2010). In this work however, (2.20) is used, and pricing is included in a quadratic manner through the matrix R by multiplying the price of activating AGC in each generator, $P=\begin{bmatrix}p_1 & \cdots & p_{m_h}\end{bmatrix}^T$, with the diagonal terms of R. This will not give a direct link between money spent and objective function, as in an economic MPC, but it will provide good knowledge to the NMPC about which generators that are more economic to use.

Using Slack Variables to Avoid Bottlenecks

Giving the NMPC constraints on the tie-line power transfer will result in a fulfillment of the transfer limit, but the NMPC won't care if it reaches the limit and stays there. During normal operating conditions it can however be beneficial to keep a certain amount of power transfer available, if a more severe situation were to happen. This is something that might be solved by using slack variables in the NMPC. Slack variables are often used to avoid infeasible solutions in an NMPC by "softening" some of the state constraints (Maciejowski, 2002). The slack variable ϵ, which must be positive, is added to the constraint which is to be softened, and it is also added to the optimization variables.

$$g\left(\bar{x}(t),\bar{u}(t)\right)\leq\epsilon \tag{2.21a}$$

$$\epsilon\geq 0 \tag{2.21b}$$

In order not to use the slack variable unless absolutely necessary, use of ϵ is penalized in the objective function

$$\min_{\bar{x},\bar{u},\epsilon}J\left(\bar{x},\bar{u},\epsilon\right)=\min_{\bar{x},\bar{u},\epsilon}\int_{t=0}^{T}\bar{x}^{T}Q\bar{x}+\bar{u}^{T}R\bar{u}+\gamma\epsilon\ dt \tag{2.22}$$

In this way, the constraints $g\left(\bar{x}(t),\bar{u}(t)\right)$ are allowed to exceed zero in severe situations. In (2.22), ϵ is linearly included in the objective function, and we have what is called exact penalty, which means that as long as γ is large enough, the constraint will not be violated unless there is no feasible solution to the original problem (Maciejowski, 2002).

Such slack variables can also be used to achieve two levels of severity on the tie-line limitations. One for normal operation, and one for severe cases. The original constraints $\Delta\bar{P}_{tie,max}$ on the tie-line power transfer is set so that there still is

available transmission capacity for emergencies. These are then implemented as soft constraints through the use of slack variables ϵ. The choice of γ compared to Q and R in the objective function will then determine when the NMPC finds it best to use the emergency transfer capacity. In order to achieve an absolute maximum limit on $\Delta\bar{P}_{tie}$, ϵ can be limited accordingly

$$\epsilon \leq \Delta\bar{P}_{tie,MAX} - \Delta\bar{P}_{tie,max} \tag{2.23}$$

where $\Delta\bar{P}_{tie,MAX}$ is the absolute maximum limit.

2.3.4 State and Parameter Estimator

The NMPC needs knowledge of the entire PM state vector $\bar{x}$. In this work, we have assumed the PRM measurements to be $y = \begin{bmatrix}\Delta\omega^k & \xi_2^i & \xi_3^i & |U|^s & \theta^s\end{bmatrix}$, where $k = 1, \ldots, m$, $i = 1, \ldots, m_h$, and $s = 1, \ldots, n$. From this, an extended Kalman filter (EKF) (Simon, 2006) based on the PM is used to estimate the PM state vector $\bar{x}$ and disturbance $\bar{w} = \Delta\bar{P}_D$. An EKF is chosen because Casadi automatically generates the system's derivatives using automatic differentiation (Andersson, 2013), making the EKF a simple and effective choice.

2.4 Case Study

Based on the information given in the first paragraph of Section 2.2, the PRM (2.1) has a total of 100 dynamic states, 72 algebraic states, 15 controllable inputs, and 21 disturbances. This system is then divided into two areas in the PM (2.15), hence $N = 2$. Area A covers South Sweden and Eastern Denmark, and Area B covers Norway, North Sweden and Finland. Between the two areas there is a tie line which represents the total power flow between the areas. In total the PM has 10 dynamic states, 15 controllable inputs, and 2 disturbances, which is a considerable reduction from the PRM. In both the PRM and the PM the AGC control signal is dispatched every 10 s.

2.4.1 Tuning the NMPC

The main tuning variables of the NMPC are the prediction horizon T, and the objective function $J(\cdot)$. The objective function is set to

$$J\left(\bar{x}, \bar{u}, \epsilon\right) = \int_{t=0}^{T} \bar{x}^T Q \bar{x} + \left(\bar{u} - \bar{u}_0\right)^T R \left(\bar{u} - \bar{u}_0\right) + \gamma\epsilon \, dt \tag{2.24}$$

The matrices Q and R are tuning matrices, where Q is real, symmetric and positive semidefinite, and R is real, symmetric and positive definite, while γ is a tuning vector containing elements greater than or equal to zero. The non-zero elements of Q are chosen as $q_{11} = \beta\frac{\left(H^1\right)^2}{(H^1+H^2)^2}$, $q_{66} = \beta\frac{\left(H^2\right)^2}{(H^1+H^2)^2}$, $q_{16} = q_{61} = \beta\frac{H^1H^2}{(H^1+H^2)}$, where

$\beta = 10^5$. This choice of Q originates from punishing deviation in overall system frequency (2.12). The matrix R is given as $R = \text{diag}\,(m_{\text{base}} \cdot P)$, where m_{base} is a vector containing the hydro generators' base rating and P is a vector containing the price of activating AGC. By including m_{base} in R the actual produced power from each power plant is included in the objective function, and not only the per unit-based $\bar{u}$, and there is also the possibility of including pricing information through P. The use of primary control is driven by Δf, so lowering the frequency deviation will also lower the use of primary reserves.

As mentioned in Section 2.3.3, the choice of γ compared to Q and R decides when the NMPC will find it beneficial to break the constraints. In this work, slack variables are included for the tie-line between Area A and B, which means that γ is a vector of dimension 2. The tuning of γ differs in the examples given in Section 2.4.3, depending on whether we want to achieve exact penalty or a two-level tie-line limit. The exact value of γ will therefore be stated for each case.

In order to match the control signal dispatching in the system, the NMPC was set to have a time step of 10 s, and the optimization horizon T was chosen to be 3 minutes, a decision based on a compromise between system time constants and complexity.

2.4.2 PI Controller

The presented NMPC will be tested against conventional PI controllers, where one is situated in each of the two areas. These two are given by

$$\bar{u}^A = K_p^A \Delta \bar{f}^A + K_i^A \int \Delta \bar{f}^A dt \tag{2.25}$$

$$\bar{u}^B = K_p^B \Delta \bar{f}^B + K_i^B \int \Delta \bar{f}^B dt \tag{2.26}$$

where K_p is the proportional constant and K_i the integral constant. The control signals from the PI controllers, $\bar{u}^A$ and $\bar{u}^B$, are distributed to the hydro generators through the participation factors α, which are constant. The PI controllers are tuned based on the SIMC method presented in Skogestad (2003). In order to compare the two controllers, a control performance measure (CPM) is applied. It basically measures the average frequency deviation, and it is calculated in the following manner: First, Δf is averaged over windows of 30 s to filter out fast fluctuations. Then, the CPM is found by again averaging Δf over all these windows. This CPM is inspired by the CPS1 and CPS2 performance criteria used by the North American electric reliability corporation (NERC) (Gross and Lee, 2001).

2.4.3 Simulation Results

In Case A-C, the AGC pricing P is equal for all generators, and $\gamma_1 = \gamma_2 = 10^5$ so that exact penalty for the slack variables are achieved. Hence there is no two-level limit for the tie-line in these cases.

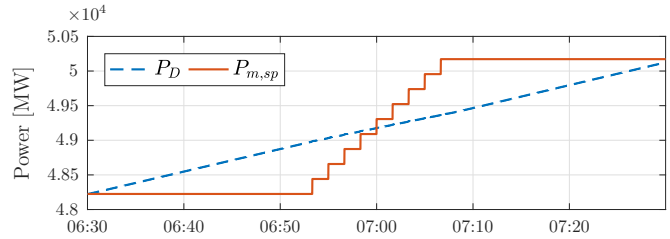

(a) Total P_D and the set point to P_m.

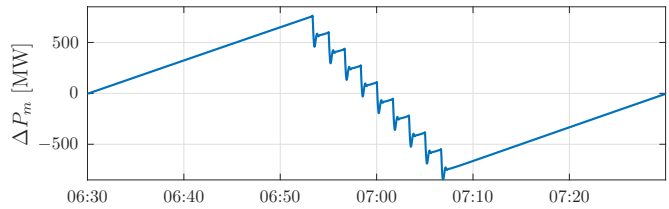

(b) Total $\Delta P_m = P_m - P_{m,sp}$.

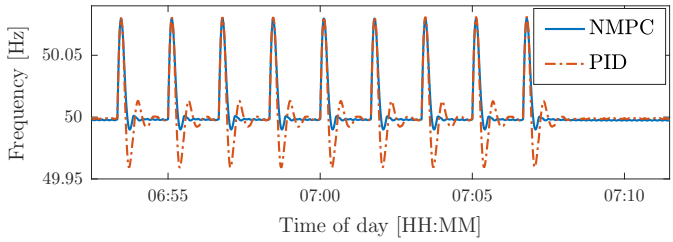

(c) Frequency response at set point changes.

Figure 2.6: Case A: Frequency response during hourly set-point changes. The change is spread over 15 minutes, and 9 smaller intervals.

Case A

The change in production set point $P_{m,sp}$ takes place on the hour in the Nordic power system, while the changes in power demand happens during the hour (Statnett, 2012). This leads to large frequency deviations at these hourly set-point changes. In Case A, such a situation is recreated, and Figure 2.6(a) shows how P_D changes continuously over the hour from 06 : 30 to 07 : 30, while $P_{m,sp}$ changes in smaller steps over 15 minutes at 07 : 00. Figure 2.6(c) and 2.6(b) shows the resulting frequency response and the deviation in P_m from $P_{m,sp}$, and Table 2.1 displays the CPM and reserve usage. From Figure 2.6(c) it is seen that the NMPC manages to keep the frequency closer to 50 Hz than the PI controller, and this is also supported by the CPM in Table 2.1. The reason the NMPC performs better than the PI controller is that the NMPC is able to take the actions of the primary controller (governor) into account when planing the optimal input. This results in a better

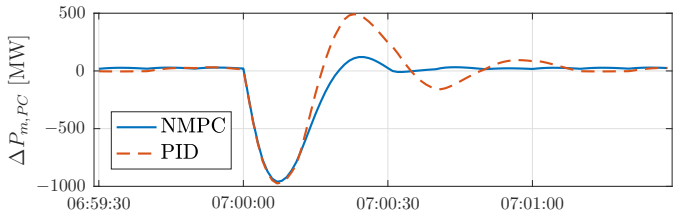

(a) Primary control

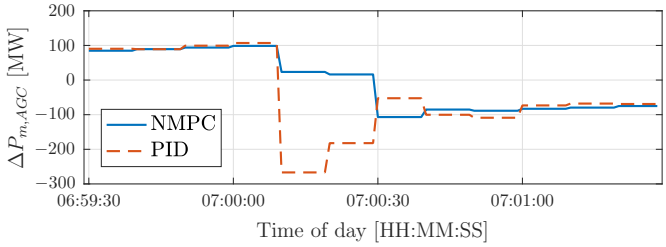

(b) AGC set-point

Figure 2.7: Case A: Use of primary control and AGC at one of the smaller set-point changes.

cooperation between primary control and AGC, as seen in Figure 2.7. The NMPC is much less aggressive, which results in a lower frequency overshoot. From Table 2.1 it is seen that the PI controller uses less AGC than the NMPC. This is because the NMPC in this case has to use more AGC than the PI controller to lower both the CPM and the use of the more expensive primary control reserves.

Case B

In Case B, the disturbance pictured in Figure 2.8(a) is imposed on the system, and in addition it is assumed that there is an upper limit of 300 MW on the tie-line power transfer from Area A to Area B. This limit is included as a constraint in the NMPC. In a PI solution, such limits would be fulfilled by the TSO through pricing, but this is not included here since such a solution is not automatic and hence not part of the automatic AGC control. Note that the Nordic system has a common market, hence there is no control of the tie-line power transfers. The only issue of interest is that they keep within their limitations. In this example, the disturbance is generated using the same method as in Cecílio et al. (2013), hence it is more realistic and fluctuating than in Case A.

In Table 2.1 it is seen that the NMPC performs better than the PI controller according to the CPM, and as seen in Figure 2.8(b) the PI controller eventually violates the tie-line limit whereas the NMPC does not. This illustrates how the NMPC is able to take into account tie-line limitations in the network in an automatic manner, which is not easily done with a PI controller. Figure 2.9(a) shows

Table 2.1: CPM and reserves usage (given in MWh).

		CPM	Primary Control	AGC
Case A	PI	$1.28 \cdot 10^{-4}$	58	**359**
	NMPC	$\mathbf{1.15 \cdot 10^{-4}}$	**55**	371
	Difference	-10%	-5%	$+3\%$
Case B	PI	$2.1 \cdot 10^{-4}$	541	173
	NMPC	$\mathbf{1.9 \cdot 10^{-4}}$	**529**	**159**
	Difference	-10%	-2%	-8%
Case C	PI	$6.7 \cdot 10^{-8}$	492	182
	NMPC	$\mathbf{6.3 \cdot 10^{-8}}$	**489**	**169**
	Difference	-6%	-0.6%	-7%

how the NMPC initially lets Area B cover most of the power imbalance (since Area B has more available resources than Area A), and then switches to use more of the resources in Area A and less in Area B once the tie-line limit is reached. In this way, the NMPC is able to fulfill the tie-line limit. From Figure 2.8(b) it is seen that with the PI controller it takes longer time for the tie-line power transfer to reach its limit. This is because the PI controller divides the responsibility of covering the power imbalance equally between Area A and Area B, as seen in Figure 2.9(b). Eventually, Area A needs so much help from Area B, that the tie-line limit is violated. From Table 2.1, it is seen that the NMPC actually uses less of both primary control and AGC to achieve better results, with a decrease of respectively 2% and 8%. The use of primary control is much higher in this example due to the fluctuating nature of the disturbance.

In this specific case, the fact that the PI controller divides the load equally between Area A and Area B has the positive effect that it takes longer before the tie-line limit is violated. However, there are disadvantages connected to such a rigid allocation. In this specific case there are less available resources in Area A, and the equal load sharing between Area A and B leads to a higher percentage of the available resource being allocated in Area A than Area B. This is not always optimal, and as seen from the example the PI controller uses more resources, and hence money. In general, a rigid allocation also leads to the controller being less able to adapt to individual cases, since each case is treated equal.

Case C

The NMPC should also improve frequency stability during normal operating conditions, and in order to compare the performance of the NMPC against the PI-controller, a Monte Carlo simulation is performed, where disturbances based on

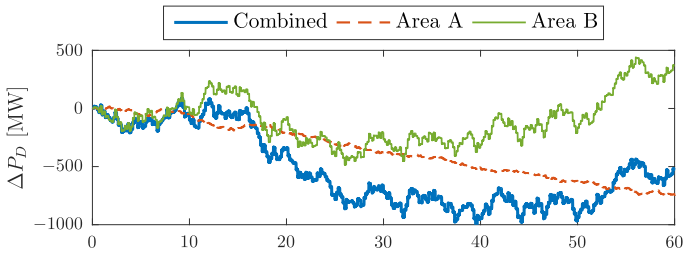

(a) ΔP_D for Area A, Area B and the two combined.

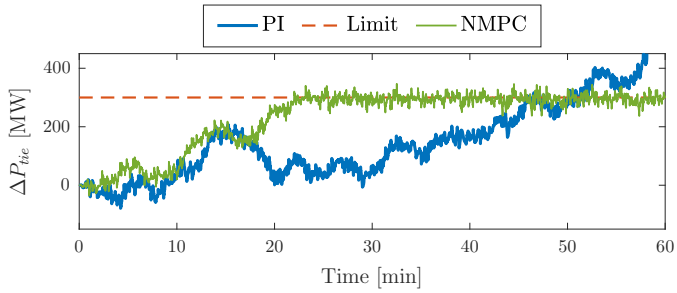

(b) Tie-line power flow from Area A to Area B.

Figure 2.8: Case B: ΔP_D and tie-line power flow.

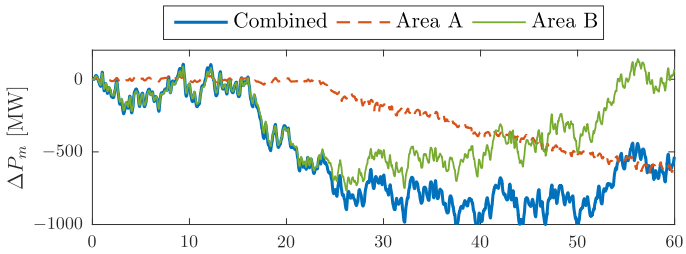

(a) NMPC

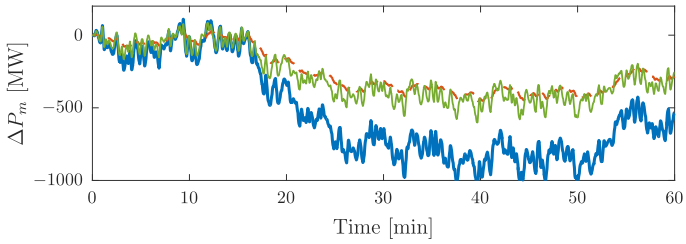

(b) PI

Figure 2.9: Case B: ΔP_m for Area A, Area B and the two combined.

random numbers are imposed on the system loads. These disturbances are smaller in size compared to the previous examples, so that they resemble normal load variations. The average numerical results from 200 simulations can be seen in Table 2.1. It shows that the NMPC uses less resources than the PI controller, especially AGC which has a decrease of 7%. This demonstrates that there is potential for reducing the expenses associated with both primary control and AGC during normal operating conditions. Table 2.1 also shows that the NMPC performs better than the PI controller, according to the CPM. The PI controller does however perform close to the NMPC, which supports that it is tuned reasonably.

Case D

In Case D the potential of including pricing information in the NMPC is illustrated. The slack variables still have exact penalty, while P is changed so that there is a difference in the AGC pricing of the generators. This is illustrated through a situation where a generator in South Sweden suddenly is disconnected. It is first simulated without there being any economic difference between the generators, then information is added to the NMPC that using AGC from the generator at node 5500 is more expensive than the other generators. In Figure 2.10 the total use of Δu and the use of Δu in generator 5500 is depicted, and it shows that the NMPC lowers the use of AGC from generator 5500 (Figure 2.10(b)). Figure 2.10(a) shows that the total amount of activated resources stays approximately the same, hence most of the shortage from generator 5500 is covered by the less expensive generators. This is of course a simplified example, however it shows how the NMPC can include pricing information in an automatic manner when executing AGC. This is something which would be difficult to achieve with a PI controller without interference from the TSO.

Case E

In Case E, P is again equal for all generators, but now $\gamma_1 = \gamma_2 = 10^3$ and a two-level limit on the tie-line power transfer is included. To illustrate the idea, a large generator in South Sweden is suddenly disconnected. The soft transfer limit from Area B to Area A is set to 400 MW and the hard transfer limit to 800 MW. As seen from Figure 2.11, the NMPC allows the $\Delta\bar{P}_{tie,max}$-limit to be violated for a couple of time steps. This is because it in total gives a better system behavior, both with regards to frequency response and use of AGC. However, the NMPC will bring $\Delta\bar{P}_{tie}$ back to the soft transfer limit after the situation has calmed, and the clearance up to the hard transfer limit is restored.

2.5 Discussion

The simulations presented in Section 2.4.3 show that the presented NMPC works in a satisfying manner. The PM in the NMPC is a smaller and simplified version of the

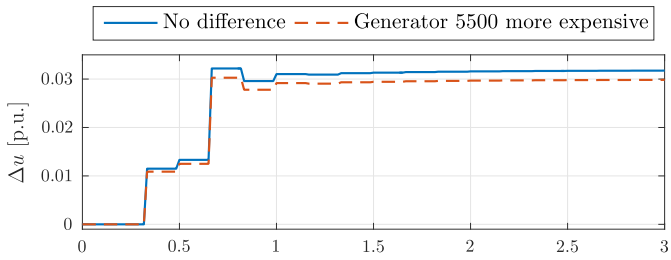

(a) Total Δu for all generators combined.

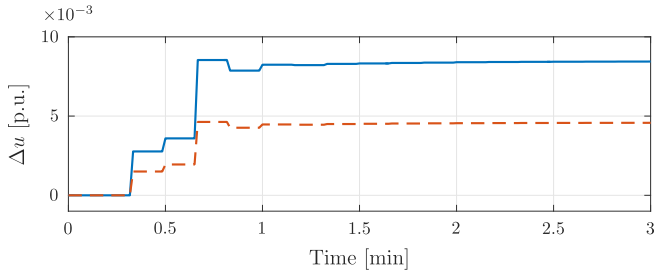

(b) Δu for the generator at node 5500.

Figure 2.10: Case D: How the input from the NMPC changes when one generator is more expensive.

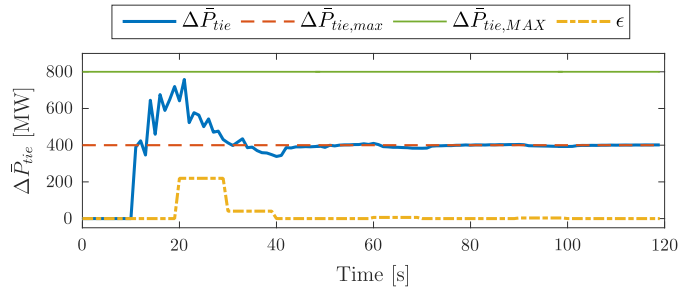

Figure 2.11: Case E: Use of slack variable ϵ to achieve two sets of tie line limits. The figure shows tie line power flow from Area B to Area A.

PRM used for simulation. This causes a model-plant mismatch, which the NMPC is robust against. An EKF is used to estimate the PM states and disturbance, hence it adapts the PM to the PRM and through this it helps the NMPC deal with the model-plant mismatch. There is not given a measurement or direct information to the NMPC about the PM system disturbance $\Delta\bar{P}_D$, it is only estimated using the EKF, which is applied as the future $\Delta\bar{P}_D$ when predicting the system behavior.

The simulations still show that the NMPC is able to both perform better than the PI controller, and to do so using less resources. In addition the NMPC is able to take into account system limitations such as limitations on generator capacity, generator rate of change, and tie-line power transfer.

One of the reasons that the NMPC is performing well is that it is able to take into account the actions of the governor, and coordinate the inputs with regards to this. In addition it can coordinate the inputs with respect to each other in a more flexible manner than the PI controller. It is also able to use the information from the disturbance estimate to plan ahead.

With the computer and software used here, the NMPC based on a two-area PM keeps well within the range of the real time requirements, with an average optimization time of less than 10 s. As an example the maximum and average optimization time for Case B in Section 2.4.3 is 0.73 s and 0.66 s, respectively. It is therefore believed that it will stay within these requirements if the PM is augmented to more than two areas.

2.6 Conclusion

An NMPC based on a simplified system model is used for AGC in the Nordic power system, represented by a larger, more complex proxy model. Both descriptive examples and extensive simulation has shown that applying NMPC to AGC can lead to both better control performance as well as a reduction in use of reserves, which again will reduce the costs associated with LFC. Ideas to how NMPC can be applied to include economics in the AGC as well as methods for ensuring tie line capacity, are also presented.

The work presented here shows some of the benefits an NMPC can provide with regards to LFC, such as flexibility and coordination between multiple inputs, taking into account system limitations, and exploiting knowledge about the disturbance acting on the system. All of these are qualities which could help in bringing about a more flexible AGC which is able to deal with the challenges that power systems are facing. It is also the authors' opinion that since the prediction model in the NMPC is a significant reduction of the plant replacement model, it is reasonable to believe that an NMPC-based solution for AGC could work in a real situation.

Chapter 3

Model predictive load-frequency control taking into account imbalance uncertainty

The work in this chapter was published in Ersdal et al. (2016b), which is an extension of the work in Ersdal et al. (2014).

Summary

Nonlinear model predictive control (NMPC) is investigated for load frequency control (LFC) of an interconnected power system which is exposed to increasing wind power penetration. The robustified NMPC (RNMPC) proposed here uses knowledge of the estimated worst-case deviation in wind-power production to make the NMPC more robust. The NMPC is based on a simplified system model that is updated using state- and parameter estimation by Kalman filters, and takes into account limitations on among others tie-line power flow. Tests on a proxy of the Nordic power system, shows that the RNMPC is able to fulfill system constraints under worst-case deviations in wind-power production in cases where the nominal NMPC is not.

3.1 Introduction

Power systems around the world have been through great development during the last two decades. First with the liberalization of the power markets in the 1990's, and second with the increasing amount of renewable energy resources, distributed generation, and increasing energy need seen around the world. These are all elements which cause challenges for the operation of power systems, and especially with regards to load frequency control (LFC).

LFC is a term applied to describe the continuous operation of keeping the frequency of a power system stable. The frequency of a power system is connected to the balancing of produced and consumed power in the way that if there is a surplus of produced power the frequency will rise, and if there is a lack of produced power the frequency will fall. It is very important that this power balance is maintained, if not the generators could lose synchronism, and the power system would collapse. Traditionally, LFC has a hierarchical structure with primary, secondary,

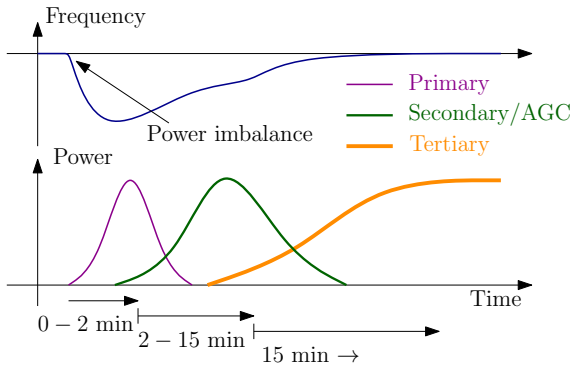

Figure 3.1: Activation of primary, secondary (AGC) and tertiary control after a power imbalance.

and tertiary control[1], see Figure 3.1. Primary control is continuous, automatic control placed locally at the generators. It is often based on proportional control, and it instantaneously covers the power imbalance between produced and consumed power. It does not, however, ensure that the frequency is restored to its set point. For this, secondary control is needed. Secondary control is a slower, centralized, and automatic controller which releases primary control. It is often referred to as automatic generator control (AGC), and this term will be applied in the following. Tertiary control is an even slower, centralized controller, which again releases the AGC. This is manually operated by the transmission system operator (TSO). In the Nordic network, consisting of Norway, Sweden, Finland, and the eastern parts of Denmark, hydro generators are the main provider for primary control, while other generating units such as thermal and nuclear power generators as well as some controllable loads participate in tertiary control (Statnett, 2012). AGC was first implemented here in 2012/2013, and it is assumed that hydro generators will be the main provider for this as well.

In the Nordic Network, the TSOs aim at keeping the frequency between 49.9 and 50.1 Hz. This has proven to be increasingly difficult, and as seen from Figure 3.2, the number of frequency incidents (minutes spent outside 49.9 and 50.1 Hz) has increased concurrently with installed wind power capacity over the last decade. It is confirmed by Statnett, the Norwegian TSO, that the increasing amount of intermittent energy resources is part of the reason for the decreasing control performance, along with a heavier loaded network and an increasing amount of bottlenecks, which at times excludes some of the resources from participating in LFC (Statnett, 2012).

There have been many suggestions to how LFC can be improved to better cope with these challenges. In Short et al. (2007) and Fabozzi et al. (2013) loads are included in LFC, while Suvire et al. (2012) concentrate on effective energy storage, and Chang-Chien et al. (2011) suggests how wind generators can participate in LFC.

[1]Also known as frequency containment reserves (FCR), frequency restoration reserves (FRR), and replacement reserves (RR).

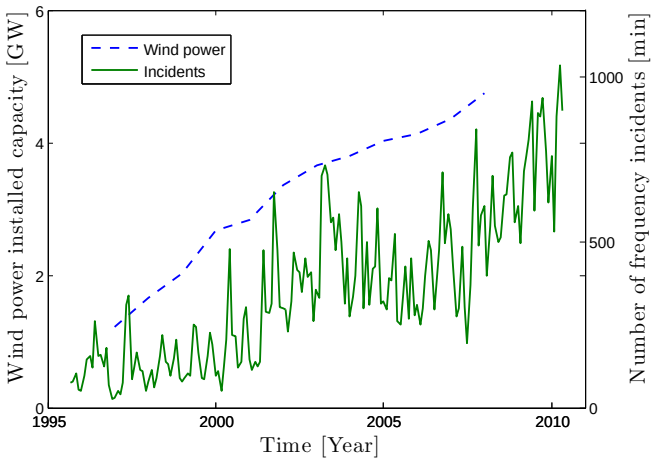

Figure 3.2: Number of frequency incidents per month (Whitley and Gjerde, 2011) and installed wind power capacity (Nordel, 2008) in the Nordic system.

Others concentrate on new control methods for LFC, such as including primary control in local decentralized generators (Marinovici et al., 2013), or improving LFC through fuzzy logic (Yousef et al., 2014), sliding mode control (Vrdoljak et al., 2010), internal model control (Saxena and Hote, 2013), and various PID tuning methods (Tan, 2010). Many have also investigated model predictive control (MPC) as a way of improving LFC, e.g. through building climate control (Halvgaard et al., 2012), or control of power flows in high voltage direct current (HVDC) lines (McNamara et al., 2013). In Otomega et al. (2007); Carneiro and Ferrarini (2010) MPC is used as a special protection scheme to prevent severe line-overloads.

Some have also investigated MPC for AGC, for example Venkat et al. (2008); Shiroei et al. (2013); Mohamed et al. (2012). However, none of these consider model-plant mismatch. Others discuss robust MPC (Shiroei et al., 2013), but this is mainly against system parameter uncertainties, and the fulfillment of system constraints is not considered. Other control methods have also been suggested for robust LFC, such as H_∞ control (Singh et al., 2013; Bevrani et al., 2011), fuzzy logic (Çam and Kocaarslan, 2005), and robust PD tuning methods (Khodabakhshian and Edrisi, 2008).

Rather generally, robust MPC is formulated in a min-max framework, where the optimization seek to find minimizing inputs for the disturbances that maximize the objective function. See for example Rawlings and Mayne (2009), Mayne et al. (2000) (nonlinear systems), Löfberg (2003) for linear systems, and various approaches to ease the computational load, e.g. based on precomputation of invariant sets (e.g. tube-based MPC (Langson et al., 2004)). Despite recent progress, min-max MPC still gives prohibitive complexity as problem dimensions grow. In this chapter, a simple approximation is chosen as the maximizing disturbances that

gives reasonable computational performance, but will not give recursive feasibility and guaranteed stability in general. The work presented in this chapter shows that this approach will still be able to handle many, or most, disturbances in the proposed setup.

In Ersdal et al. (2016a) a nonlinear MPC (NMPC) based on a simplified system model was designed for AGC of the Nordic power system and tested against conventional PI controllers. Through both descriptive examples and Monte Carlo simulations, it was shown that an NMPC can be beneficial in AGC, both with regards to control performance and reserve usage. It was also shown how the NMPC can take system constraints into account, such as limitations on tie-line power transfers. This is something which is not easily done with a PI controller. Ersdal et al. (2014) presented an NMPC for AGC which is robustified against variations in produced wind power. This robustified NMPC (RNMPC) was tested without any model-plant mismatch, and it showed how the RNMPC was able to plan production so that it could handle a worst-case wind-power production scenario without breaking any system constraints.

This chapter is an extension of the work presented in Ersdal et al. (2014, 2016a). The RNMPC from Ersdal et al. (2014) is implemented and tested with the proxy system and prediction model from Ersdal et al. (2016a), hence there is a more realistic test of the controller on a large, realistic simulator. Ersdal et al. (2016a) presented a complete solution to the LFC problem by including generator participation-factors in the optimization problem as well as state estimation for full state feedback. This chapter will be an extension of this by including knowledge of worst-case predictions of future wind power production to robustify the NMPC. If the RNMPC can plan so that there always is enough transfer capacity on important tie-lines to handle some worst-case scenario, all generators are able to participate in LFC at all times, which will improve the system frequency.

In this work a centralized MPC (CMPC) is implemented, i.e. it is based on a model of the full system and it controls all the controllable system inputs. There are several examples where distributed MPC (DMPC) has been applied for LFC, such as Venkat et al. (2008); Mohamed et al. (2011). In DMPC separate MPCs, based on single-area models, controls the inputs to each area, and the main benefits are less demands for communication and smaller optimization problems for each MPC, hence shorter optimization time. The main drawback of DMPC is that it may result in poor systemwide control performance if the subsystems interact significantly (Venkat et al., 2008). For large power systems, such as the Central European system or the Eastern Interconnection in North America, the benefits of DMPC are very relevant. With a considerable smaller network, such as the Nordic network, on the other hand, there is not that much to gain by applying DMPC compared to CMPC, especially when considering that the CMPC presented here is based on a simplified model with a rather small amount of optimization variables. In addition to this, using a DMPC would complicate the tie-line constraint handling, which is an important feature of the presented controller.

The remainder of this chapter is organized as follows. In Section 3.2 the proxy

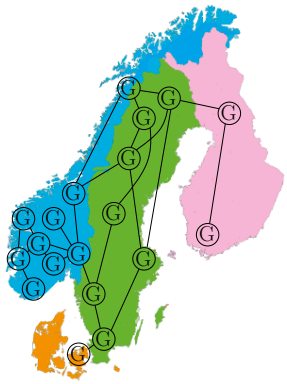

Figure 3.3: An overview of the generators in the SINTEF model (Norheim et al., 2005).

system used to represent the Nordic power system and the prediction model used in the NMPC are presented. The nominal NMPC (NNMPC) is then discussed in Section 3.3, before the details of the RNMPC are given in Section 3.4. In Section 3.5 the case study is presented along with the results from the tests on the proxy system, which then are discussed in Section 3.6. Final conclusions on the presented work are given in Section 3.7.

3.2 Modeling

The proxy system and the prediction model used in this work are the same as the ones used in Ersdal et al. (2016a). This section is therefore a condensed version of Section 2.2. All variables, in both the proxy system and the prediction model, are given in per unit [p.u.], see Appendix A in Machowski et al. (2008) for details.

The transmission grid is a critical infrastructure which cannot be used as a test-bed. For research in grid transmission control, it is therefore always necessary to use a simulation as a proxy for the physical system. The power system model used here is a model of the Nordic power system developed by SINTEF Energy Research (Norheim et al., 2005). It includes 15 hydro generators, 5 non-hydro generators, 21 composite loads, and 36 nodes. The placement of the generators can be seen in Figure 3.3, and they are chosen so that the model reflects the real production and most interesting bottlenecks in the Nordic power system (Norheim et al., 2005).

3.2.1 SINTEF Proxy System

In general a power system can be modeled by a differential algebraic equation

$$\dot{x} = f(x, z, u, w) \tag{3.1a}$$
$$0 = g(x, z, u, w) \tag{3.1b}$$

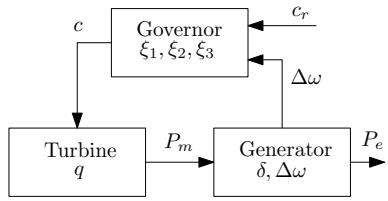

Figure 3.4: Overview of states, inputs and outputs of the dynamic system equation.

where x are the dynamic system states, z the algebraic system states, u the controllable input and w the system disturbance.

The dynamics of the model consists of the electromechanical dynamics of the rotor as well as the dynamics of the turbines and their governing systems (primary control). Since it is mainly the hydro turbines which provide primary control in the Nordic network, and most likely will provide the majority of AGC as well, only the hydro turbine and governor dynamics are included. Note that the rotor dynamics of the synchronous generator are modeled for all generators of the network.

Figure 3.4 shows a simplified diagram of the states, inputs and outputs of the dynamic system equation. Generators are modeled by what is usually denoted the swing equation, while the hydro turbines and governors are modeled as the nonlinear model of Machowski et al. (2008), usually denoted HYGOV. The states of the swing equation are the rotor angle and angular velocity, δ and $\Delta\omega$, the state of the turbine is the penstock flowrate q and the governor has the internal states ξ_1, ξ_2, ξ_3, representing the valve opening of the pilot servomotor and main servomotor (ξ_1 and ξ_3) as well as the integral of the controller part of the governor (ξ_2). The valve opening is $c = \text{sat}(\xi_3) = 0 \leq \xi_3 \leq 1$, and c_r is the valve opening set point provided by the TSO, while P_m and P_e are the mechanical and electrical power outputs, respectively. It is the valve opening set-point c_r which will be controlled by the NMPC.

The algebraic system equations describe the current flow in the network, and it is found using the internal node representation, where Kirchoff's current law is applied at each node. A node can contain only a junction of current flows, or it may have an aggregated load and/or an aggregated generator connected to it. Figure 3.5 shows the currents flowing into a node with both an aggregated load and an aggregated generator connected to it, where I_g is the current delivered from the generator, I_L the current from the load and I_{sys} the current from all the other nodes of the network. Based on the reactive power balance in the network, there is also the resulting nodal voltage $U = |U| e^{j\theta}$. When applying Kirchoff's current law in all nodes, the result is one complex equation in polar form with two unknown: $|U|$ and θ, the magnitude and angle of the nodal voltages.

Given a large power system consisting of n nodes, where m of these have generators connected to them, and where m_h of these are hydro turbines, the total system

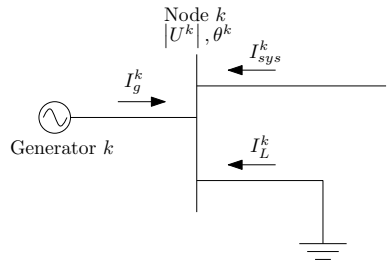

Figure 3.5: Internal node representation.

can be written as (3.1) with the following dynamic equations

$$\dot{\delta}^k = \Delta\omega^k \cdot \omega_n \tag{3.2a}$$

$$\Delta\dot{\omega}^k = \frac{1}{2H^k}\left(P^k_m - P^k_e(z) - D^k_g\left(\Delta\omega^k - \Delta\omega_n\right)\right) \tag{3.2b}$$

$$\dot{q}^i = \frac{1}{T^i_w}\left(1 - \left(\frac{q^i}{c^i}\right)^2\right) \tag{3.2c}$$

$$\dot{\xi}^i_1 = \frac{1}{T^i_g T^i_p}\left(c^i_r - \Delta\omega^i + \frac{r^i}{T^i_r}\xi^i_2 - \left(r^i + \rho^i\right)c^i - T^i_g\xi^i_1\right) \tag{3.2d}$$

$$\dot{\xi}^i_2 = -\frac{1}{T^i_r}\xi^i_2 + c^i \tag{3.2e}$$

$$\dot{\xi}^i_3 = \mathrm{sat}^i_{\dot{c}}(\xi^i_1) \tag{3.2f}$$

for each generator $k = 1, \ldots, m$ and each hydro turbine $i = 1, \ldots, m_h$. Where

$$\Delta\omega_n = \frac{\sum_{j=1}^m H^j \Delta\omega^j}{\sum_{j=1}^m H^j} \tag{3.2g}$$

$$c^i = \mathrm{sat}^i_c(\xi^i_3) \tag{3.2h}$$

$$P^i_m = A^i_t\left(q^i/c^i\right)^2\left(q^i - q^i_{nl}\right) - D^i_t c^i\left(\Delta\omega^i - \Delta\omega_n\right) \tag{3.2i}$$

and ω_n is the nominal rotor-speed of the generator, H the rotor inertia, D_g the generator damping coefficient, T_w the water starting time of the hydro turbine, T_g and T_p time constants in the servo motor of the governor, T_r the time constant of the transient droop, ρ the constant-droop coefficient, r the transient-droop coefficient, $\mathrm{sat}_{\dot{c}/c}(\cdot)$ saturations, q_{nl} the no-load flow of the turbine, A_t a factor that accounts for the different per-unit bases in the turbine and generator, and D_t the turbine damping coefficient. The algebraic equation is as follows

$$\begin{aligned} 0 &= P_e(z) - \mathcal{R}e\left(EI^*_g\right) \\ &= P_e(z) - \mathcal{R}e\left(E\left(Y^*_c\left|U\right|e^{-j\boldsymbol{\theta}} + \left|I_l\right|e^{-j\theta}\right)\right)\frac{s_{\text{base}}}{m_{\text{base}}} \end{aligned} \tag{3.3}$$

where E is the internal voltage of the generators, I_g^* the complex conjugate of the current delivered from the generators, Y_c^* the complex conjugate of the network admittance matrix, I_l the absolute value of the active load currents, s_{base} the network base rating, and m_{base} the base rating of the generators.

This gives the following state, input and disturbance vectors

$$x = \begin{bmatrix} \delta^k & \Delta\omega^k & q^i & \xi_1^i & \xi_2^i & \xi_3^i \end{bmatrix}^T \tag{3.4a}$$

$$z = \begin{bmatrix} |U^s| & \theta^s \end{bmatrix}^T \tag{3.4b}$$

$$u = c_r^i \tag{3.4c}$$

$$w = \begin{bmatrix} |I_l^s| & P_m^p \end{bmatrix}^T \tag{3.4d}$$

where $k = 1, \ldots, m$, $i = 1, \ldots, m_h$, $s = 1, \ldots, n$, and $p = m_h + 1, \ldots, m$. This means that for each generator k (regardless of type), there are two dynamic states, for each hydro generator i there are in addition four extra dynamic states, and for each node s there are two algebraic states. In total $2m + 4m_h$ dynamic states, $2n$ algebraic states, m_h controllable inputs, and $n + m - m_h$ disturbances.

3.2.2 Prediction Model for Model Predictive Control

The prediction model (PM) is the model used by the NMPC to predict how the system will behave in the future, based on the inputs to-be-optimized and a disturbance model. In real-life situations, these models are always simplifications and approximations to the actual processes which are being controlled. In this work, the NMPC is based on a reduced and simplified version of the system presented in the previous section. This is done to ease the computational load of the NMPC and the state estimator, but it also incurs a natural model-plant mismatch in the testing of the controller. To find the PM, the larger model of the previous section is first divided into N areas connected to each other by tie lines. All states, inputs and disturbances are given relative an initial steady state where both active and reactive power supply and consumption are balanced.

The dynamics affecting the frequency response of a power system are relatively slow, and neglecting the fast dynamics reduces the complexity of the model (Bevrani, 2014). The nodal voltages and the electromechanical dynamics of the swing equation are considered to be fast dynamics, and can therefore be neglected. The dynamics of area i, including the generators, can in this case be represented by one single differential equation (Bevrani, 2014)

$$\Delta\dot{\bar{f}}^i = \frac{1}{2\bar{H}^i}\left(\Delta\bar{P}_m^i - \Delta\bar{P}_D^i - \Delta\bar{P}_{tie}^i\right) \tag{3.5}$$

where $\Delta\bar{f}$ is the deviation from the nominal frequency f_n, $\Delta\bar{P}_m$ the total change in power from primary control and AGC combined, $\Delta\bar{P}_D$ the total change in load power and uncontrollable production, $\Delta\bar{P}_{tie}$ the change in total power flow from

the area on all its tie lines, and $\bar{H}$ the inertia of the rotating masses of the area. The change in total tie-line power flow from area i is (Bevrani, 2014)

$$\Delta\dot{\bar{P}}^i_{tie} = 2\pi\left(\Delta\bar{f}^i\sum_{j=1,j\neq i}^{N}\bar{T}_{ij} - \sum_{j=1,j\neq i}^{N}\bar{T}_{ij}\Delta\bar{f}^j\right) \tag{3.6}$$

where $\Delta\bar{f}^{i/j}$ is the local frequency in area i/j, and $\bar{T}_{ij}$ the synchronizing torque coefficient between area i and j. The frequency deviation of the entire system is defined as

$$\Delta\bar{f} = \frac{\sum_{i=0}^{N}\bar{H}^i\Delta\bar{f}^i}{\sum_{i=0}^{N}\bar{H}^i} \tag{3.7}$$

The hydraulic turbines and governor equations are simplified by modeling all the hydraulic power stations of an area as one aggregated hydraulic turbine and governor. The dynamics of the turbine can in turn be represented by a linearized version of the nonlinear model used in the proxy system, where the reference points for the PM system states are used for linearization. This gives the following dynamic equation for the aggregated turbine of area i

$$\Delta\dot{\bar{q}}^i = -\frac{2}{\bar{T}^i_w\bar{c}^{i2}_{ss}/\bar{q}^i_{ss}}\left(\Delta\bar{q}^i - \frac{\bar{q}^{i2}_{ss}}{\bar{c}^{i2}_{ss}}\Delta\bar{c}^i\right) \tag{3.8a}$$

$$\Delta\bar{P}^i_m = \bar{A}^i_t\frac{\bar{q}^{i2}_{ss}}{\bar{c}^{i2}_{ss}}\left(3\Delta\bar{q}^i - 2\frac{\bar{q}^{i2}_{ss}}{\bar{c}^{i2}_{ss}}\Delta\bar{c}^i\right) \tag{3.8b}$$

where $\Delta\bar{c}$ and $\Delta\bar{q}$ are the change in valve opening and water flow rate from $\bar{c}_{ss}$ and $\bar{q}_{ss}$, respectively. In the governor equations, one of the time constants is several times smaller than the others, and it can therefore be neglected. This results in the following governor dynamic equations for area i

$$\Delta\dot{\bar{\xi}}^i_2 = -\frac{1}{\bar{T}^i_r}\Delta\bar{\xi}^i_2 + \Delta\bar{c}^i \tag{3.9a}$$

$$\Delta\dot{\bar{\xi}}^i_3 = \mathrm{sat}^i_{\dot{c}}\left(\frac{1}{\bar{T}^i_g}\left(\Delta\bar{c}^i_r - \Delta\bar{f}^i + \frac{\bar{r}^i}{\bar{T}^i_r}\Delta\bar{\xi}^i_2 - \left(\bar{r}^i + \bar{\rho}^i\right)\Delta\bar{c}^i\right)\right) \tag{3.9b}$$

$$\Delta\bar{c}^i = \mathrm{sat}^i_c\left(\Delta\bar{\xi}^i_3\right) \tag{3.9c}$$

The manipulated input is still the valve opening set point $\Delta\bar{c}_r$.

Disturbance Model

The balancing of power is managed by market transactions in most systems, and through these markets the predicted power demand and supply are balanced on slots of normally one hour. The markets take into account variations in production from traditional power stations as well as the daily/weekly/annually deterministic load variation patterns. Because

1. load variation patterns as well as production from some generators are difficult to predict in detail, and

2. changes in production set-point $P_{m,sp}$ takes place on the hour, while changes in power demand happens during the hour (Statnett, 2012)

there will always be deviations from the hourly market balance. In order to keep the power system safe and stable, it is important that this unpredicted power imbalance is covered by the primary control and the AGC.

By choosing the initial steady state of the PM as the marked balance, the disturbance of the PM $\Delta\bar{P}_D^i$ represents the total unpredicted power imbalance of each area. This unpredicted power imbalance can roughly be divided into two different dynamic components. One is a continuously, slowly varying imbalance due to intermittent energy resources and loads. The other is an imbalance caused by sudden disconnections of loads or generators, which results in steep and sudden changes in the power imbalance. Both of these components are important to consider when dealing with robust LFC. However, here we focus on the effects of an increasing wind-power penetration, and we will therefore concentrate on the former.

When dealing with power systems including a certain amount of wind power, such as the Nordic grid, one can for simplicity assume that this intermittent unpredicted power imbalance is dominated by the fluctuations in produced wind power. If, in addition, it is assumed that the majority of wind power is situated in area p, $\Delta\bar{P}_D$ of all the other areas can be neglected, and the model is affected by one single disturbance $\Delta\bar{P}_D = \Delta\bar{P}_D^p$. With the Nordic network in mind, Denmark and South Sweden contribute with about 80% of the total wind power production (Statnett, 2012). In Ersdal et al. (2016a) the disturbance $\Delta\bar{P}_D$ was kept constant over the prediction horizon. In this work however, the idea from Ersdal et al. (2014) to make the NMPC more robust against fluctuations in produced wind power by using different disturbance scenarios in the predicted system behavior, is implemented.

Depending on the number of areas N, the simplified system is represented by one differential equation

$$\dot{\bar{x}} = \bar{f}\left(\bar{x}, \bar{u}, \bar{w}\right) \tag{3.10a}$$

where

$$\bar{x} = \begin{bmatrix} \Delta\bar{f}^i & \Delta\bar{q}^i & \Delta\bar{\xi}_2^i & \Delta\bar{\xi}_3^i & \Delta\bar{P}_{tie}^i \end{bmatrix}^T \tag{3.10b}$$

$$\bar{u} = \Delta\bar{c}_r^i \tag{3.10c}$$

$$\bar{w} = \Delta\bar{P}_D^i \tag{3.10d}$$

and $i = 1, \ldots, N$. In total $5N$ dynamic state variables, N controllable inputs, and one disturbance. The bar notation represents the simplified system states, inputs and parameters.

3.3 Controller

3.3.1 Control Problem

The main control task of the MPC is to balance the power production in the network against the consumption at all times, and to do so while avoiding bottleneck congestions and staying within other system bounds. When large, unexpected disturbances appear, it is a problem in the Nordic network that some of the resources participating in primary control and AGC are prevented from participating due to bottlenecks in the network. For instance, the generators in the west may not be able to participate in covering a disturbance in the east if the east-west transmission lines are already transferring close to maximum.

In addition to this primary control task, the MPC should also keep the costs associated with LFC at a minimum. The cost of primary control is often higher than AGC, and lowering the use of primary control by keeping the frequency closer to f_n through use of AGC is desirable. When it comes to use of AGC, it is advantageous to keep the input in the PM $\bar{u}$ as close to its hourly set-point value $\bar{u}_0$ as possible. This is because the TSO has to pay more per delivered MWh the more they require the generators to deviate from the initial hourly set point. In Ersdal et al. (2016a) it was shown how a NMPC can lower the costs associated with LFC compared to tradition PI-control. In this work the aim is not to further improve the reserve usage, but rather expand the NMPC while maintaining the results from Ersdal et al. (2016a).

3.3.2 MPC

MPC is a framework for advanced control that has seen widespread use, especially within chemical process industries, and it is believed that the optimizing and constraint-handling nature of MPC makes it suitable also for LFC. MPC uses a model of the system to predict how it will behave in the future, and then optimizes the controlled input with regards to an objective function measuring predicted performance. Mathematically, it can be formulated as a continuous time optimal control problem on the form (3.11a) subject to (3.11b) - (3.11d) (Biegler, 2010)

$$\min_{\bar{x}(\cdot),\bar{u}(\cdot)} J\left(\bar{x}(t),\bar{u}(t)\right) \tag{3.11a}$$

$$\bar{x}(0) - \bar{x}_0 = 0 \text{ Fixed initial state} \tag{3.11b}$$

$$\dot{\bar{x}}(t) - \bar{f}\left(\bar{x}(t),\bar{u}(t),\bar{w}(t)\right) = 0 \text{ System model} \tag{3.11c}$$

$$g\left(\bar{x}(t),\bar{u}(t)\right) \leq 0 \text{ Constraints} \tag{3.11d}$$

where $\bar{x}(t)$ are the system states, $\bar{u}(t)$ the controlled inputs, $\bar{w}(t)$ the predicted disturbances, and $J\left(\bar{x}(t),\bar{u}(t)\right)$ the control objective function.

Figure 3.6 shows the basics of how an MPC works. The idea is to solve an optimization problem at each time step to find the optimal system input $\bar{u}(t)$ over

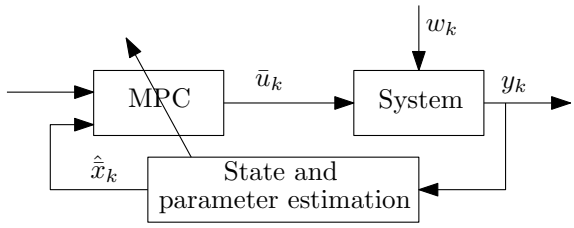

Figure 3.6: Overview of MPC-loop.

a fixed time horizon with respect to the objective function $J(\cdot)$, and then apply the first element of $\bar{u}(t)$ as input to the system. The loop is closed by the measurements $y(t)$, and a state estimator is also included as the MPC needs knowledge of the entire state vector $\bar{x}(t)$.

3.3.3 MPC Design for AGC

An MPC will be applied for AGC in this work. It will control the proxy system of Section 3.2.1, from now referred to as the plant replacement model (PRM), while using the prediction model (PM) of Section 3.2.2 to predict future system behavior. Hence there is a natural model-plant mismatch between PM and PRM. The control of, and contribution from tertiary control is omitted in this work, as it is manually operated over a longer time scale.

The dynamic equation of the PM (3.10) is implemented as the system model (3.11c), and the constraints (3.11d) includes limitations on generation capacity, generation rate of change, as well as on tie-line power transfer. Since the saturations in (3.9) are nonlinear, this will result in a nonlinear MPC (NMPC), and the optimization problem is therefore non-convex. The continuous time optimization problem (3.11) in the NMPC is solved with direct methods, that is, it is discretized and transformed into a nonlinear program (NLP) (Biegler, 2010). This NLP is then solved numerically by the use of collocation, where both the control inputs and states are discretized on a fixed grid. In order to avoid convergence issues with the NLP solver, related to the non-smooth saturation functions in (3.9), these are replaced by smooth approximations as in Ersdal et al. (2016a).

In the PM, there is one input per area, which leads to N optimal inputs from the NMPC: $\Delta\bar{c}_r^i$, where $i = 1, \ldots, N$. These N inputs are then distributed to the hydro generators of each area by individual participation factors α_j^i. As seen from Figure 3.7

$$c_{rj}^i = c_{r0j}^i + \alpha_j^i \Delta\bar{c}_r^i \tag{3.12}$$

where $j = 1, \ldots, m_h^i$ and m_h^i is the number of hydro generators in area i. Bear in mind that $\sum_{i=0}^{N} m_h^i = m_h$. However, each of the valve set points of the PRM c_r has individual constraints, and in Ersdal et al. (2016a) the participation factors α were included in the optimization problem as optimization variables. This both

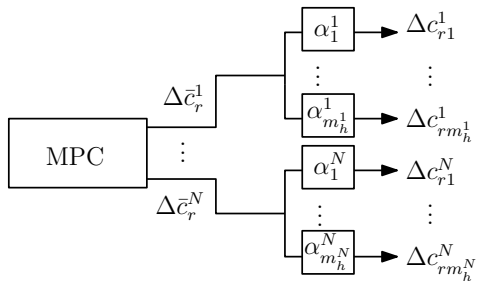

Figure 3.7: Participation factors α_j^i, where m_h^i is the number of hydro generators in area i.

allows for individual input constraints and greater flexibility and better use of the NMPC's strength on coordination of multiple inputs, however at the expense of a larger optimization problem. This extension of the PM is also included in this work, and the PM now has $5N$ dynamic states, m_h optimization variables and one disturbance.

3.3.4 State and Parameter Estimation

The MPC relies on knowledge of the entire PM state vector $\bar{x} = \left[\Delta\bar{f}^i, \Delta\bar{q}^i, \Delta\bar{\xi}_2^i, \Delta\bar{\xi}_3^i, \Delta\bar{P}_{tie}^i\right]^T$ as well the current PM disturbances $\bar{w} = \Delta\bar{P}_D^i$. In order to find an estimate of these, it is assumed that the following PRM states are measured

$$y = \begin{bmatrix}\Delta\omega^k & \xi_2^i & \xi_3^i & |U|^s & \theta^s\end{bmatrix} \tag{3.13}$$

where $k = 1, \ldots, m$, $i = 1, \ldots m_h$, and $s = 1, \ldots n$. In practice $|U|$ and θ are measured using phasor measurement units (PMU), while $\Delta\omega$, ξ_2, and ξ_3 are measurable at the generators and governors. From these, the equivalent PM states $\Delta\bar{f}^i = 2\pi\Delta\bar{\omega}^i$, $\Delta\bar{\xi}_2^i$, and $\Delta\bar{\xi}_3^i$ can be calculated, and the power flow between all network nodes, including $\Delta\bar{P}_{tie}^i$, can be found using $|U|$ and θ. Hence the PM measurements are

$$\bar{y} = \begin{bmatrix}\Delta\bar{f}^i & \Delta\bar{\xi}_2^i & \Delta\bar{\xi}_3^i & \Delta\bar{P}_{tie}^i\end{bmatrix}^T \tag{3.14}$$

where $i = 1, \ldots, N$.

An extended Kalman filter (EKF) (Simon, 2006) based on the PM is then applied to estimate the full PM state vector as well as the PM disturbances, $\Delta\bar{P}_D^i$. In order to estimate the change in load power and uncontrollable production of each area ($\Delta\bar{P}_D^i$), the PM is augmented to include $\Delta\bar{P}_D^i$ as states with zero derivatives. To illustrate the EKF, a simulation is performed using the proxy system. The PM is set to have one area, hence $N = 1$. The resulting estimate of $\Delta\bar{q}$ and $\Delta\bar{P}_D$, $\Delta\hat{\bar{q}}$ and $\Delta\hat{\bar{P}}_D$, can be seen in Figure 3.8, and it illustrates that the implemented EKF manages to estimate the unmeasured state and disturbance in a satisfying manner. The EKF is chosen because the software used for implementation, Casadi (Andersson, 2013), automatically generates the system's derivatives, making the EKF a simple and effective choice.

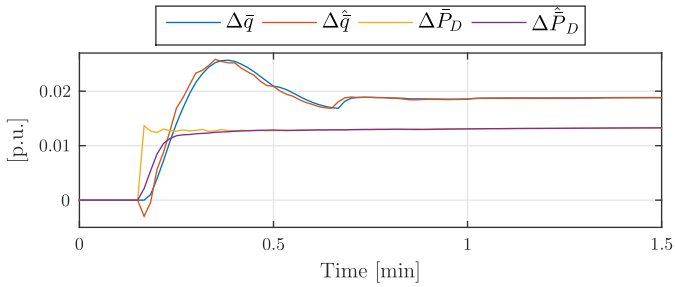

Figure 3.8: Results from EKF: The estimate of $\Delta\bar{q}$ and $\Delta\bar{P}_D$, $\Delta\hat{\bar{q}}$ and $\Delta\hat{\bar{P}}_D$.

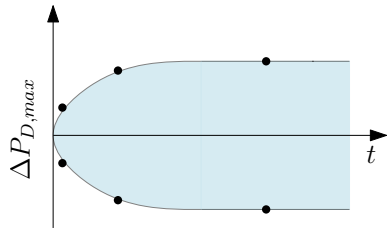

Figure 3.9: An example of how a worst-case estimate for ΔP_D could look.

3.4 Robustified NMPC

3.4.1 Worst-Case Estimate of ΔP_D

For a given wind farm, a worst-case estimate of the variation from the predicted power output can be estimated, and Holttinen (2004) provides such data one second, one minute and one hour into the future t. If this information is combined for several wind farms, one can create a total worst-case estimate for the future variation in wind-power production of one area, see Figure 3.9.

If the wind farms are distributed more evenly in the system, so that the assumption in Section 3.2.2 no longer applies, the disturbance would enter at several points and a worst case combination of the disturbances, where system dynamics are considered, has to be calculated.

3.4.2 Robustified NMPC

In the RNMPC a new state vector is constructed by combining the original state vector $\bar{x}$ (3.10b) and input $\bar{u}$ (3.10c) exposed to three different future disturbances: The zero, negative, and positive worst-case estimate for $\Delta\bar{P}_D$ added to the current estimated disturbance $\bar{w}$ (3.10d), see Figure 3.10. The system equation for the

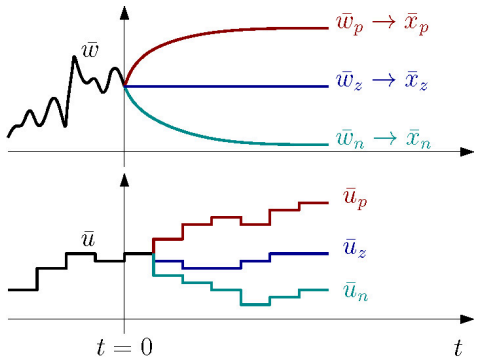

Figure 3.10: Robustified NMPC. For simplicity, $\bar{u}$ is considered to be scalar.

combined system used in (3.11c) is

$$\dot{\tilde{x}} = \begin{bmatrix} \dot{\bar{x}}_z \\ \dot{\bar{x}}_p \\ \dot{\bar{x}}_n \end{bmatrix} = \begin{bmatrix} \bar{f}\left(\bar{x}_z, \bar{u}_z, \bar{w}_z\right) \\ \bar{f}\left(\bar{x}_p, \bar{u}_p, \bar{w}_p\right) \\ \bar{f}\left(\bar{x}_n, \bar{u}_n, \bar{w}_n\right) \end{bmatrix} = \tilde{f}\left(\tilde{x}, \tilde{u}, \tilde{w}\right) \tag{3.15}$$

where $\tilde{u} = \begin{bmatrix} \bar{u}_z & \bar{u}_p & \bar{u}_n \end{bmatrix}^T$ and $\tilde{w} = \begin{bmatrix} \bar{w}_z & \bar{w}_p & \bar{w}_n \end{bmatrix}^T$. At each optimization it is required that for the first element of $\tilde{u}(t)$, $\bar{u}_z$, $\bar{u}_n$ and $\bar{u}_p$ must be equal. After this, they are free to vary in manners optimal for their designated system states, see Figure 3.10. In this way the optimal input trajectory for all three scenarios, fulfills all system constraints and is therefore a feasible input (on the control horizon).

3.4.3 Stability of the RNMPC

A common approach for achieving robust NMPC is the concept of min-max NMPC (Rawlings and Mayne, 2009), which often results in large and complex optimization problems. The RNMPC presented in the previous section is a simplified, nonlinear version of the min-max feedback MPC presented in Scokaert and Mayne (1998). It is well known that min-max approaches are computationally intractable, especially in the nonlinear case. This motivates us to only consider predefined approximate worst case scenarios instead of letting the optimizer find the real worst case disturbance, which is an approach that has similarities to what is done in scenario-based NMPC (Huang et al., 2009; Goodwin and Medioli, 2013). A drawback with doing this is however that the recursive feasibility property is lost. This is important in proving closed-loop stability of MPC schemes (Mayne et al., 2000), and stability of the RNMPC can therefore not be guaranteed. In this work, stability is rather approached by choosing long horizons and tuning weights to achieve convergent behavior in simulations. "Stabilizing ingredients" such as terminal costs could have been added, but this is not included in this study.

To handle possible instability/infeasible optimization problems, a supervising agent must be devised that interferes when problems are detected, as a fallback

mechanism. This could involve automatic fail-to-safe transitions, possible restart of the NMPC, or switching to manual control. It can be argued that such a mechanism will have to be installed in any case, since it is very hard (and conservative) to include all thinkable disturbance scenarios in the prediction model. The role of the robustified NMPC is then to handle the disturbances most likely to happen.

An exact solution to such a supervising agent is not implemented in this work. However, some possible solutions are discussed in the following. The return codes and warning signals from the numerical optimization solver can be applied to detect convergence problems and other computational issues. Moreover, one may monitor the performance of the NMPC alongside the fallback controller. Motivated by the discussions in Johansen (2015) on dependable embedded MPC, an idea is a control selection scheme where the value of the NMPC objective function evaluated in simulations on a system model (in this case, the PRM would be natural, if available, if not the PM should be used) is used as a measure to select either the NMPC or the fallback controller. The idea is that unstable/infeasible and poor solutions from the NMPC will be discarded in favor of the fallback controller. With regards to the actual fallback controller, it could for example be conventional PI-based AGC, or in some cases manual control. In any case, such an event must generate an alarm to the TSO, so that the situation can be supervised in a proper manner. A mechanism must also be devised for re-connecting the NMPC, this can for instance be running the NMPC in open-loop for some time-steps to verify feasibility before it is manually re-connected by the TSO.

while *true* **do**
  1. Gather measurements, y;
  2. Calculate PM measurements, $\bar{y}$;
  3. Use EKF to find estimate of PM state vector and disturbance, $\hat{\bar{x}}$ and $\hat{\bar{P}}_D$, for use in the NMPC;
  4. Find optimal inputs u using NMPC based on PM;
  5. Check the computed input for problems (numerical/performance), e.g. as discussed above;
  if *Problems* **then**
    A. Calculate system input using fallback controller, u_{fb};
    B. Apply u_{fb} to system;
  else
    Apply input u from NMPC to system;
  end
end

Algorithm 1: Implementation of NMPC.

The main parts of the controller are summarized in Algorithm 1. The reconnection of the NMPC is not included, as this would be a manual operation conducted by the TSO.

3.5 Case Study

The PRM (3.1) has a total of 100 dynamic states, 72 algebraic states, 15 controllable inputs, and 21 disturbances. This system is divided into two areas in the PM (3.10), hence $N = 2$. One area covers South Sweden and Eastern Denmark (area A), and the other covers Norway, North Sweden and Finland (area B), and according to the assumptions made in Section 3.2.2, $\Delta\bar{P}_D^B = 0$ and $\Delta\bar{P}_D = \Delta\bar{P}_D^A$. There is also a tie line between the two areas which represents the total power flow between them. This tie line has a maximum power-transfer capacity of 2000 MW. With $N = 2$, the PM has 10 dynamic sates, 15 controllable inputs, and one disturbance, which is a significant reduction from the PRM. The AGC control signal is dispatched every 10 s for both the PRM and the PM.

The performance of the RNMPC is compared to the NNMPC, which is based on $\dot{\bar{x}}_z = \bar{f}\left(\bar{x}_z, \bar{u}_z, \bar{w}_z\right)$. In order to compare the two controllers, a control performance measure (CPM) is applied. It is inspired by the CPS1 and CPS2 performance criteria used by the North American electric reliability corporation (NERC) (Gross and Lee, 2001), and it basically measures the average frequency deviation: first Δf is averaged over windows of 30 s to filter out fast fluctuations, then the CPM is found by again averaging Δf over all these windows.

3.5.1 Tuning the NMPC

The main tuning variables of the NMPC are the prediction horizon T, and the objective function $J\left(\cdot\right)$. The objective function is set to

$$J\left(\bar{x}, \bar{u}\right) = \int_{t=0}^{T} \bar{x}^T Q \bar{x} + \left(\bar{u} - \bar{u}_0\right)^T R \left(\bar{u} - \bar{u}_0\right) \, dt \tag{3.16}$$

where $Q = \text{diag}\left(\bar{Q}_z, \bar{Q}_p, \bar{Q}_n\right)$ and $R = \text{diag}\left(\bar{R}_z, \bar{R}_p, \bar{R}_n\right)$ for the RNMPC, and $Q = \bar{Q}$ and $R = \bar{R}$ for the NNMPC. Q is real, symmetric and positive semidefinite, while R is real, symmetric and positive definite. The non-zero elements of $\bar{Q}$ are chosen so that the deviation in overall system frequency (3.7) is punished: $\bar{q}_{11} = \beta \frac{\left(H^1\right)^2}{\left(H^1+H^2\right)^2}$, $\bar{q}_{66} = \beta \frac{\left(H^2\right)^2}{\left(H^1+H^2\right)^2}$, $\bar{q}_{16} = \bar{q}_{61} = \beta \frac{H^1 H^2}{\left(H^1+H^2\right)^2}$, where $\beta = 10^5$. The use of primary control is actuated by Δf, so minimizing Δf will also minimize the use of primary reserves. The matrix R is set to $R = \text{diag}\left(\eta m_{\text{base}}\right)$, where m_{base} is a vector containing the hydro generators' base rating, and $\eta = 0.1$. With m_{base} included in R, the actual produced power from the hydro generators are included in the objective function, and not only the per-unit based $\bar{u}$. In order to place more emhasis on deviations in $\bar{x}_z$, $\bar{Q}_z$ is set equal to $\bar{Q}$, while $\bar{Q}_p = \bar{Q}_n = 0.1\bar{Q}$. The three systems are all punished equally when it comes to deviations in input: $\bar{R}_z = \bar{R}_p = \bar{R}_n = \bar{R}$.

The control horizon T is 3 minutes, a decision based on a compromise between system time constants and complexity, and the time step of the NMPCs is 10 s in order to match the control signal dispatching in the system.

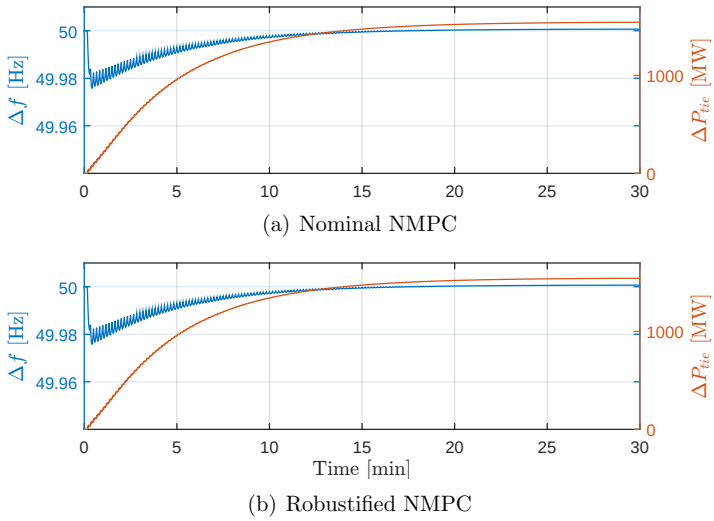

(a) Nominal NMPC

(b) Robustified NMPC

Figure 3.11: Case A: Δf and ΔP_{tie} for NNMPC and RNMPC.

3.5.2 Software

The proxy system and both NMPCs were implemented in Python using Casadi. Casadi is a framework for solving dynamic optimization or optimal control problems (OCP). Casadi has been developed with focus on allowing users to implement their method of choice with any complexity, rather than being a black-box OCP-solver (Andersson, 2013). The name Casadi originates from its form as a minimalistic computer algebra system (Cas) with a general implementation of automatic differentiation (ad). It is interfaced to various NLP solvers, and in using these solvers from Casadi there is no need to implement functions for the derivatives, as they are automatically generated and interfaced by Casadi using automatic differentiation (Andersson, 2013). In this work the interior point optimizer IPOPT (Wächter and Biegler, 2006) is applied, using the exact Hessian.

3.5.3 Tests on the SINTEF proxy system

The NMPC has been tested on the SINTEF Nordic system model described earlier. As discussed, it is normal practice in power system research to use high fidelity validated models to test operational and research concepts since the transmission system itself cannot be used for experimentation.

In Case A, the disturbance (entering in area A) is small enough so that ΔP_{tie} does not reach its limit. Figure 3.11 shows the resulting Δf and ΔP_{tie}, and it is clear that in this case the response is very similar for the NNMPC and the RNMPC. This is confirmed by the CPM in Table 3.1. It is also seen from Figure 3.11 that there are oscillations in the system frequency. These oscillations are mainly caused

Table 3.1: CPM and reserves usage (given in MWh).

		CPM	Primary Control	AGC
Case A	NNMPC	$\mathbf{3.73 \cdot 10^{-5}}$	26.0	**768.7**
	RNMPC	$3.75 \cdot 10^{-5}$	**25.9**	769.2
	Difference	+0.5%	−0.4%	≈ ±0%
Case B	NNMPC	$1.28 \cdot 10^{-3}$	**88.2**	2525
	RNMPC	$\mathbf{1.27 \cdot 10^{-3}}$	89.4	**2518**
	Difference	−0.8%	+1%	−0.3%
Case C	NNMPC	$\mathbf{3.5 \cdot 10^{-3}}$	**2298**	**746**
	RNMPC	$3.9 \cdot 10^{-3}$	2463	777
	Difference	+11%	+7%	+4%

by the fast, electromechanical dynamics of the system, which the NMPC is not able to account for due to turbine time constants and NMPC sampling time.

In Case B the initial state of the system has $\Delta P_D \neq 0$ (and thus $\Delta P_{tie} \neq 0$), and after approximately 4 minutes, the disturbance (still entering in area A) follows the negative worst-case scenario of Figure 3.10, $\bar{w}_n$. The test results can be seen in Figure 3.12 - 3.14. Figure 3.12(b) shows that in the initial steady state, the limit of ΔP_{tie} is reached by the NNMPC, while the RNMPC stabilizes the tie-line power transfer at a lower level, ensuring that there still is some transfer capacity left. This is very beneficial when the worst-case disturbance sets in, and Figure 3.12(b) clearly shows that the RNMPC manages to keep within the limit of 2000 MW while the NNMPC does not. Figure 3.13 illustrates how ΔP_m is allocated between the two areas with the NNMPC and the RNMPC, and in Figure 3.14 the total input $\sum u = \sum c_r$ of each area can be seen.

It is clear from both Figure 3.12 and 3.13 that the NNMPC experiences larger system oscillations than the RNMPC. This is because the NNMPC is at the tie-line constraint, causing the inputs to constantly having to adjust in an attempt to fulfill the system constraints, see Figure 3.14(a). These input oscillations are not seen with the RNMPC (Figure 3.14(b)), and they cause oscillations in generated power as well as amplifying the oscillations in system frequency. They are not beneficial for the hydro generators as they will cause wear and tear on their valves and other mechanical parts.

The last case, Case C, is a Monte Carlo simulation where disturbances based on random numbers, generated using the method of Cecílio et al. (2013) are imposed on the system. These disturbances are much more fluctuating and smaller in size compared to the previous cases, so that they resemble normal disturbance patterns. The Monte Carlo simulation is included to show the average performance of the RNMPC against the NNMPC, and the average results from 100 simulations can

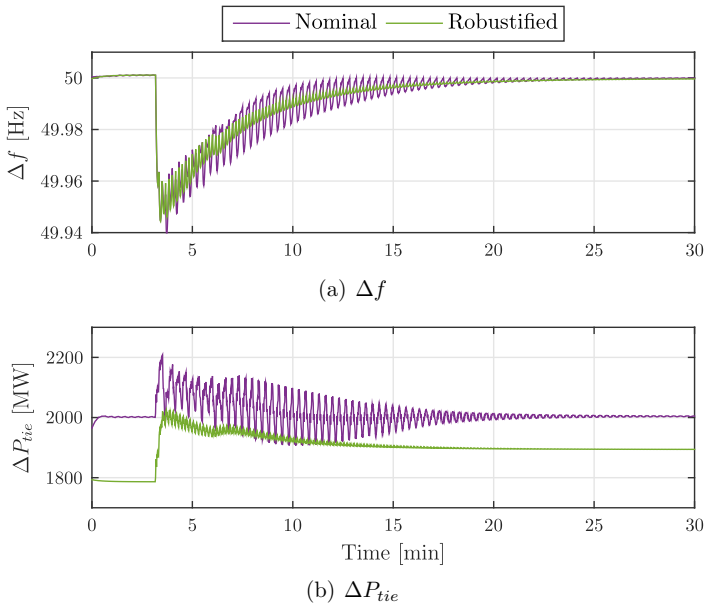

(a) Δf

(b) ΔP_{tie}

Figure 3.12: Case B: Δf and ΔP_{tie} for NNMPC and RNMPC.

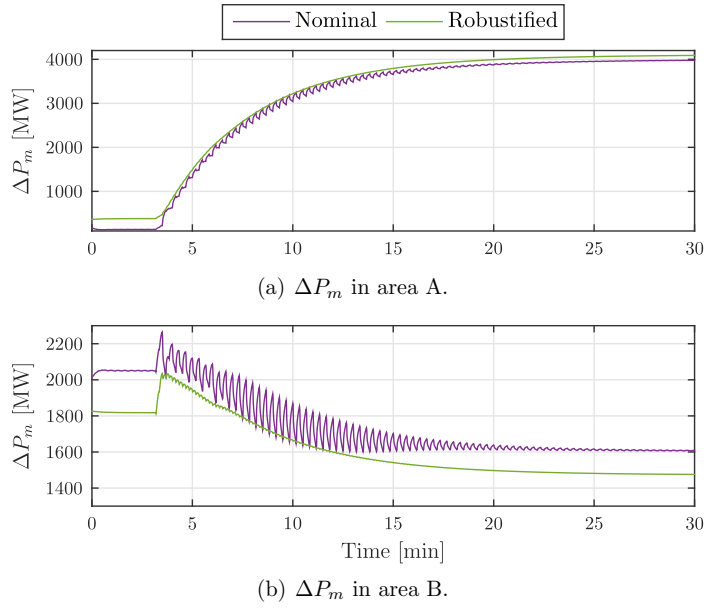

(a) ΔP_m in area A.

(b) ΔP_m in area B.

Figure 3.13: Case B: total use of ΔP_m in area A and area B with nominal and robustified controller.

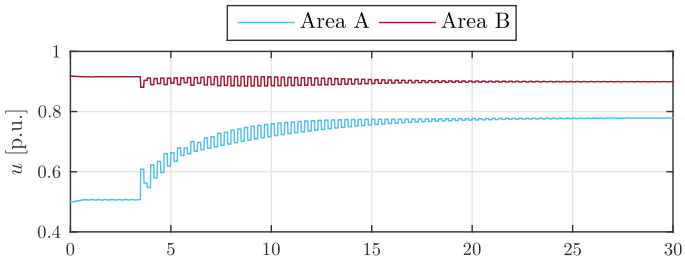

(a) $\sum u = \sum c_r$ in area A and B with NNMPC.

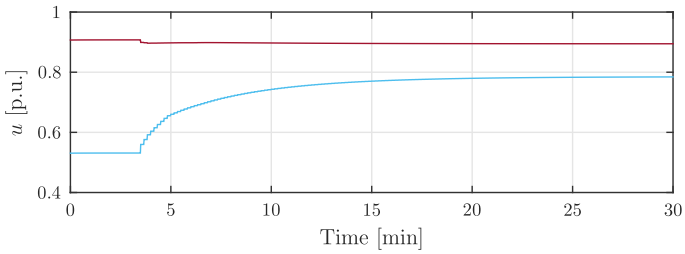

(b) $\sum u = \sum c_r$ in area A and B with RNMPC.

Figure 3.14: Case B: total input in area A and area B with nominal and robustified controller.

be seen in Table 3.1. It shows that the NNMPC in general performs slightly better than the RNMPC, both with regards to frequency control and reserve usage. This is however not very surprising, as robust control methods tends to be more conservative, which often leads to poorer control performance.

3.6 Discussion

In Ersdal et al. (2016a) it was shown through both descriptive examples and thorough simulation, that applying NMPC for AGC can be beneficial with regards to control performance and reserves usage. In this work, the emphasis has been placed on making the NMPC presented in Ersdal et al. (2016a) more robust against fluctuating wind power production.

In Case A it was demonstrated that when no system constraints are met, the NNMPC and RNMPC results in almost identical system behavior and reserve usage. On average however, the Monte Carlo simulation showed that the NNMPC does perform better than the RNMPC while using less resources. This is however something that must be expected when trying to robustify the NMPC. Another result from the Monte Carlo simulation is data on how often the RNMPC results in infeasible optimization problems. For 100 successful simulations, there where 12 that ended with infeasibility (hence 11%). With the NNMPC, the tie-line constraints were broken in these cases, and the only reason why infeasibility was not

encountered is that the NNMPC has slack variables to handle this. Adding slack variables to system constraints is a common way of avoiding infeasibility in optimization problems (Maciejowski, 2002), as they allow the solution to break certain constraints if absolutely necessary. Slack variables were not included in the RNMPC because they would deteriorate the aim of keeping clearances to system constraints.

Even though the RNMPC showed to be more conservative when more realistic, fluctuating disturances were imposed on the system, it is still less conservative than the RNMPC in Ersdal et al. (2014). The main reason for this difference is that in Ersdal et al. (2014) there was only one input per area, whereas here there are several. Several inputs per area makes it easier for the RNMPC to fulfill the system constraints, also in case of worst-case disturbance scenarios, and it does not need to be as conservative.

In case B the difference between the NNMPC and RNMPC is displayed. When the disturbance is at a level so that ΔP_{tie} approaches its limit, the NNMPC will stabilize ΔP_{tie} at the limit, while the RNMPC will keep some clearance to it in case of a new worst-case disturbance. And as seen from Figure 3.12(b), the RNMPC manages to keep within the tie-line limit when the worst-case disturbance sets in, while the NNMPC does not. In Figure 3.13 it is seen how the NNMPC and RNMPC allocates ΔP_m in area A and area B differently. It shows that the two controllers gives similar results, only that the RNMPC in general allocates more of ΔP_m to area A where the disturbance enters, resulting in a lower ΔP_{tie}. Both Figure 3.12(a) and Table 3.1 shows that the control performance of the NNMPC and RNMPC in case B are very similar, and there is some increase in the use of primary control while the use of AGC is lowered. However, these are very small numbers, and for all practical purposes the two controllers performs equally with regards to frequency restoration and reserves usage.

3.7 Conclusion

The negative trend seen in the quality of LFC in the Nordic power system over the last decades indicates that something must be done to better cope with the challenges of intermittent energy resources and network bottlenecks. In Ersdal et al. (2016a) it was shown how applying NMPC for AGC can improve the LFC by better coordination of AGC and primary control, as well as including power-transfer limits as constraints in the NMPC. In this work, this has been extended to include the robustified NMPC (RNMPC) from Ersdal et al. (2014), and simulations show that also with a more realistic simulation setup (including model-plant mismatch and state estimation), the RNMPC manages to keep transfer capacity available for severe situations of unpredicted fluctuations in produced wind power from the area of South Sweden and East Denmark. The behavior of the RNMPC was compared to that of the nominal NMPC (NNMPC) from Ersdal et al. (2016a), and Monte Carlo simulations show that the NNMPC is not able to avoid bottlenecks in the same way as the RNMPC. The NNMPC does perform better than the RNMPC on

average, but there will almost always be a trade off between system performance and robustness of a controller. The difference in performance and reserve usage is however not deterrent, and this work shows that the scheme presented here could be a realistic way of dealing with bottlenecks in the Nordic network, ensuring available transfer capacity so that all available resources are able to participate in the LFC.

Chapter 4

Scenario-based approaches for handling uncertainty in MPC for power system frequency control

The work in this chapter is submitted to IFAC World Congress 2017.

Summary

A stochastic nonlinear model predictive controller (SNMPC) is designed for automatic generator control of a proxy of the Nordic power system, and it is compared with a multi-stage nonlinear model predictive controller (MNMPC). Both controllers are scenario based, but originate in two different disturbance modeling paradigms; stochastic and deterministic. A simulation study indicates that the two controllers behave similarly. The MNMPC is however less exposed to infeasibility issues, and it also has better tractability than the SNMPC. On the other hand, the SNMPC gives probabilistic guarantees for constraint fulfillment; a feature whose practical implications are debatable.

4.1 Introduction

Model predictive control (MPC) is a framework for advanced control that has its roots in optimal control, and is one of the few advanced control methods that has made a significant impact on industrial control engineering (Maciejowski, 2002). In short, the MPC solves an optimal control problem (OCP) at each time step and then implements the first instant of the solution in a receding horizon manner.

The MPC relies on good knowledge of the system it is controlling, and the system model is very important. Full knowledge and 100% accurate models are however extremely rare, and in practise the MPC must be able to account for uncertainties and/or unmeasurable disturbances acting on the system. One way to systematically address this issue is through robust MPC (RMPC), which consideres uncertainties that are assumed to be deterministic and lie in a bounded set (Mesbah, 2016; Bemporad and Morari, 1999). The work on RMPC has been dominated by min-max OCP formulations (Bemporad et al., 2003; Scokaert and Mayne, 1998), and relaxations such as tube-based MPC (Langson et al., 2004). The RMPC is designed so that system constraints are fulfilled for all possible disturbances within the prediction horizon, which often can lead to conservative results. A practical approach to

achieve robust MPC which is not as conservative, is multi-stage MPC. The multi-stage MPC is based on a representation of the evolution of the uncertainty as a scenario tree (Lucia et al., 2013), where the uncertainty is assumed to be discrete. The concept of future feedback is also included by allowing different inputs for different disturbance scenarios, reducing the conservativeness of the robust approach (Lucia et al., 2013). Allowing feedback in the MPC results in what is known as feedback MPC, and in the presence of uncertainty, feedback MPC is known to be superior to nominal MPC, though resulting in a more complex OCP (Rawlings and Mayne, 2009). An alternative approach to implementing feedback MPC is optimizing over control laws $u = \mu(x)$, rather than control actions (Rawlings and Mayne, 2009). This is used in e.g. tube-base MPC. For the general nonlinear case, there are no guarantees that the multi-stage MPC results in robust constraints satisfaction for scenarios that are not included in the scenario tree, but it has been shown to give good results in practice (Lucia et al., 2013, 2014a).

An alternative to RMPC is stochastic MPC (SMPC), where the uncertainties are considered to be of probabilistic nature. The probabilistic description of uncertainties are used to define chance constraints (Li et al., 2002; Primbs and Sung, 2009) which enable systematic use of the stochastic description of uncertainties to define stochastic levels of acceptable closed-loop constraint violation (Mesbah, 2016), i.e. a small constraint violation probability is allowed. Chance-constrained optimization problems are hard to solve in general, and sample-based approximations such as the scenario approach (Campi et al., 2009) has been presented as tractable alternatives. In the scenario approach only a finite number of uncertainty realizations are considered, and the chance-constraint optimization problem is approximated by replacing the chance constraint with hard constraints associated with the extracted disturbance realizations only.

This work compares the performance of a stochastic nonlinear MPC (SNMPC) inspired by Campi et al. (2009) and a multi-stage nonlinear MPC (MNMPC) similar to the robustified NMPC in Ersdal et al. (2016b), for automatic generator control (AGC) of the Nordic power system. AGC is currently facing challenges related to stability and reliability due to more intermittent energy resources in the system as well as an increasing power demand, and during the last decade there has been an increasing interest in applying MPC for AGC, see for example Venkat et al. (2008); Shiroei et al. (2013); Ersdal et al. (2016a,b). SMPC has also been investigated as a method for reserve scheduling for power systems with wind power generation (Rostampour et al., 2013). In this work, the uncertainty of the model is dominated by the fluctuations in produced wind power, and the aim is to design an NMPC for AGC which is robust against these fluctuations.

The remainder of this chapter is organized as follows. In Section 4.2 the system model is presented, before the SNMPC and the MNMPC are discussed in Section 4.3. In Section 4.4, the details of the case study are given, and the results from simulations on the proxy model are presented. The concluding remarks are summarized in Section 4.5.

4.2 Model description

In large, complex power systems, such as the Nordic power system, one important control aspect is load frequency control (LFC). This is a term applied to describe the continuous operation of keeping the frequency of a power system stable, which is strongly connected to the balancing of produced and consumed power. It is vital for the power system that this power balance is maintained and that the produced power matches the consumed power at all times, if not the generators could loose synchronism and the power system would collapse.

AGC is the part of LFC that automatically controls the generator production set points, and in Ersdal et al. (2016a) a NMPC is designed for AGC of the Nordic power system. This is extended in Ersdal et al. (2016b) to a robustified NMPC which is designed to be more robust against fluctuations in produced wind power, by including worst-case scenarios of these. In both Ersdal et al. (2016a,b) the NMPC is based on a simplified model, while tested on a more rigorous and realistic proxy model. In this work, the same models will be used, however, only the equations for the NMPC prediction model (PM) are repeated here. The interested reader is referred to Ersdal et al. (2016b) for details of the SINTEF model, which is used as a proxy for the physical system.

In the Nordic power system the hydro turbines account for nearly 100% of the AGC, and so only the hydro turbine dynamics are included in the model. Other turbines are included as constant power inputs. The PM model is divided into N areas, and the equations for each area i are as follows

$$\Delta\dot{\bar{f}}^i = \frac{1}{2\bar{H}^i}\left(\Delta\bar{P}_m^i - \Delta\bar{P}_D^i - \Delta\bar{P}_{tie}^i\right) \tag{4.1a}$$

$$\Delta\dot{\bar{q}}^i = -\frac{2}{\bar{T}_w^i \bar{c}_{ss}^{i2}/\bar{q}_{ss}^i}\left(\Delta\bar{q}^i - \frac{\bar{q}_{ss}^{i2}}{\bar{c}_{ss}^{i2}}\Delta\bar{c}^i\right) \tag{4.1b}$$

$$\Delta\dot{\bar{\xi}}_2^i = -\frac{1}{\bar{T}_r^i}\Delta\bar{\xi}_2^i + \Delta\bar{c}^i \tag{4.1c}$$

$$\Delta\dot{\bar{\xi}}_3^i = \mathrm{sat}_{\dot{c}}^i\left(\frac{1}{\bar{T}_g^i}\left(\Delta\bar{c}_r^i - \Delta\bar{f}^i + \frac{\bar{r}^i}{\bar{T}_r^i}\Delta\bar{\xi}_2^i - \left(\bar{r}^i + \bar{\rho}^i\right)\Delta\bar{c}^i\right)\right) \tag{4.1d}$$

$$\Delta\dot{\bar{P}}_{tie}^i = 2\pi\left(\Delta\bar{f}^i \sum_{j=1,j\neq i}^{N} \bar{T}_{ij} - \sum_{j=1,j\neq i}^{N} \bar{T}_{ij}\Delta\bar{f}^j\right) \tag{4.1e}$$

where

$$\Delta\bar{P}_m^i = \bar{A}_t^i \frac{\bar{q}_{ss}^{i2}}{\bar{c}_{ss}^{i2}}\left(3\Delta\bar{q}^i - 2\frac{\bar{q}_{ss}^{i2}}{\bar{c}_{ss}^{i2}}\Delta\bar{c}^i\right) \tag{4.1f}$$

$$\Delta\bar{c}^i = \mathrm{sat}_c^i\left(\Delta\bar{\xi}_3^i\right) \tag{4.1g}$$

and $\Delta\bar{f}$ is the frequency, $\Delta\bar{P}_m$ the produced power, $\Delta\bar{P}_D$ the unpredicted power imbalance, $\Delta\bar{P}_{tie}$ the total power flow from the area to all other areas, $\bar{H}$ the inertia

of the rotating masses of the area, $\bar{T}_{ij}$ the synchronizing torque coefficient between area i and j, $\Delta\bar{c}$ and $\Delta\bar{q}$ the changes in valve opening and water flow rate from $\bar{c}_{ss}$ and $\bar{q}_{ss}$, respectively, $\bar{T}_w$ the water starting time of the hydro turbine, $\bar{A}_t$ a factor that accounts for the different per-unit bases in the turbine and generator, $\Delta\bar{\xi}_2$ the integral of the governor, $\Delta\bar{\xi}_3$ the valve opening of the main servo motor of the governor, $\bar{T}_g$ the time constant of the servo motor, $\bar{T}_r$ the time constant of the transient droop, $\bar{r}$ the transient-droop coefficient, $\bar{\rho}$ the constant-droop coefficient, $\Delta\bar{c}$ the saturated valve opening, $\Delta\bar{c}_r$ the reference point for the valve opening, and $i = 1, \ldots, N$. All defined relative an initial steady state. The controllable input to the system is the valve-opening setpoint for each area $\Delta\bar{c}_r^i$ and the participation factor for each generator j in area i, α_j^i, and the disturbance acting on the system is the unpredicted power imbalance for each area $\Delta\bar{P}_D^i$.

4.2.1 System disturbance

The only disturbance we consider is that of the unpredicted power imbalance $\Delta\bar{P}_D^i$. The main components of the unpredicted power imbalance with regards to LFC is the imbalance in production and consumption from intermittent generators and loads, respectively. When dealing with power systems including a certain amount of wind power, such as the Nordic system, one can for simplicity assume that $\Delta\bar{P}_D^i$ is dominated by the fluctuations in produced wind power. If, in addition, it is assumed that the majority of wind power is situated in area p, $\Delta\bar{P}_D$ of all the other areas can be neglected, and the model is affected by one single disturbance $\Delta\bar{P}_D = \Delta\bar{P}_D^p$. With the Nordic network in mind, Denmark and South Sweden contribute with about 80% of the total wind power production (Statnett, 2012).

The complete model is thus given by the nonlinear model

$$\dot{\bar{x}} = \bar{f}\left(\bar{x}, \bar{u}, \bar{w}\right) \tag{4.2}$$

where $\bar{x} = \begin{bmatrix}\Delta\bar{f}^i & \Delta\bar{q}^i & \Delta\bar{\xi}_2^i & \Delta\bar{\xi}_3^i & \Delta\bar{P}_{tie}^i\end{bmatrix}$, $\bar{u} = \begin{bmatrix}\Delta\bar{c}_r^i & \alpha_j^i\end{bmatrix}$, $\bar{w} = \Delta\bar{P}_D$, $i = 1, \ldots, N$, $j = 1, \ldots, m_h^i$, and m_h^i is the number of hydro generators in area i. The system is also subjected to both input and state constraints

$$\bar{g}\left(\bar{x}, \bar{u}\right) \leq 0 \tag{4.3}$$

including generation constraints, generator rate constraints, and constraints on the tie-line power transfer.

4.3 Controller

4.3.1 Disturbance modeling, deterministic vs stochastic.

When modeling a disturbance's influence on a system, it is common to differentiate between deterministic and stochastic modeling. A system disturbance w is in general defined by an admissible set of disturbance signals $w \in \mathcal{W}$, and the difference

between deterministic and stochastic modeling is whether or not one attempts to assign probabilities to the elements of the set $\mathcal{W}$ (Levine, 2010). With a deterministic disturbance model all realizations in $\mathcal{W}$ are bounded and considered equally likely to occur, while they are appointed different probabilities $\mathcal{P}[w]$ and are not necessarily bounded when applying a stochastic disturbance model.

The disturbance acting on the system presented in Section 4.2 is the unpredicted power imbalance $\bar{w} = \Delta\bar{P}_D$, which is assumed to be dominated by fluctuations in produced wind power in area p. For each wind farm in area p, the probability space of the future variation from the predicted power output can be estimated (Holttinen, 2004), and from this one can find the probability space of the future variation from the predicted power output for all wind farms in area p combined, i.e. $\bar{w} \in \mathcal{W}$, see Figure 4.2. The estimate of $\mathcal{W}$ is primarily based on weather prognoses, which are stochastic by nature through the use of ensemble forecasting and model output statistics (Barry and Chorley, 2003). Hence, it would in many ways be natural to assign probabilities to the elements of $\mathcal{W}$. However, it is not necessarily the best choice when taking other aspects into account, and in this chapter two scenario-based approaches are compared, the SNMPC that is based on a stochastic disturbance model, and the MNMPC that is based on a deterministic disturbance model. The aim of this chapter is to compare the two approaches, and discuss their strengths and weaknesses in view of their performance in the case study.

4.3.2 Stochastic NMPC

Given a system such as (4.2). If the disturbance signal $\bar{w}$ is modeled as a stochastic disturbance with probability space $\mathcal{W}$ and probability distribution $\mathcal{P}[\bar{w}]$ over $\mathcal{W}$, then it makes sense to replace hard constraints with chance constraints

$$\mathcal{P}_{\bar{w}}\left[\bar{g}\left(\bar{x},\bar{u}\right) \leq 0 \ \forall \ t\right] \geq 1-\sigma \tag{4.4}$$

where $\sigma \in (0,1)$ is the admissible constraint violation parameter, $t = 1,\ldots,T$, T is the optimization horizon, and $\mathcal{P}_{\bar{w}}$ denotes the dependency of $\bar{g}\left(\bar{x},\bar{u}\right)$ on the stochastic signal $\bar{w}$. It basically states that the constraints are allowed to be violated with a probability no higher than $1-\sigma$.

In scenario-based approaches to stochastic NMPC (Campi et al., 2009), S independent identically distributed samples of $\bar{w}$ $(\bar{w}^1,\ldots,\bar{w}^S)$ are used to approximate the chance constraint, where only the constraints corresponding to the extracted disturbance realizations are considered. The result is the SNMPC which includes a standard OCP with a finite number of constraints

$$\min_{\bar{u},\bar{x}^j} \sum_{j=1}^{S} J\left(\bar{x}^j,\bar{u}\right) \tag{4.5a}$$

$$\dot{\bar{x}}^j - \bar{f}\left(\bar{x}^j,\bar{u},\bar{w}^j\right) = 0 \text{ System model} \tag{4.5b}$$

$$\bar{g}\left(\bar{x}^j,\bar{u}\right) \leq 0 \text{ Constraints} \tag{4.5c}$$

where $j = 1, \ldots, S$, $\bar{x}^j$ and $\bar{w}^j$ are the state and disturbance associated with scenario j, $\bar{u}$ the input, and $J(\bar{x}^j, \bar{u})$ the following objective function.

$$J\left(\bar{x}^j, \bar{u}\right) = \int_{t=0}^{T} \bar{x}^{jT} Q^j \bar{x}^j + \bar{u}^T R \bar{u} \; dt \tag{4.6}$$

For convex OCPs, the scenario approach can be used to find the number of scenarios needed to guarantee that the optimal solution to (4.5), $\bar{u}^*$, satisfies all constraints except a user-chosen fraction that tends rapidly to zero as S increases (Campi et al., 2009). The OCP (4.5) in the SNMPC has a quadratic objective function and linear state and input constraints. The constraints imposed by the system model (4.5b) are however nonlinear because of the saturations in (4.1), hence the OCP is non-convex. It can however be argued that this is a modest nonlinearity, and we will apply the theory in Campi et al. (2009) as if we have a linear model and hence a convex OCP.

Generating scenarios

The scenarios used in the SNMPC are found by applying random numbers to generate S independent and identically distributed disturbance realizations $\bar{w}^j(t) = \Delta\bar{P}_D^j(t)$, $j = 1, \ldots, S$, $t = 0, \ldots, T$ using the method in Cecílio et al. (2013) with the probability space $\mathcal{W}$ as input. This method results in an unknown probability distribution $\mathcal{P}$, however, using the method of Campi et al. (2009) there is no need to know $\mathcal{W}$ or $\mathcal{P}$ explicitly, only S realizations fulfilling this probability distribution is needed. When selecting the number of scenarios S, Theorem 1 in Campi et al. (2009) states that given the number of optimization variables n_u, if S fulfills

$$S \geq \frac{2}{\kappa}\left(\ln\frac{1}{\beta} + n_u\right) \tag{4.7}$$

the resulting solution to (4.5), $\bar{u}^*$, will satisfy the chance constraints (4.4) with a probability no smaller than $1 - \beta$, except for at most an κ-fraction. Theorem 1 in Campi et al. (2009) is developed with one common input $\bar{u}$ for all scenarios, and so $\bar{u}$ is equal for all j in the SNMPC (4.5).

4.3.3 Multi-stage NMPC

In Ersdal et al. (2016b) an NMPC for AGC of the Nordic power system which is robustified against fluctuations in produced wind power is presented. It is a special case of the multi-stage NMPC (MNMPC) presented in Lucia et al. (2013), and it is also inspired by the min-max feedback MPC presented in Scokaert and Mayne (1998). In both Lucia et al. (2013) and Scokaert and Mayne (1998) the concept of future feedback is included in the NMPC. The idea is that the future control inputs can be adapted to the future disturbance measurements/estimates, and that only decisions based on the same information must be equal (Lucia et al.,

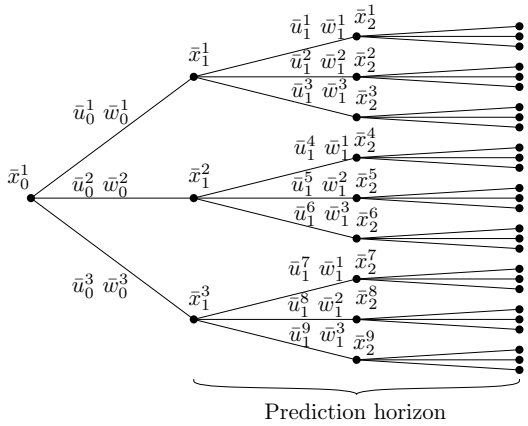

Figure 4.1: Scenario tree representation of the discrete uncertainty evolution for multi-stage NMPC (Lucia et al., 2013).

2013). A scenario tree is presented in Lucia et al. (2013), where the uncertainty is represented by discrete scenarios and the branches are combinations of values from the assumed extreme values of the disturbance, see Figure 4.1. If future feedback is not included, as is the case with the SNMPC, the input $\bar{u}$ would have to be equal for all disturbances and state evolutions in the scenario-tree. With a discrete disturbance representation, as depicted in Figure 4.1, this means that

$$\bar{u}_0^1 = \bar{u}_0^2 = \bar{u}_0^3 \tag{4.8}$$
$$\bar{u}_1^1 = \bar{u}_1^2 = \cdots = \bar{u}_1^9. \tag{4.9}$$

With the MNMPC, however, only the inputs originating in the same state must be equal, i.e.

$$\bar{u}_0^1 = \bar{u}_0^2 = \bar{u}_0^3 \tag{4.10}$$
$$\bar{u}_1^1 = \bar{u}_1^2 = \bar{u}_1^3 \tag{4.11}$$
$$\bar{u}_1^4 = \bar{u}_1^5 = \bar{u}_1^6 \tag{4.12}$$
$$\bar{u}_1^7 = \bar{u}_1^8 = \bar{u}_1^9 \tag{4.13}$$

Hence, the future inputs are allowed to change in accordance with new information received through feedback. This increases the flexibility of the NMPC and reduces the conservativeness of the robust approach (Lucia et al., 2013).

The robustified NMPC from Ersdal et al. (2016b) is from now on referred to as the multi-stage NMPC (MNMPC), and for this three disturbance realizations are considered; one following the positive border of $\mathcal{W}$, one following the negative border of $\mathcal{W}$, and one neutral in the middle. Compared to the scenario tree in Figure 4.1, this means that three paths are included: $\bar{w}^1 = \{\bar{w}_0^1, \bar{w}_1^1, \bar{w}_2^1, \ldots\}$, $\bar{w}^2 = \{\bar{w}_0{}^2, \bar{w}_1^2, \bar{w}_2^2, \ldots\}$, and $\bar{w}^3 = \{\bar{w}_0^3, \bar{w}_1^3, \bar{w}_2^3, \ldots\}$. These corresponds to $\bar{w}^p$, $\bar{w}^z$, and

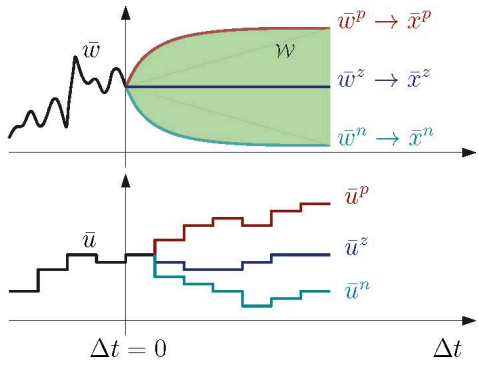

Figure 4.2: Sketch of how the MNMPC works. For simplicity of illustration, $\bar{u}$ is considered to be scalar.

$\bar{w}^n$ in Figure 4.2. In accordance to Lucia et al. (2013), the first element of $\bar{u}$ must be equal for all three scenarios ($\bar{u}_0^p = \bar{u}_0^z = \bar{u}_0^n$), after this, they are free to vary in manners optimal for their designated system states, see Figure 4.2.

The OCP solved at each time instant in the MNMPC is then

$$\min_{\bar{u}^j, \bar{x}^j} \sum_{j=\{p,z,n\}} J\left(\bar{x}^j, \bar{u}^j\right) \tag{4.14a}$$

$$\dot{\bar{x}}^j - \bar{f}\left(\bar{x}^j, \bar{u}^j, \bar{w}^j\right) = 0 \quad \text{System model} \tag{4.14b}$$

$$\left.\begin{array}{l} \tilde{g}\left(\bar{x}^j, \bar{u}^j\right) \leq 0 \\ \bar{u}_0^z = \bar{u}_0^p = \bar{u}_0^n \end{array}\right\} \text{ Constraints} \tag{4.14c}$$

where $j = \{p, z, n\}$, $\bar{x}^j$, $\bar{w}^j$, $\bar{u}^j$ the state, disturbance and input associated with scenario j, and $J(\bar{x}^j, \bar{u}^j)$ the following objective function.

$$J\left(\bar{x}^j, \bar{u}^j\right) = \int_{t=0}^{T} \bar{x}^{jT} Q^j \bar{x}^j + \bar{u}^{jT} R^j \bar{u}^j \; dt \tag{4.15}$$

4.4 Case Study

The SNMPC is tested on the SINTEF Nordic power system test bed from Ersdal et al. (2016b) and compared against the MNMPC. The PM is chosen to have 2 areas, hence $N = 2$. One area covers South Sweden and Eastern Denmark (area A), and the other covers Norway, North Sweden and Finland (area B), and according to the assumptions made in Section 4.2, $\Delta\bar{P}_D^B = 0$ and $\Delta\bar{P}_D = \Delta\bar{P}_D^A$. There is also a tie line between the two areas which represents the total power flow between them, and has a positive direction from area B to area A. The extended Kalman filter (EKF) presented in Ersdal et al. (2016b) is also applied here to close the control loop. The proxy system and both NMPCs were implemented in Python using Casadi, where the continuous time OCPs (4.5) and (4.14) are discretized and transformed into

nonlinear programs. Collocation has been used for discretization, and the OCPs are solved using the interior point optimizer IPOPT (Wächter and Biegler, 2006), using exact Hessian.

In order to obtain acceptable probability results in (4.7), the number of scenarios in the SNMPC-OCP should approach $S = 1000$. With the hardware and software used in this work, such a large number of scenarios imposes computer memory issues that are difficult to handle. This seems to be a problem for others who have implemented stochastic NMPC as well. In Rostampour et al. (2015), for example, it takes more than 5 days to solve the OCP with $S = 100$, while the sampling time of the NMPC is 15 s. We therefore limited us to $S = 65$. It is seen through simulations that the behavior of the SNMPC in the test case does not change much from $S = 10$ to $S = 65$, and so it is assumed that for the purpose of comparison with the MNMPC, the simulation results from $S = 65$ can be used as a representation of a stochastic NMPC scheme with more realistic values for β and κ.

In order to compare the performance of the two controllers, a control performance measure (CPM) is applied. It is inspired by the CPS1 and CPS2 performance criteria used by the North American electric reliability corporation (NERC) (Gross and Lee, 2001), and it basically measures the average frequency deviation: first $\Delta\bar{f}$ is averaged over windows of 30 s to filter out fast fluctuations, then the CPM is found by again averaging $\Delta\bar{f}$ over all these windows.

4.4.1 Tuning the NMPC

The main tuning variables for the NMPCs are the prediction horizon T and the objective function $J(\cdot)$.

$$J\left(\bar{x}^j, \bar{u}^j\right) = \int_{t=0}^{T} \bar{x}^{jT} Q^j \bar{x}^j + \bar{u}^{jT} R^j \bar{u}^j \; dt \tag{4.16}$$

For both the SNMPC and the MNMPC, Q is real, symmetric and positive semidefinite, while R is real, symmetric and positive definite. The non-zero elements of Q are chosen so that the deviation in overall system frequency is punished (Ersdal et al., 2016b): $q_{11} = \gamma \frac{\left(H^1\right)^2}{(H^1+H^2)^2}$, $q_{66} = \gamma \frac{\left(H^2\right)^2}{(H^1+H^2)^2}$, $q_{16} = q_{61} = \gamma \frac{H^1 H^2}{(H^1+H^2)^2}$, where $\gamma = 10^5$. The matrix R is set to $R = \text{diag}\left(\eta m_{\text{base}}\right)$, where m_{base} is a vector containing the hydro generators' base rating, and $\eta = 0.1$. For the MNMPC $Q^p = Q^n = 0.1Q^z$ in order to place more emphasis on deviations in x^z. The three systems are all punished equally when it comes to deviations in input: $R^z = R^p = R^n$. For the SNMPC all scenarios have the same Q and R.

The control horizon T is 3 minutes for both NMPCs, a decision based on a compromise between system time constants and complexity, and the time step of the NMPCs is 10 s in order to match the control signal dispatching in the system.

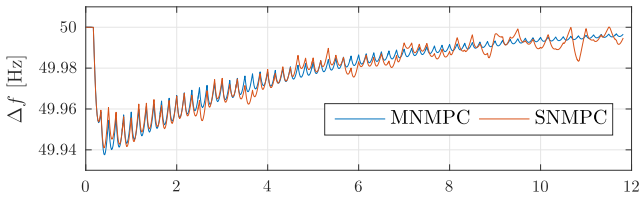

Figure 4.3: Case A: Frequency deviation Δf for MNMPC and SNMPC.

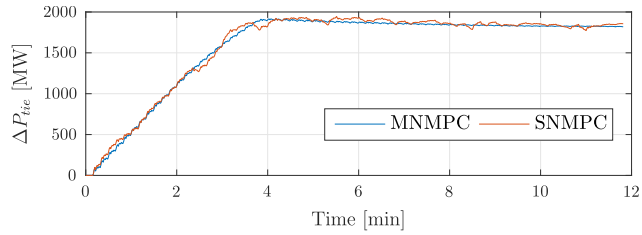

Figure 4.4: Case A: Tie-line power flow ΔP_{tie} for MNMPC and SNMPC.

4.4.2 Simulation results

Case A

Both the SNMPC and the MNMPC are simulated with a disturbance $\bar{w} = \bar{w}_n$, see Figure 4.2, and a maximum transfer limit from area B to area A at $\Delta \bar{P}_{tie,max} = 2000$ MW. The resulting Δf and ΔP_{tie} (without bar notation, as they are simulation-results from proxy model) can be seen in Figure 4.3 and 4.4. They show that the resulting frequency deviation and tie-line power flow is very similar in the two cases. Both controllers brings the frequency back to 50 Hz while keeping a clearance to the tie-line limit of 2000 MW in case of new disturbances. This is supported by the CPM given in Table 4.1. It is assumed that the similarity in behavior will increase concurrently with S, which makes sense as $\bar{w}^p$ and $\bar{w}^n$ defines the boundaries for $\mathcal{W}$ and hence for the scenarios $\bar{w}^j$. When the number of scenarios S is increased, so will the scenario's coverage of $\mathcal{W}$, resulting in a SNMPC which must take into account disturbance scenarios similar to $\bar{w}^n$ and $\bar{w}^p$. The SNMPC will also naturally place more emphasis on the average disturbance scenario through a higher scenario density near the center of $\mathcal{W}$, while the MNMPC does the same by applying a

Table 4.1: CPM and average optimization time T_{opt} for Case A.

Controller	CPM ($\cdot 10^{-5}$)	T_{opt}
Multi-stage	11.18	1.98 s
Stochastic	11.23	40.18 s
Difference	+0.5%	+1910%

higher weight to Q^n in the objective function.

However, as seen in Figure 4.3 and 4.4, the SNMPC results in a more "noisy" system behavior than the MNMPC. There are two main reasons for this. First of all, the scenarios used in the SNMPC fluctuate more than the smooth disturbance scenarios used in the MNMPC. These high frequency fluctuations will excite the fast system dynamics in the predictions, resulting in a more fluctuating and conservative controller. Secondly, the fact that the SNMPC has one common optimized input for all scenarios forces the input to fluctuate in order to fulfill system constraints for all scenarios, which again excites the dynamics of the actual system.

Case B

In Case B the transfer capacity on the tie line is changed so that the transfer window is more narrow than in Case A. The limits are now set to $\Delta\bar{P}_{tie,min} = -100$ MW and $\Delta\bar{P}_{tie,max} = 1000$ MW, resulting in a transfer window of 1100 MW. Figure 4.5 shows the predictions associated with $\bar{w}^p$ and $\bar{w}^n$ from the MNMPC-optimization at $t = 0$, and Figure 4.6 shows the predictions associated with two of the disturbance realizations from the last attempt at solving the SNMPC-optimization at $t = 0$.

In this case, the SNMPC was not able to find a feasible solution, and the reason for this is illustrated in Figure 4.6. It shows that the SNMPC is simply not able to find a common input which fulfills the system constrains for all disturbance scenarios over the entire prediction horizon. Up until approximately 2.5 minutes into the prediction horizon, the tie-line power transfer associated with $\bar{w}^{31}$ and $\bar{w}^{40}$ are kept at, or within, the transfer limits by keeping the total input relatively low. After this, however, it seems that some adjustments has to made, and the input is increased, likely as an effort to keep $\Delta\bar{P}^{31}_{tie}$ within the lower transfer limit. This in turn causes $\Delta\bar{P}^{40}_{tie}$ to increase, and violate the upper transfer limit, as seen in the zoomed square of Figure 4.6(a).

The MNMPC is on the other hand able to find a feasible solution, and even though both $\Delta\bar{P}^{p}_{tie}$ and $\Delta\bar{P}^{n}_{tie}$ stay at the limits, they never violate them. Figure 4.5(b) shows how the inputs associated with $\bar{w}^p$ and $\bar{w}^n$ are free to vary after the first two time steps (this is increased from one because of delays connected to the EKF), and this is the reason why the MNMPC is able to find a feasible solution while the SNMPC is not.

4.4.3 Discussion

The benefit of the SNMPC is clearly the stochastic guarantees for constraint fulfillment given by Theorem 1 in Campi et al. (2009). With $S \approx 1000$, it would be guaranteed that with no probability smaller than 0.99, $\bar{u}^*$ would satisfy all system constraints for all $\bar{w} \in \mathcal{W}$ except for a small fraction of them whose probability is smaller than or equal to 0.07. These are theoretical guarantees which cannot be made for the MNMPC. They are however made under unrealistic assumptions such as perfect prediction model, and the practical implications are therefore arguable.

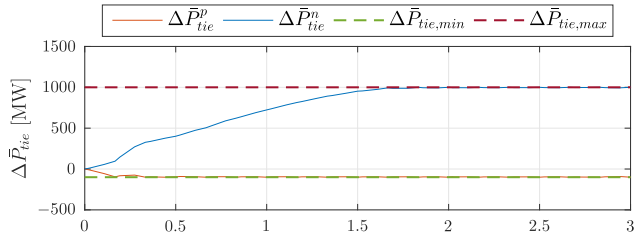

(a) Predicted tie-line power flow associated with $\bar{w}^p$ and $\bar{w}^n$.

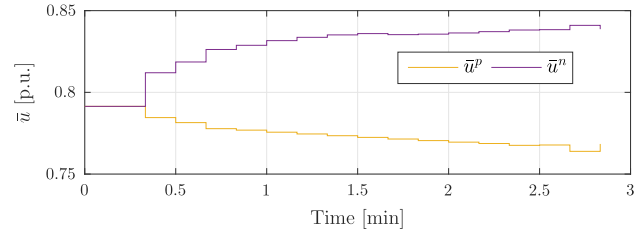

(b) Sum of predicted input associated with $\bar{w}^p$ and $\bar{w}^n$.

Figure 4.5: Case B MNMPC: Predicted input and tie-line power flow.

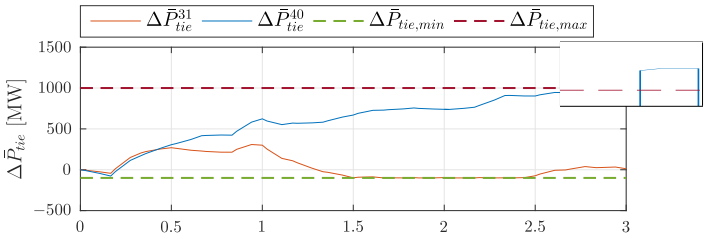

(a) Predicted tie-line power flow associated with $\bar{w}^{31}$ and $\bar{w}^{40}$.

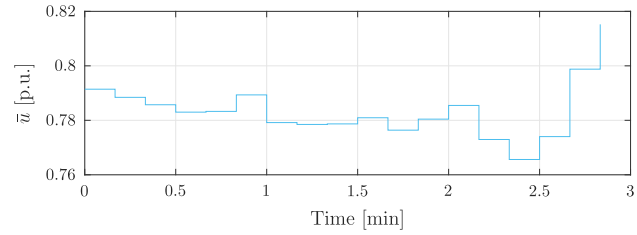

(b) Sum of predicted input for both $\bar{w}^{31}$ and $\bar{w}^{40}$.

Figure 4.6: Case B SNMPC: Predicted input and tie-line power flow.

It is the authors' opinion that the constraints of the control problem presented in this chapter are of such a nature that the practical difference with respect to constraint fulfillment is not prominent. However, it should be mentioned that the SNMPC does have the advantage of freedom to tune the conservativeness through the choice of η and β (and hence S), which is not as easy for the MNMPC.

There are also some issues with the tractability of the SNMPC as S increases. The MNMPC considers much fewer scenarios than the SNMPC, and therefore solves a much smaller OCP. This is reflected in the maximum optimization time in Case A, which was 2.1 s and 59.8 s for the MNMPC and the SNMPC, respectively, with an average optimization time of 2.0 s and 40.2 s. If a successful simulation of SNMPC with $S = 1000$ could be conducted, the optimization time would increase even further, and with a time step of 10 s, this means that the MNMPC is able to run in real time, whereas the SNMPC is not. It can be argued that some of these tractability issues can be resolved using more memory etc., however, the MNMPC will still solve the OCP in less time.

Another issue is the feasibility and recursive feasibility of the OCP. For both the MNMPC and the SNMPC there are no guarantees for neither feasibility nor recursive feasibility. However, in the MNMPC the optimization variable $\bar{u}$ for each disturbance realization $\{\bar{w}^z, \bar{w}^p, \bar{w}^n\}$ only needs to be equal for the first instant, before they are free to do what is optimal for their associated system states $\{\bar{x}^z, \bar{x}^p, \bar{x}^n\}$, whereas for the SNMPC $\bar{u}$ is equal for all disturbance realizations and their associated system states. This complicates matters for the SNMPC with regards to feasibility, as seen in Case B. When the scenarios included in the SNMPC results in diverging system behavior and thereby diverging inputs needs, it becomes increasingly difficult as S increases to find one common input to satisfy them all. It could be argued that feedback could be included in the SNMPC as well, this would however increase the already prominent tractability issues. If each of the scenarios of the SNMPC were to have their own input, the size of the OCP would increase substantially. In addition, since Theorem 1 from Campi et al. (2009) is developed with one common input for all scenarios, it may not hold if feedback was included. When it comes to recursive feasibility, the MNMPC results in a standard, nominal NMPC, and recursive feasibility can be guaranteed using classical methods such as terminal constraint regions which are control invariant (Maiworm et al., 2015), provided that such terminal ingredients can be calculated a priori. In the general nonlinear case it is however very challenging to find the necessary terminal ingredients, and if they can be found, they often lead to overly conservative control laws (Lucia et al., 2014b).

The MNMPC and the SNMPC are based upon two different disturbance modeling paradigms; deterministic and stochastic. And even though it could be argued that it is intuitive to view the future variation from the predicted wind-power production as stochastic, the robust control issue in this work is mainly handling the worst case disturbance, since handling of the worst-case disturbance implies that less severe disturbances can be handled as well. The case study presented in this chapter illustrates that the SNMPC and the MNMPC have some similarities in practice,

however, the MNMPC is less conservative and less likely to encounter feasibility issues because it takes into account feedback in its predictions.

4.5 Conclusion

This chapter presents a stochastic NMPC (SNMPC) for frequency control of the Nordic power system, and compares it with the multi-stage NMPC (MNMPC) presented in Ersdal et al. (2016b). The nonlinearities of the SNMPC are very modest, and the theory on stochastic assurance of constraint fulfillment from Campi et al. (2009) is used as if the optimal control problem of the SNMPC was convex.

Simulations on a proxy of the Nordic power system show that the SNMPC and the MNMPC behaves similarly, and it argued that the SNMPC and the MNMPC share some properties in practice. However, the MNMPC does not give stochastic guarantees for constraint fulfillment, such as the SNMPC. The practical consequences of this are unclear, especially given that these guarantees does not take into account other unknown disturbances and model errors. On the other hand, the MNMPC is less likely to encounter infeasibility, and there are also tractability and real-time issues with the SNMPC which are not seen in the MNMPC.

Chapter 5

Coordinated control of multiple HVDC links using backstepping

The work in this chapter was published in Ersdal et al. (2012).

Summary

This chapter regards a power system containing multiple High Voltage Direct Current (HVDC) links. The topic is to exploit the HVDC lines' ability to control the power supplied by them to increase the stability of the system. The nonlinear controller-design method backstepping is applied to design a controller for the direct current (DC) through each HVDC link. The simulation results show that the controller increases both transient stability and damping when some non-permanent errors are imposed on the system.

5.1 Introduction

The electric power systems in Europe today are complex dynamical systems of high dimension consisting of interconnected generators, transmission lines, loads etc. In order to keep the power supply safe and stable, it is important that all the generating units of an alternating current (AC) power system operate at the same frequency. The recent and ongoing liberalization of the energy market as well as increasing demand has in some cases reduced the stability margin of the power systems (Morison et al., 2004), and it has become important to augment their stability. Some of the possibilities for improving the power system stability are:

1. building new transmission lines,
2. installing new generation capacity,
3. better utilize the existing equipment in the power system.

High Voltage Direct Current (HVDC) links are in general used to transmit large amounts of energy over long distances. Norway is for example connected to the Netherlands and Denmark with underwater HVDC cables. But HVDC lines also

have the ability of direct control of its power flow (Casazza and Delea, 2003), and the current through already existing HVDC lines can therefore serve as a control input to help stabilize the AC network.

Improving system stability using a single HVDC link has been discussed in several papers, examples being Smed and Andersson (1993) and Li (2003). Applying more than one HVDC link for stability improvement allows for coordinated control of the HVDC links, and perhaps improving the stability even more (Eriksson et al., 2010). Coordinated control of several HVDC links is discussed in e.g. Eriksson et al. (2010), Eriksson and Knazkins (2008) and Pilotto et al. (1995).

Even though the current through the HVDC lines can be directly controlled, there are of course some restraints on both the amount of current that can pass, as well as the rate of change. The limitation on the power transmission capacity of HVDC lines is dominated by the maximum allowed conductor temperature (Weimers, 2000). The NorNed transmission line between Norway and the Netherlands, for example, has a capacity of 700 MW which is transferred at 450 kV. This gives a maximum current of approximately 780 A.

The problem investigated in this chapter is inspired by the work in Eriksson et al. (2010) on utilization of HVDC links to enhance system stability and dampen system oscillations. A major difference is that here the backstepping method will be applied in designing the nonlinear controller, instead of input-output exact linearization. Backstepping allows reduced control effort by not canceling damping terms.

The outline of the chapter is as follows. In Section 5.2 an overall system description is given, and the control problem is defined. Section 5.3 is devoted to designing the state feedback law using the backstepping method. The specific network used for simulation is presented in Section 5.4, along with the simulation results. These are then discussed in Section 5.5 and the conclusion is drawn in Section 5.6.

5.2 System description

Consider two separated power systems connected by p HVDC links. Each of the two power systems contains m and n nodes, respectively. Each of these nodes is connected to a synchronous generator and a load, which represents the equivalent of a larger, more complex network. Each of these separated power systems can therefore represent systems of various size and complexity.

The swing equation for generator k is given as

$$\dot{\delta}_k = \omega_k \tag{5.1a}$$

$$\dot{\omega}_k = \frac{1}{H_k}\left(P_{mk} - \mathcal{R}e\left(E_{gk}I_{gk}^*\right) - D_k\omega_k\right) \tag{5.1b}$$

where δ_k is the rotor angle and ω_k the rotor angular velocity, both given in reference to the 50 Hz reference frame, P_{mk} the mechanical power produced by the turbine, $P_{ek} = \mathcal{R}e\left(E_{gk}I_{gk}^*\right)$ the electrical power acting on the rotor, E_{gk} the voltage of the

internal bus, I_{gk} the current from generator k, H_k the moment of inertia, and D_k the damping coefficient.

From (5.1), it can be shown that the set of nonlinear differential equations for several generators connected by a power grid and HVDC lines can be written

$$\dot{\delta} = \omega \tag{5.2a}$$
$$\dot{\omega} = \psi(\delta, \omega) + \phi(\delta) I_{DC} \tag{5.2b}$$

where $\delta = \begin{bmatrix} \delta_1 & \cdots & \delta_{m+n} \end{bmatrix}^T$, $\omega = \begin{bmatrix} \omega_1 & \cdots & \omega_{m+n} \end{bmatrix}^T$, and I_{DC} is a $p \times 1$-vector containing the current through the HVDC lines. The connection between $I_{DC} = \begin{bmatrix} I_{DC,1} & \cdots & I_{DC,p} \end{bmatrix}^T$ and the currents from the generators $I_G = \begin{bmatrix} I_{g1} & \cdots & I_{g(m+n)} \end{bmatrix}^T$, is given by the algebraic equations for the network, and the procedure is explained in more detail in Section 5.4.

Since the networks are connected through DC lines, the frequencies can be different at each network. However, for stability reasons, they should be equal for the generators working together in the same AC grid. The purpose of the controller designed here is to make sure that this is fulfilled by asymptotically stabilizing the generator frequency differences.

The system states to be stabilized for each AC network are therefore chosen as

$$\begin{aligned} \eta_{i1} &= \delta_{i1} - \delta_{i2} \\ &\vdots \\ \eta_{is-1} &= \delta_{i1} - \delta_{is} \\ \zeta_{i1} &= \omega_{i1} - \omega_{i2} \\ &\vdots \\ \zeta_{is-1} &= \omega_{i1} - \omega_{is} \end{aligned}$$

where $i = \{1, 2\}$ specifies the AC network, $s = \{m, n\}$ is the number of nodes in the AC network, and δ_{ij} and ω_{ij} are associated with the generator at node ij. The system dynamics for the two AC networks combined then become

$$\begin{aligned} \dot{\eta}_{ij} &= \zeta_{ij} \\ \dot{\zeta}_{ij} &= \Psi_{ij}(\eta_{ij}, \zeta_{ij}, t) + \Phi_{ij}(\eta_{ij}, t) I_{DC} \end{aligned}$$

With $\eta = \begin{bmatrix} \eta_{11} & \cdots & \eta_{1m} & \eta_{21} & \cdots & \eta_{2n} \end{bmatrix}^T$ and $\zeta = \begin{bmatrix} \zeta_{11} & \cdots & \zeta_{1m} & \zeta_{21} & \cdots & \zeta_{2n} \end{bmatrix}^T$, we can collect

$$\dot{\eta} = \zeta \tag{5.3a}$$
$$\dot{\zeta} = \Psi(\eta, \zeta, t) + \Phi(\eta, t) I_{DC} \tag{5.3b}$$

where

$$\Psi(\eta,\zeta,t)=\begin{bmatrix}\Psi_{11}(\eta,\zeta,t)\\ \vdots\\ \Psi_{1m}(\eta,\zeta,t)\\ \Psi_{21}(\eta,\zeta,t)\\ \vdots\\ \Psi_{2n}(\eta,\zeta,t)\end{bmatrix},\ \Phi(\eta,t)=\begin{bmatrix}\Phi_{11}(\eta,t)\\ \vdots\\ \Phi_{1m}(\eta,t)\\ \Phi_{21}(\eta,t)\\ \vdots\\ \Phi_{2n}(\eta,t)\end{bmatrix}.$$

It is not possible to write $\dot{\zeta}$ merely as a function of η, ζ and I_{DC}, there will also be dependencies on the original system variables ω and δ. This is solved by regarding δ and ω as time varying signals, hence the time-dependence in the system.

Since η does not necessarily have an equilibrium at the origin, a change of variables is made so that $\bar{\eta}=\eta-\eta_0$:

$$\dot{\bar{\eta}}=\zeta \tag{5.4a}$$

$$\dot{\zeta}=\Psi(\bar{\eta}+\eta_0,\zeta,t)+\Phi(\bar{\eta}+\eta_0,t)\,I_{DC} \tag{5.4b}$$

where η_0 is the equilibrium of (5.3a) and

$$\Psi(\bar{\eta}+\eta_0,\zeta,t)=\Psi_R(\bar{\eta}+\eta_0,\zeta,t)-D\zeta \tag{5.5}$$

where $D\zeta$ contains the "good" damping terms of $\Psi(\bar{\eta}+\eta_0,\zeta,t)$, and $\Psi_R(\bar{\eta}+\eta_0,\zeta,t)$ contains the remaining elements. The good damping terms consists of terms that provides desirable damping to the system states. The matrix D is a $r\times r$ diagonal matrix containing combinations of $\frac{D_k}{M_k}$, where $r=m+n$. The equilibrium of ζ is $\zeta=0$, and the system (5.4) therefore has its equilibrium at the origin.

Assumption 1. *It is in the following assumed that $\Phi(\bar{\eta}+\eta_0,t)$ is quadratic, that is, ζ and I_{DC} have the same dimension, and invertible.*

This assumption is restrictive with regards to the configuration of the power system, and future work should include relaxing this assumption and considering a more general network configuration.

5.3 Controller Design

Backstepping is a recursive procedure for designing nonlinear controllers. It requires full state feedback, and it is therefore assumed that all system states are either measured by phasor measurement units (PMU) or that they are estimated by a state estimator.

Consider systems on the form

$$\dot{\eta}=f(\eta)+g(\eta)\,\zeta \tag{5.6a}$$

$$\dot{\zeta}=u \tag{5.6b}$$

The idea behind backstepping is to break the design problem for the full system into a sequence of design problems for lower order subsystems (Krstić et al., 1995). First ζ is viewed as a virtual input to stabilize η, then the stabilizing virtual input is "backstepped" through the integrator to find the actual input u which stabilizes both η and ζ.

Applying backstepping to systems on the form (5.6) is referred to as integrator backstepping (Khalil, 2002). Backstepping may also be applied to systems on the more general form

$$\dot{\eta} = f(\eta) + g(\eta)\zeta \tag{5.7a}$$

$$\dot{\zeta} = f_a(\eta, \zeta) + g_a(\eta, \zeta)u \tag{5.7b}$$

where η is known as the internal dynamics and ζ as the external dynamics. The external dynamics must have the same dimension as the input u, and it is convenient that the equilibrium point of the system is at the origin.

Since (5.4) is on this form, with I_{DC} as input u, we can design a controller for it using backstepping. This is summarized in the following Theorem, where we avoid canceling the "good" damping terms.

Theorem 1. *Under Assumption 1, the origin of (5.4) can be asymptotically stabilized by letting*

$$I_{DC} = \Phi^{-1}(\bar{\eta} + \eta_0, t)\left[-K_2^T z - \bar{\eta} - \Psi_R(\bar{\eta} + \eta_0, \zeta, t) - K_1\zeta\right] \tag{5.8}$$

where $z = \zeta + K_1\bar{\eta}$ and K_1 and K_2 are positive definite, constant matrices chosen such that

$$Q = \begin{bmatrix} K_1 & -0.5DK_1 \\ -0.5DK_1 & D^T + K_2 \end{bmatrix} \tag{5.9}$$

is positive definite.

Proof. Consider the Lyapunov function

$$V = 0.5\bar{\eta}^T\bar{\eta} + 0.5z^T z \tag{5.10}$$

where

$$z = \zeta - \gamma(\bar{\eta}) \tag{5.11}$$

$$\gamma(\bar{\eta}) = -K_1\bar{\eta} \tag{5.12}$$

Applying the controlled input I_{DC} in (5.8) on the system (5.4) results in the following time derivative of the Lyapunov function

$$\dot{V} = -\begin{bmatrix}\bar{\eta}^T & z^T\end{bmatrix}\begin{bmatrix} K_1 & -0.5DK_1 \\ -0.5DK_1 & D^T + K_2 \end{bmatrix}\begin{bmatrix}\bar{\eta} \\ z\end{bmatrix} \tag{5.13}$$

$$= -q^T Q q < 0 \tag{5.14}$$

Thus with (5.8) as input and (5.10) as Lyapunov function, it is clear that

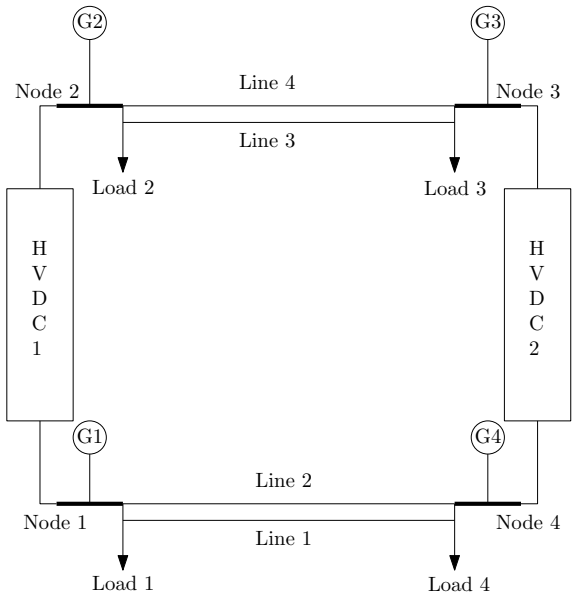

Figure 5.1: Power system consisting of four synchronous machines and two HVDC links (Eriksson et al., 2010).

1. $V(\bar{\eta}, z)$ is positive definite and decrescent with respect to (η, ζ),

2. $\dot{V}(\bar{\eta}, z)$ is negative definite with respect to (η, ζ),

and according to Theorem 4.9 in (Khalil, 2002), the origin of (5.4) is uniformly asymptotically stable. □

5.4 Network example

Both the network model and the HVDC model described in the following are mainly based on those presented in Eriksson et al. (2010), but differ somewhat in presentation. This section also serves to detail the modeling procedure outlined in Section 5.2.

The network used for testing the controller is shown in Figure 5.1. It consists of four synchronous generators, four loads, four transmission lines and two HVDC links. This network model is a special case of the model presented in Section 5.2, with $p = m = n = 2$. The detailed model of the HVDC lines and the AC network are presented in the following.

5.4.1 HVDC model

As in Eriksson et al. (2010), the HVDC lines are of conventional type, meaning that reactive power is consumed by them and that the active power through them can be controlled via the DC current. It is assumed that the HVDC lines are lossless and have ideal control capabilities. It is also assumed that the power factors on both the inverter and rectifier side are equal. Positive direction for the current through HVDC link 1 and 2 are from node 1 to node 2 and from node 4 to node 3, respectively. This means that the current injected from the HVDC links have positive sign at node 2 and 3 and negative sign at node 1 and 4 of Figure 5.1.

Assuming that the absolute value of the node voltages at each side of the HVDC links are approximately equal, the injected current at node k by HVDC link l is given as

$$I_{HVDC,kl} = I_{DC,kl} \cdot e^{j\theta_k} \tag{5.15}$$

where θ_k is the voltage angle at node k, and $I_{DC,l}$ is the controlled DC current through HVDC link l. Assuming that node k is directly connected to HVDC link l, then $I_{DC,kl} = -I_{DC,l}$ if node k is at the rectifier side, and $I_{DC,kl} = I_{DC,l}$ if node k is at the inverter side. If node k and HVDC link l are not directly connected, $I_{DC,kl} = 0$.

Defining $I_{HVDC,k}$ as the total current injected at node k by both HVDC-links, leads to the following

$$I_{HVDC} = \begin{bmatrix} I_{HVDC,1} \\ I_{HVDC,2} \\ I_{HVDC,3} \\ I_{HVDC,4} \end{bmatrix} = \begin{bmatrix} -e^{i\theta_1} & 0 \\ e^{i\theta_2} & 0 \\ 0 & e^{i\theta_3} \\ 0 & -e^{i\theta_4} \end{bmatrix} I_{DC} \tag{5.16}$$

where $I_{DC} = \begin{bmatrix} I_{DC,1} & I_{DC,2} \end{bmatrix}^T$.

5.4.2 Network model

The algebraic equation for the current flow in the network is found using the internal node representation, where it is assumed that the loads in the network are constant resistances. Defining all currents as positive into node k, Kirchoff's current law gives

$$I_{gk} + I_{Lk} + I_{HVDC,k} + \sum_{l=1}^{n+m} Y_{kl} U_l = 0 \tag{5.17}$$

where I_{gk} is the current injected by generator k, I_{Lk} the current from load k, $I_{HVDC,k}$ the current injected by the HVDC-links, Y_{kl} the systems admittance matrix at position (k, l), U_l the voltage at node l, and $n + m$ the number of nodes in the network.

The current injected from generator k into node k is given by

$$I_{gk} = \frac{E_{gk} - U_k}{jx'_{dk}}, \; \forall \; k = 1, \ldots, 4 \tag{5.18}$$

where E_{gk} is the voltage at the internal bus of generator k, and x'_{dk} is the generators transient reactance. The current from load k into node k is given by

$$I_{Lk} = -\frac{U_k}{R_k} \tag{5.19}$$

where R_k is the load resistance.

Combining (5.17)-(5.19) gives the following compact equation

$$\begin{bmatrix} I_G \\ I_{HVDC} \end{bmatrix} = \begin{bmatrix} Y_A & Y_B \\ Y_C & Y_D \end{bmatrix} \begin{bmatrix} E \\ U \end{bmatrix} \tag{5.20}$$

where $I_G = \begin{bmatrix} I_{g1} & \dots & I_{g4} \end{bmatrix}^T$. Eliminating U from the equation yields

$$\begin{aligned} I_G &= \left(Y_A - Y_B Y_D^{-1} Y_C\right) E + Y_B Y_D^{-1} I_{HVDC} \\ &= Y_{RNM} E + Y_{HVDC} I_{HVDC} \end{aligned} \tag{5.21}$$

Replacing I_{gk} in (5.1) with (5.21), and assuming that the absolute value of the generator's internal voltage $|E_{gk}|$ is constant, the system can be written as a set of nonlinear differential equations $\dot{x} = h\left(x, I_{DC}\right)$:

$$\dot{\delta}_1 = \omega_1 \tag{5.22}$$

$$\dot{\delta}_2 = \omega_2 \tag{5.23}$$

$$\dot{\delta}_3 = \omega_3 \tag{5.24}$$

$$\dot{\delta}_4 = \omega_4 \tag{5.25}$$

$$\begin{aligned} \dot{\omega}_1 = \frac{1}{M_1}\big[& P_{m1} - D_1\omega_1 - G_{11}E_{g1}^2 \\ & - E_{g1}E_{g4}\left(B_{14}\sin\left(\delta_1 - \delta_4\right) + G_{14}\cos\left(\delta_1 - \delta_4\right)\right) \\ & + E_{g1}\left(F_{11}\cos\left(\delta_1 - \theta_1\right) + K_{11}\sin\left(\delta_1 - \theta_1\right)\right) I_{DC,1} \\ & + E_{g1}\left(F_{14}\cos\left(\delta_1 - \theta_4\right) + K_{14}\sin\left(\delta_1 - \theta_4\right)\right) I_{DC,2}\big] \end{aligned} \tag{5.26}$$

$$\begin{aligned} \dot{\omega}_2 = \frac{1}{M_2}\big[& P_{m2} - D_2\omega_2 - G_{22}E_{g2}^2 \\ & - E_{g2}E_{g3}\left(B_{23}\sin\left(\delta_2 - \delta_3\right) + G_{23}\cos\left(\delta_2 - \delta_3\right)\right) \\ & - E_{g2}\left(F_{22}\cos\left(\delta_2 - \theta_2\right) + K_{22}\sin\left(\delta_2 - \theta_2\right)\right) I_{DC,1} \\ & - E_{g2}\left(F_{23}\cos\left(\delta_2 - \theta_3\right) + K_{23}\sin\left(\delta_2 - \theta_3\right)\right) I_{DC,2}\big] \end{aligned} \tag{5.27}$$

$$\begin{aligned} \dot{\omega}_3 = \frac{1}{M_3}\big[& P_{m3} - D_3\omega_3 - G_{33}E_{g3}^2 \\ & - E_{g3}E_{g2}\left(B_{32}\sin\left(\delta_3 - \delta_2\right) + G_{32}\cos\left(\delta_3 - \delta_2\right)\right) \\ & - E_{g3}\left(F_{32}\cos\left(\delta_3 - \theta_2\right) + K_{32}\sin\left(\delta_3 - \theta_2\right)\right) I_{DC,1} \\ & - E_{g3}\left(F_{33}\cos\left(\delta_3 - \theta_3\right) + K_{33}\sin\left(\delta_3 - \theta_3\right)\right) I_{DC,2}\big] \end{aligned} \tag{5.28}$$

$$\begin{aligned}\dot{\omega}_4 = \frac{1}{M_4}\big[&P_{m4} - D_4\omega_4 - G_{44}E_{g4}^2 \\ &- E_{g4}E_{g1}\left(B_{41}\sin\left(\delta_4-\delta_1\right)+G_{41}\cos\left(\delta_4-\delta_1\right)\right) \\ &+ E_{g4}\left(F_{41}\cos\left(\delta_4-\theta_1\right)+K_{41}\sin\left(\delta_4-\theta_1\right)\right)I_{DC,1} \\ &+ E_{g4}\left(F_{44}\cos\left(\delta_4-\theta_4\right)+K_{44}\sin\left(\delta_4-\theta_4\right)\right)I_{DC,2}\big]\end{aligned} \tag{5.29}$$

where $Y_{RNM}(k,l) = G_{kl} + jB_{kl}$, and $Y_{HVDC}(k,l) = F_{kl} + jK_{kl}$, which easily can be written as (5.2). The system is then written as (5.4) with $\eta = \begin{bmatrix}\delta_2 - \delta_3 & \delta_1 - \delta_4\end{bmatrix}^T$ and $\xi = \begin{bmatrix}\omega_2 - \omega_3 & \omega_1 - \omega_4\end{bmatrix}^T$.

For this system, the "good" damping terms in D of (5.5) is equal to

$$D = \begin{bmatrix}\frac{D_2}{M_2} + \frac{D_3}{M_3} & 0 \\ 0 & \frac{D_1}{M_1} + \frac{D_4}{M_4}\end{bmatrix} \tag{5.30}$$

These contribute to stabilization, and the controller should therefore not cancel them.

Because of $I_{HVDC,kl}$'s dependency on θ_k, it is not possible to entirely eliminate the nodal voltages from the differential equations, but

$$I_G = Y_A E + Y_B U \tag{5.31}$$

from (5.20) may be applied to find U at each time step by knowledge of the previous I_G and E:

$$U(t) = Y_B^{-1}\left(I_G(t-1) - Y_a E(t-1)\right) \tag{5.32}$$

5.4.3 Simulation

In this section the controller is tested with different types of faults imposed on the system. None of these faults are known beforehand. During the simulations, P_{mk} is kept constant for all generators, and the tuning parameters were in all four cases set to $K_1 = 70\mathcal{I}$ and $K_2 = 160\mathcal{I}$, where $\mathcal{I}$ is the 2×2 identity matrix. The maximum current through the HVDC lines were set to be 1.5 pu.

Case A

First the controller is tested with no model-plant mismatch, and initial conditions outside the equilibrium. The simulation results with and without controller can be seen in Figure 5.2, and it shows that the controller clearly dampens the oscillations in a satisfying manner, and makes the system states converge.

Case B

Second, the controller is tested with the system fault identified as Case III in Eriksson et al. (2010): Load 4 is doubled for 100 ms at $t = 0.5$ s, while the controller is based on the nominal load. Figure 5.3 shows simulations with initial condition at the equilibrium, with and without controller. Clearly the controller handles the fault satisfyingly, by both decreasing the amplitude and eliminating oscillations.

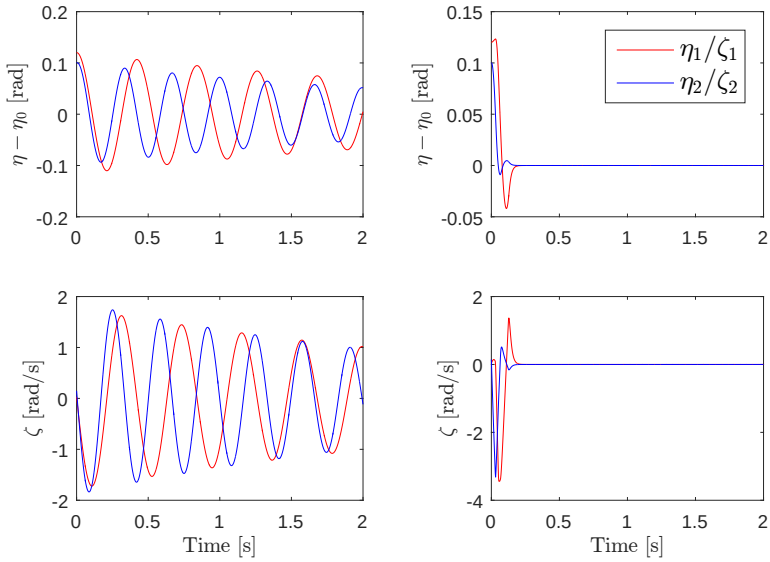

(a) Without controller. (b) With controller.

Figure 5.2: Simulation results with error from Case A: Initial conditions outside the equilibrium.

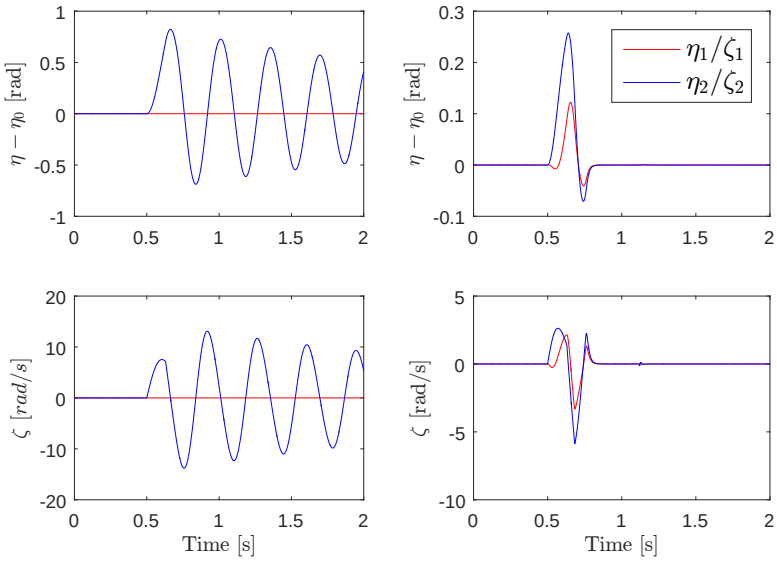

(a) Without controller. (b) With controller.

Figure 5.3: Simulation results with error from Case B: Load 4 is doubled for 100 ms.

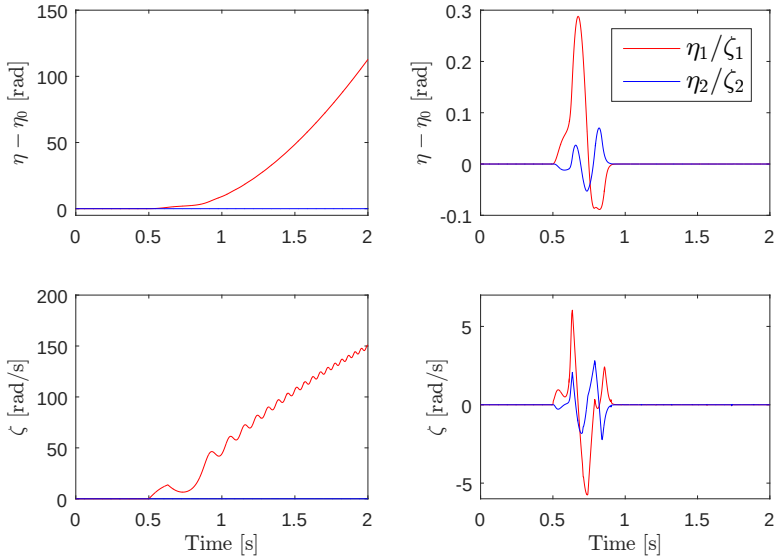

(a) Without controller. (b) With controller.

Figure 5.4: Simulation results with error from Case C: Three phase to ground error in line 4.

Case C

Next, a fault similar to that identified as case II in Eriksson et al. (2010) is introduced to the system. Here, line 4 has a three phase to ground error at $t = 0.5$ which lasts for 130 ms. The simulation results with and without controller, and with initial conditions at the equilibrium can be seen in Figure 5.4. The open-loop system diverges, but also here the controller performs well and stabilizes the system.

Case D

Last the controller was tested with a permanent fault of 5% increase in the load at node 4 occuring at $t = 0.5$ s. Since the fault is permanent the system's equilibrium is altered. This means that after $t = 0.5$ s, not only is the controller based on the wrong system model but it is also trying to control the system to a state that is no longer its equilibrium. Figure 5.5 shows the results from the simulations with and without controller, and with initial conditions at the equilibrium. It shows that the controller manages to stabilize the system, however at an equilibrium different than that of the non-faulty system.

5.4.4 Current through the HVDC lines

For all the examples given above, the value of I_{DC} is saturated due to the limitation on power transmission capacity. If one were to simulate without these limitations,

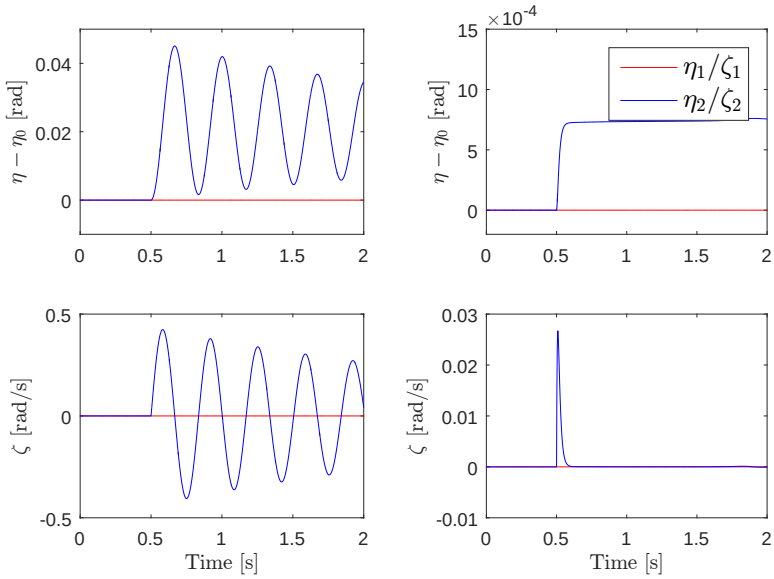

(a) Without controller. (b) With controller.

Figure 5.5: Simulation results with error from Case D: Permanent 5% increase in load 4.

one would see that the maximum value of I_{DC} is dominated by current peaks, often occurring during steady state. These peaks can also be seen when studying the input during simulations including saturation, but naturally their amplitude is then equal to the saturation limit. See for example Figure 5.6, which displays I_{DC} for Case B. It can be seen from Figure 5.3 that the system is at steady state from $t \approx 0.8$ s, and yet there are current peaks in the control signals at $t \approx 1.12$ s and $t \approx 1.28$ s.

5.5 Discussion

When the faults imposed on the system only last for a short while, and the amount of time where the controller is based on the wrong system is relatively short, the controller both increases transient stability and dampening of the system. This is because even though the Lyapunov function may grow during the fault, it is again guaranteed to sink from the time the fault has passed, hence bringing the system back to steady state.

When relatively small permanent faults are present, the controller brings the system to a new steady state. The reason for this is that the controller does not include integral control, resulting in a steady state error in η. However, for our control objective it does not matter where the equilibrium of η is.

There is no guarantee that the controller will increase stability in the case of

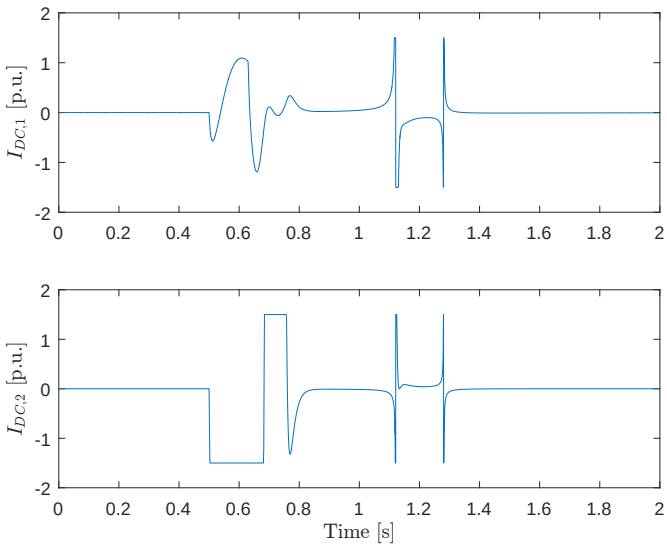

Figure 5.6: I_{DC} from simulations with the error from Case B: Load 4 is doubled for 100 ms.

arbitrarily large permanent faults. In order for the controller to handle larger permanent faults, the model should be properly updated when loads or network configuration change.

Due to the saturation in I_{DC}, it sometimes tends to rapidly shift between $\pm\sigma$ when stabilizing the system, where σ is the saturation limit. Since there in real life are limits on the current's rate of change as well, these instant shifts will rather be steep slopes limited by the current's maximum rate of change. How this will affect the controller is not investigated here.

The peaks occurring during steady state in I_{DC}, seen in Figure 5.6, arise due to singularities in $\Phi\left(\bar{\eta}+\eta_0, t\right)$. These singularities appears at arbitrary moments in time, often during steady state, because of the changes in the generator angles $\delta_k(t)$. This means that Assumption 1 does not hold for these short moments. The peaks do not affect the system states when the system is at steady state. However, when the systems' equilibrium is altered due to permanent faults, and it is at steady state outside the origin, they lead to fluctuations from the equilibrium.

This is a significant problem with the presented controller. Even with saturation, eliminating the high amplitude of these peaks, they still cause trouble especially when there are permanent faults in the system. This is therefore an issue that needs to be further addressed, and is an important part of the further work that may be done with regards to this controller.

A nice feature of the presented controller which is not illustrated in the simulations, is that when I_{DC} does not reach saturation, only the part of the system that is subjected to fault is affected by the controller. The reason for this is simply that in the closed-loop dynamics, $\dot{\eta}_1$ and $\dot{\zeta}_1$ are functions of η_1 and ζ_1 and $\dot{\eta}_2$ and $\dot{\zeta}_2$ are

functions of η_2 and ζ_2. This means that the rest of the systems stays at steady state during a fault, while the "subsystem" where the fault occurred deals with the stabilization.

5.6 Conclusion

The controller presented in this chapter is proven to asymptotically stabilize the system in theory, as long as the controller is based on the correct system. Simulations confirm that as long as the time the controller is based on an incorrect system is limited, it increases the stability of the system and brings it back to steady state.

It is also shown that during small permanent faults, the controller increases stability, but brings the system to a new equilibrium. However, it cannot necessarily handle arbitrary large permanent changes in the system. To address this issue the controller must work together with a good model updater, so that the model is updated when larger changes in loads or network configuration appears.

The main challenge of the presented controller is however the restrictive nature of Assumption 1, and the fact that the controller becomes singular for some combinations of generator angles. These singularities in the controller is an issue which must be resolved in order for the controller to function in practice. Another problem with Assumption 1 is of course that it confines the configuration of the network it may be applied on, demanding that the number of external variables ζ and the number of HVDC lines are equal.

Chapter 6

Concluding remarks

In this thesis, the advanced control method known as model predictive control (MPC) is used for automatic generator control (AGC) of the Nordic power system. In Chapter 1 the composition of the Nordic power system was presented, and the factors identified by the Norwegian transmission system operator (TSO) as the main challenges with regards to load frequency control (LFC) were presented. The Nordic power system has seen a decrease in frequency quality over the past two decades, and the aim of this thesis has been to improve the frequency quality and solve other issues related to this, such as avoiding bottleneck congestions and minimizing the effect of hourly production and trading set-point changes.

In Chapter 2 a nonlinear MPC (NMPC) was presented, including an extended Kalman filter (EKF) for state and disturbance estimation. The NMPC is based on a simplified model of the proxy system, and the constraints include limitations on tie-line power flow, generation capacity, and generation rate of change. Even though the NMPC is based on a simplified system model (based on aggregated generators), it is able to account for individual generator constraints by including the generator participation factors as optimization variables. This is an important feature, as the limitations on both total production and production rate-of-change vary a lot between the individual generating units. Simulations showed that the NMPC is able to coordinate the AGC with the primary control, resulting in reduced costs and improved frequency quality both at hour-shifts and during normal operation throughout the hour.

Performing LFC is a considerable expense for the TSO, and it is in many ways intuitive to include pricing in the NMPC in order to minimize costs. A suggestion to how this could be done is included in Chapter 2, where the cost of using the different generating units for AGC is included in the objective function in a quadratic manner. In an economic MPC, the objective function is often an economic profit function, which is linearly dependent on the state and input. The suggestion made here is therefore not an economic MPC, but rather a suggestion to how it could be included in the given framework. This was illustrated through simulations, showing that the MPC will favor the cheaper generating units.

The Nordic power system has not been sufficiently expanded since the liberalization of the power markets during the 1990s, which has led to a heavier loaded network with an increasing amount of bottlenecks. At times, these bottlenecks prevent some of the generating units in participating in LFC, which can lead to

both poorer frequency quality and higher expenses connected to LFC. In Chapter 2 another suggestion concerns how slack variables can be used to ensure available tie-line power-transfer capacity, and hence avoid tie-line bottlenecks. The presented solution requires an a-priori calculation of the need for available transfer capacity on the tie-lines. This is a somewhat rigid solution, and in Chapter 3 a more flexible solution to this problem is presented in the form of robustified NMPC. Instead of stating, for each tie-line, how much available transfer capacity is needed in case of any unforeseen event, the focus is now on unforeseen changes in wind power production, and the aim is to improve frequency quality in the presence of uncontrollable power production, such as wind power. A choice was made to focus on the slowly varying unpredicted power imbalance, and not on sudden changes caused by large loads or generators disconnecting or connecting to the system. The choice to focus only on the disturbance caused by unpredicted changes in wind power production is based on the assumption that the general slowly varying unpredicted power imbalance in the Nordic power system is dominated by unpredicted deviations in wind power production in South-Sweden and Zealand. This is a realistic assumption since (a) the overall consumption follows, to a large extent, a predictable consumption pattern, and (b) South-Sweden and Zealand contribute with approximately 80% of the total wind power production in the Nordic system (Statnett, 2012). It is assumed that a worst-case deviation from the predicted wind-power production in South Sweden and Zealand can be estimated, and the NMPC from Chapter 2 is then made more robust against such deviations using a simplified version of the multi-stage NMPC in Lucia et al. (2013) and the feedback min-max NMPC in Scokaert and Mayne (1998). This NMPC is referred to as the robustified NMPC (RNMPC) in Chapter 3 and as the multi-stage NMPC (MNMPC) in Chapter 4 and in the following. Simulations showed that the MNMPC keeps enough transfer capacity available so that it is able to use all generating units in covering a sudden drop or increase in wind-power production, resulting in better LFC. The MNMPC from Chapter 3 is based on a deterministic disturbance model, and in Chapter 4 it is compared to a stochastic NMPC (SNMPC) which is based on a stochastic disturbance model. Even though it intuitively might make more sense to view predictions of deviation in wind power production as stochastic, the results in Chapter 4 shows that in this case, the MNMPC results in a similar control result while showing better tractability and less chance of encountering infeasibility.

The prediction model (PM) used in the NMPCs divides the proxy system into two areas, which are chosen so that one area contains the majority of wind-power production. The tie-line constraints which are handled by the NMPCs are therefore constraints on the total sum of power transfer on all tie-lines connecting the two areas. If a more detailed control of power flow is wanted, the prediction model has to be expanded into more areas, which will affect the size of the OCP, and hence the time it takes to solve it. However, for the purpose of ensuring sufficient available tie-line capacity into an area with high wind-power density, it is the authors opinion that the PM used in this thesis sufficiently reflects the real power flow in the system. For the results in Chapter 3 and 4, it is also an important assumption that the

	Number of optimization variables			
Controller	u	x	ϵ	Total
Nominal NMPC	270	730	72	1072
RNMPC/MNMPC	810	2409	0	3219
SNMPC, $s = 65$	270	52195	0	52465
SNMPC, $s = 1000$	270	803000	0	803270

Table 6.1: Number of optimization variables of each NMPC. Specified for inputs u, states x and slack variables ϵ.

majority of wind power is gathered in one area, so that the disturbance in the other area can be neglected. If this is not the case, and the wind power is spread more evenly in the system, the estimate of the worst-case deviation in produced wind-power has to be adapted accordingly.

With regards to numerical issues encountered in the NMPCs of this thesis, it can be mentioned that with the smooth approximation of the saturation function, the PM is generally well behaved. With $N = 2$ areas, it is a fairly small model, and there were not any significant numerical issues. The only exception is the SNMPC from Chapter 4. With the number of scenarios included in the SNMPC approaching 100, it became very difficult to find a solution with the software and hardware used in this thesis. The OCP simply became too complex. Table 6.1 shows the size of the OCP for the different NMPCs.

With regards to nominal stability properties, none of the above NMPCs are proven to be stable. Stabilizing ingredients such as terminal constraints and terminal cost function could be added to ensure nominal asymptotic stability, this could however deteriorate the control performance by making the NMPC more conservative. In addition, terminal constraints and terminal cost functions that can be used to prove stability can be difficult to find. Nominal stability is therefore rather approach by choosing long horizons and tuning weights to achieve convergent behavior in simulations, and the Monte Carlo simulations presented in Chapter 2 and 3 supports this. However, since no stability proofs are given, it is important that the presented NMPC-based control regimes are supported by appropriate fallback controllers which ensures safe operations in case of unstable/infeasible or poor solutions from the NMPC.

The last contribution to the thesis, presented in Chapter 5, focuses on angle stability. This chapter investigates the possibility of using HVDC lines to increase angle stability in a power system, using a backstepping controller. The presented backstepping controller is tested on an arbitrary system where two synchronous power systems are connected by HVDC-lines, and simulations show that by controlling the power flow through the HVDC-lines, the electromechanical oscillations following a fault can be dampened. The same approach can also be used to stabilize the frequency of the power systems, however operating at a higher time scale. In

fact, if the controller for the power flow is properly designed, the power flow in HVDC lines can be used as a resource for both angle and frequency stability. The NMPCs presented in this thesis would however be to slow to handle the control of angle stability. In to the Nordic power system, the HVDC lines connecting the Nordic system to the Continental European system are appropriate candidates, and the NMPC schemes presented in Chapter 2 and 3 could make use of them for LFC. There are however some complicating issues that must be dealt with, one of which is scheduled power flow. The power trading between synchronous areas decides how much power that flow in the HVDC lines, which restricts how much they can be used for power-system stability purposes. However, they can be utilized when possible, and perhaps especially during hour shifts when set points for both production and power flow in HVDC lines change.

With regards to the control-design method used in Chapter 5, backstepping is very different from NMPC. They share the features that they are advanced, model-based control methods that are suitable for multivariable and nonlinear systems. However, backstepping is a theoretical approach resulting in an explicit control law which results in an asymptotically stable (nominal) system, whereas the NMPC is a practical approach which often suffers from the lack of theoretical stability proof. On the other hand, including and handling constraints and known/measurable disturbances is much easier with an NMPC than with a backtepping controller. The theoretical stability guarantees provided by the backstepping controller will also be jeopardized in the presence of model-plant mismatch and unknown disturbances, and as seen in Chapter 5, singularities in the controller is also a common issue (Khalil, 2002). Another issue for the backstepping controller from Chapter 5, which in general would not be a problem for an NMPC, is that of unequal number of inputs and outputs. The backstepping controller from Chapter 5 is not able to deal with such systems, which is a significant drawback.

Unresolved issues and possible future research directions

In this thesis, all of the NMPCs are tested under fairly realistic conditions, including model-plant mismatch as well as state and disturbance estimation. There are however some practical issues that are not yet resolved. One of these is communication. All of the NMPCs are centralized controllers which rely on measurements made in different parts of the power system. It has however not been the scope of this thesis to investigate proper solutions for safe, reliable and precise communication, this is never the less an important part of implementing the NMPCs on a real power system. The NMPCs also rely on different TSOs being willing to share measurements and information across borders.

When it comes to further development of the NMPCs, it is an evident possibility to include the costs related to AGC in order to minimize the expenses for the TSO. This was barely touched upon in Chapter 2, and it could be interesting to see if this could be included in a more holistic manner, either by including it in the presented NMPCs, or by approaching it in a hierarchic manner.

Another possibility that has not been addressed in this thesis is the use of flexible alternating current transmission systems (FACTS). FACTS are power electronics-based devices that are able to enhance power system controllability and stability and increase power transfer capability. They do so by facilitating power flow control, power oscillation damping and transient stability improvement. Including these in the NMPC would increase controllability and flexibility, at the expense of a larger and more complex OCP.

Bibliography

Almassalkhi, M. and Hiskens, I. (2015). Model-predictive cascade mitigation in electric power systems with storage and renewables; Part I: Theory and implementation. *Power Systems, IEEE Transactions on*, 30(1):67–77.

Andersson, J. (2013). *A General-Purpose Software Framework for Dynamic Optimization*. PhD thesis, Arenberg Doctoral School, KU Leuven.

Barry, R. and Chorley, R. (2003). *Atmosphere, Weather, and Climate*. Routledge.

Bemporad, A., Borrelli, F., and Morari, M. (2003). Min-max control of constrained uncertain discrete-time linear systems. *Automatic Control, IEEE Transactions on*, 48(9):1600–1606.

Bemporad, A. and Morari, M. (1999). Robust model predictive control: A survey. *Robustness in identification and control*, pages 207–226.

Bevrani, H. (2014). *Robust Power System Frequency Control*. Springer.

Bevrani, H., Hiyama, T., and Bevrani, H. (2011). Robust PID based power system stabilizer: Design and real-time implementation. *International Journal of Electrical Power & Energy Systems*, 33:179–188.

Biegler, L. T. (2010). *Nonlinear Programming: Concepts, Algorithms, and Applications to Chemical Processes*. SIAM.

Campi, M. C., Garatti, S., and Prandini, M. (2009). The scenario approach for systems and control design. *Annual Reviews in Control*, 33(2):149–157.

Carneiro, J. and Ferrarini, L. (2010). Preventing thermal overloads in transmission circuits via model predictive control. *Control Systems Technology, IEEE Transactions on*, 18(6):1406–1412.

Casazza, J. and Delea, F. (2003). *Understanding Electric Power Systems*. IEEE Press.

Çam, E. and Kocaarslan, I. (2005). Load frequency control in two area power system using fuzzy logic controller. *Energy Conversion Management*, 46:233–243.

Cecílio, I. M., Ersdal, A. M., Fabozzi, D., and Thornhill, N. F. (2013). An open-source educational toolbox for power system frequency control tuning and optimization. In *Innovative Smart Grid Technologies Europe (ISGT EUROPE), 2013 4th IEEE/PES*. IEEE.

Chang-Chien, L.-R., Lin, W.-T., and Yin, Y.-C. (2011). Enhancing frequency response control by DFIGs in the high wind penetrated power systems. *Power Systems, IEEE Transactions on*, 26(2):710–718.

Dvorkin, Y., Pandic, H., Ortega-Vazquez, M. A., and Kirschen, D. S. (2015). A hybrid stochastic/interval approach to transmission-constrained unit commitment. *IEEE Transactions on Power Systems*, 30(2):621–631.

ENTSO-E (2012). Operational reserve ad hoc team report. Technical report. Available at `https://www.entsoe.eu/fileadmin/user_upload/_library/resources/LCFR/2012-06-14_SOC-AhT-OR_Report_final_V9-3.pdf`.

ENTSO-E (2014). Yearly statistics & adequacy retrospect 2012-2014. Technical report. Available at `https://www.entsoe.eu/publications/statistics/yearly-statistics-and-adequacy-retrospect/Pages/default.aspx`.

ENTSO-E (2015). ENTSO-E at a glance. Technical report. Available at `https://www.entsoe.eu/Documents/Publications/ENTSO-E%20general%20publications/entsoe_at_a_glance_2015_web.pdf`.

Eriksson, R. and Knazkins, V. (2008). On the Coordinated Control of Multiple HVDC Links: Modal Analysis Approach. *GMSARN International Journal*, 2:15–20.

Eriksson, R., Knazkins, V., and Söder, L. (2010). Coordinated control of multiple HVDC links using input-output exact linearization. *Electric Power Systems Research*, 80(12):1406–1412.

Ersdal, A., Imsland, L., and Uhlen, K. (2016a). Model predictive load-frequency control. *Power Systems, IEEE Transactions on*, 31(1):777–785.

Ersdal, A. M., Cecílio, I. M., Fabozzi, D., Imsland, L., and Thornhill, N. F. (2013). Applying model predictive control to power system frequency control. In *Innovative Smart Grid Technologies Europe (ISGT EUROPE), 2013 4th IEEE/PES*. IEEE.

Ersdal, A. M., Fabozzi, D., Imsland, L., and Thornhill, N. F. (2014). Model predictive control for power system frequency control taking into account imbalance uncertainty. In *IFAC World Congress*, volume 19, pages 981–986.

Ersdal, A. M. and Imsland, L. (2017). Scenario-based approaches for handling uncertainty in MPC for power system frequency control. In *IFAC World Congress (submitted)*.

Ersdal, A. M., Imsland, L., and Uhlen, K. (2012). Coordinated control of multiple HVDC links using backstepping. In *Control Applications (CCA), 2012 IEEE International Conference on*, pages 1118–1123.

Ersdal, A. M., Imsland, L., Uhlen, K., Fabozzi, D., and Thornhill, N. F. (2016b). Model predictive load-frequency control taking into account imbalance uncertainty. *Control Engineering Practice*, 53:139 – 150.

Fabozzi, D., Thornhill, N. F., and Pal, B. C. (2013). Frequency restoration reserve control scheme with participation of industrial loads. In *Proc. 2013 IEEE Grenoble PowerTech conf.*

Goodwin, G. C. and Medioli, A. M. (2013). Scenario-based, closed-loop model predictive control with application to emergency vehicle scheduling. *International Journal of Control*, 86(8):1338–1348.

Gross, G. and Lee, J. W. (2001). Analysis of load frequency control performance assessment criteria. *Power Systems, IEEE Transactions on*, 16:520–525.

Grüne, L. and Pannek, J. (2011). *Nonlinear Model Predictive Control. Theory and Algorithms.* Springer.

Halvgaard, R., Poulsen, N. K., Madsen, H., and Jørgensen, J. B. (2012). Economic model predictive control for building climate control in a smart grid. In *Innovative Smart Grid Technologies (ISGT), 2012 IEEE PES*, pages 1–6. IEEE.

Holttinen, H. (2004). *The impact of large scale wind power production on the Nordic electricity system.* PhD thesis, Helsinki University of Technology.

Hovgaard, T. G., Edlund, K., and Bagterp Jorgensen, J. (2010). The potential of economic MPC for power management. In *Decision and Control (CDC), 2010 49th IEEE Conference on*, pages 7533–7538. IEEE.

Huang, R., Patwardhan, S. C., and Biegler, L. T. (2009). Multi-scenario-based robust nonlinear model predictive control with first principle models. *Computer Aided Chemical Engineering*, 27:1293–1298.

Johansen, T. (2015). Toward dependable embedded model predictive control. *Systems Journal, IEEE.* (to appear).

Khalil, H. K. (2002). *Nonlinear Systems.* Prentice Hall, 3rd edition.

Khodabakhshian, A. and Edrisi, M. (2008). A new robust PID load frequency controller. *Control Engineering Practice*, 16:1069–1080.

Krstić, M., Kanellakopoulos, I., and Kokotović, P. (1995). *Nonlinear and Adaptive Control Design.* John Wiley & Sons, Inc.

Kundur, P. (1994). *Power system stability and control.* The EPRI power system engineering series. McGraw-Hill.

Kundur, P., Paserba, J., Ajjarapu, V., Andersson, G., Bose, A., Canizares, C., Hatziargyriou, N., Hill, D., Stankovic, A., Taylor, C., Van Custem, T., and Vittal, V. (2004). Definition and Classification of Power System Stability. *IEEE Transactions on Power Systsems*, 19(2):1387–1401.

Langson, W., Chryssochoos, I., Raković, S., and Mayne, D. Q. (2004). Robust model predictive control using tubes. *Automatica*, 40(1):125–133.

Levine, W. (2010). *The Control Handbook, Second Edition: Control System Fundamentals, Second Edition*. Electrical Engineering Handbook. CRC Press.

Li, P., Wendt, M., and Wozny, G. (2002). A probabilistically constrained model predictive controller. *Automatica*, 38(7):1171–1176.

Li, X. (2003). A nonlinear emergency control strategy for HVDC transmission systems. *Electric Power System Research*, 67(3):153 – 159.

Löfberg, J. (2003). *Minimax approaches to robust model predictive control*. PhD thesis, Linköping University.

Lucia, S., Andersson, J. A., Brandt, H., Diehl, M., and Engell, S. (2014a). Handling uncertainty in economic nonlinear model predictive control: A comparative case study. *Journal of Process Control*, 24(8):1247–1259.

Lucia, S., Finkler, T., and Engell, S. (2013). Multi-stage nonlinear model predictive control applied to a semi-batch polymerization reactor under uncertainty. *Journal of Process Control*, 23(9):1306 – 1319.

Lucia, S., Limon, D., and Engell, S. (2014b). Stability properties of multi-stage robust nonlinear model predictive control. *Automatica (Submitted)*.

Machowski, J., Bialek, J. W., and Bumby, J. R. (2008). *Power System Dynamics. Stability and Control*. Wiley.

Maciejowski, J. M. (2002). *Predictive Control with Constraints*. Pearson Education.

Maiworm, M., Bäthge, T., and Findeisen, R. (2015). Scenario-based model predictive control: Recursive feasibility and stability. *The 9th IFAC Symposium on Advanced Control of Chemical Processes ADCHEM 2015*, 48(8):50 – 56.

Marinovici, L., Lian, J., Kalsi, K., Du, P., and Elizondo, M. (2013). Distributed hierarchical control architecture for transient dynamics improvement in power systems. *Power Systems, IEEE Transactions on*, 28(3):3065–3074.

Mayne, D. (2001). Control of constrained dynamic systems. *European Journal of Control*, 7(2):87 – 99.

Mayne, D., Rawlings, J., Rao, C., and Scokaert, P. (2000). Constrained model predictive control: Stability and optimality. *Automatica*, 36(6):789 – 814.

McNamara, P., Negenborn, R. R., De Schutter, B., and Lightbody, G. (2013). Optimal coordination of a multiple HVDC link system using centralized and distributed control. *Control Systems Technology, IEEE Transactions on*, 21(2):302–314.

Mesbah, A. (2016). Stochastic model predictive control: An overview and perspectives for future research. *Control Systems Magazine, IEEE*. (to appear).

Mohamed, T., Bevrani, H., Hassan, A., and Hiyama, T. (2011). Decentralized model predictive based load frequency control in an interconnected power system. *Energy Conversion and Management*, 52(2):1208 – 1214.

Mohamed, T. H., Morel, J., Bevrani, H., and Hiyama, T. (2012). Model predictive based load frequency control design concerning wind turbines. *International Journal of Electrical Power & Energy Systems*, 43(1).

Morison, K., Wang, L., and Kundur, P. (2004). Power System Security Assessment. *Power & Energy magazine, IEEE*, 2(5):30–39.

Nocedal, J. and Wright, S. J. (2006). *Numerical Optimization*. Springer, second edition.

Nordel (2008). Nordel annual statistics 1997-2008. Technical report. `https://www.entsoe.eu/news-events/former-associations/nordel/annual-statistics/Pages/default.aspx`.

Norheim, I., Lindgren, E., Uski, S., Srensen, P., and Jauch, C. (2005). WILMAR WP5 - Deliverable D5.1. System Stability Analysis. Technical report, SITNEF Energy Research.

Otomega, B., Marinakis, A., Glavic, M., and Van Cutsem, T. (2007). Emergency alleviation of thermal overloads using model predictive control. In *Proc. 2007 IEEE PES PowerTech Conference*.

Pilotto, L., Szechtman, M., Wey, A., Long, W., and Nilsson, S. (1995). Synchronizing and damping torque modulation controllers for multi-infeed HVDC systems. *IEEE Transactions on Power Delivery*, 10(3):1505–1513.

Primbs, J. A. and Sung, C. H. (2009). Stochastic receding horizon control of constrained linear systems with state and control multiplicative noise. *Automatic Control, IEEE Transactions on*, 54(2):221–230.

Rawlings, J. B. and Amrit, R. (2009). Optimizing process economic performance using model predictive control. In *Nonlinear model predictive control*, pages 119–138. Springer.

Rawlings, J. B. and Mayne, D. Q. (2009). *Model Predictive Control: Theory and Design*. Nob Hill Publishing.

Rostampour, V., Esfahani, P. M., and Keviczky, T. (2015). Stochastic nonlinear model predictive control of an uncertain batch polymerization reactor. In *IFAC Conference on Nonlinear Model Predictive Control*.

Rostampour, V., Margellos, K., Vrakopoulou, M., Prandini, M., Andersson, G., and Lygeros, J. (2013). Reserve requirements in AC power systems with uncertain generation. In *IEEE PES ISGT Europe 2013*, pages 1–5.

Saxena, S. and Hote, Y. (2013). Load frequency control in power systems via internal model control scheme and model-order reduction. *Power Systems, IEEE Transactions on*, 28(3):2749–2757.

Scokaert, P. and Mayne, D. (1998). Min-max feedback model predictive control for constrained linear systems. *IEEE Transactions on Automatic Control*, 43(8):1136–1142.

Shiroei, M., Toulabi, M. R., and Ranjbar, A. M. (2013). Robust multivariable predictive based load frequency control considering generation rate constraint. *International Journal of Electrical Power & Energy Systems*, 46:405–413.

Short, J., Infield, D., and Freris, L. (2007). Stabilization of grid frequency through dynamic demand control. *Power Systems, IEEE Transactions on*, 22(3):1284–1293.

Simon, D. (2006). *Optimal State Estimation*. Wiley.

Singh, V. P., Mohanty, S. R., Kishor, N., and Ray, P. K. (2013). Robust H-infinity load frequency control in hybrid distributed generation systems. *International Journal of Electric Power & Energy Systems*, 46:294–305.

Skogestad, S. (2003). Simple analytic rules for modeling reduction and PID controller tuning. *Journal of Process Control*, 13:291–309.

Smed, T. and Andersson, G. (1993). Utilizing HVDC to damp power oscillations. *IEEE Transactions on Power Delivery*, 8(2):620 – 627.

Statnett (2012). Systemdrifts- og markedsutviklingsplan 2012. Technical report. available at `issuu.com/statnett/docs/statnett_smup`.

Statnett (2015). Årsrapprt fra systemansvarlig 2015. Technical report.

Suvire, G., Molina, M., and Mercado, P. (2012). Improving the integration of wind power generation into AC microgrids using flywheel energy storage. *Smart Grid, IEEE Transactions on*, 3(4):1945–1954.

Tan, W. (2010). Unified tuning of PID load frequency controller for power systems via IMC. *Power Systems, IEEE Transactions on*, 25(1):341–350.

Venkat, A., Hiskens, I., Rawlings, J., and Wright, S. (2008). Distributed MPC strategies with application to power system automatic generation control. *Control Systems Technology, IEEE Transactions on*, 16(6):1192–1206.

Vrdoljak, K., Perić, N., and Petrović, I. (2010). Sliding mode based load-frequency control in power systems. *Electric Power Systems Research*, 80(5):514–527.

Wächter, A. and Biegler, L. T. (2006). On the implementation of an interior-point filter line-search algorithm for large-scale nonlinear programming. *Mathematical Programming*, 106(1):25–57.

Weimers, L. (2000). Bulk power transmission at extra high voltages, a comparison between transmission lines for HVDC at voltages above 600 kV DC and 800 kV AC.

Whitley, D. and Gjerde, O. (2011). LFC/AGC-Nordic and European perspective. Presentation at workshop: Exchange of balancing services between the Nordic and the Central European synchronous systems. Available at http://www.sintef.no/globalassets/project/balance-management/gardermoen/8---gjerde-statnett---lfc-and-agc---nordic-perspective.pdf.

Yousef, H., AL-Kharusi, K., Albadi, M., and Hosseinzadeh, N. (2014). Load frequency control of a multi-area power system: An adaptive fuzzy logic approach. *Power Systems, IEEE Transactions on*, 29(4):1822–1830.